The Thesis Committee for Logan Joseph Santos
Certifies that this is the approved version of the following thesis:

Solvent Annealing and Thickness Control for the Orientation of Silicon-containing Block Copolymers for Nanolithographic Applications

APPROVED BY
SUPERVISING COMMITTEE:

Supervisor:

C. Grant Willson

Christopher J. Ellison

Solvent Annealing and Thickness Control for the Orientation of Silicon-containing Block Copolymers for Nanolithographic Applications

by

Logan Joseph Santos, B.S.

Thesis

Presented to the Faculty of the Graduate School of

The University of Texas at Austin

in Partial Fulfillment

of the Requirements

for the Degree of

Master of Science in Engineering

The University of Texas at Austin

May 2012

Dedication

I dedicate this thesis to my family and all of the friends. Without you, I am nothing.

Acknowledgements

Usually, the best place to start is with what comes first, and family is always first. In the beginning, there were my parents. My father, Stanley Joseph Santos, and my mother, Tammie Darlene Norton, have always wanted what is best for their children. My sister, Blair Elizabeth Santos, has always been there to protect and support her big brother. Together, we lived in the small town of Tioga, Louisiana across the street from my grandmother, Joyce ("Momo") Santos, who also played a giant part in my upbringing, particularly in the spiritual aspect. My aunts – Victoria Hyatt, Loretta Gaspard, and Catherine Mosby – have always been very supportive of me and have set excellent examples of how good human beings should live. I have always enjoyed their telephone calls throughout my college career, which put me at ease. My cousins Catherine Pearson, Lauren Hyatt, and Melissa Mosby rounded out the rambunctious bunch of children who would always be playing in the old neighborhood.

Some of the best times of my life involved playing baseball in Tioga where I made many childhood friends. The best of which is Casey Henagan who I am still friends with even to this very day. Perhaps my longest friendship, as we were playing against each other at the age of four, Casey is my most interesting friend. During a summer job, we once tried to figure out why we were such good friends. Even though our personalities and interests are almost polar opposites, we seem to keep each other in check. I was honored to recently be in his wedding to his lovely, witty wife Andrea. I was so honored that I passed out in the middle of the ceremony.

For elementary school, I attended Our Lady of Prompt Succor in Alexandria, LA to receive the best education my hometown had to offer. I attended Country Day for

junior high and Holy Savior Menard for high school. I was offered the chance to attend the Louisiana School for Math, Science, and the Arts (LSMSA). After much consideration, my family and I decided to enroll me. It was a difficult decision as I was giving up my starting position at third base on Menard's baseball team as well as leaving my friends and family two years early. I am convinced that this is the best decision we have ever made. I had to stay in a dorm for two years on a college campus and take advanced classes offered nowhere else in the state from professors who were required to have PhDs. It was here that I grew from a nerdy, antisocial child to my present nerdy, slightly-more-social self. For the first time in my life, I had many friends. Through these comrades, I matured and broadened my horizons further that I had ever imagined. The two most prominent influences from LSMSA have been Anthony McDavid and John Bourgeois. Anthony, who recently departed to live in Japan, has been a model for the type of attitude I'd like to have in life. He sees what he wants and goes for it – like a boss. He also offered me great life advice when I was struggling both at work and personally in graduate school. I recently had the great honor of being in John's wedding (at which I did not pass out). I wish him and his new bride Amanda a wonderful future. The teachers that helped shape me the most include: Mrs. Jowers, Mr. Keys, Mr. Sanders, Mrs. Hernandez, Mrs. Chapman, Dr. Hynes, and Dr. McMullen. Without these educators, I would not have been able to go to a good, out-of-state engineering college and become the chemical engineer I am today.

At Texas A&M University, I received a quality industry-oriented education and met my two best friends, Alek Schmidt and Devin Garcia. Never have I met two people so like me with so similar interests. Their friendship has meant the world to me. They, together with my friends Andrew House, Dr. Rebecca McMahon, Alba Lucía Pineda Solano, and Christina Chern, made my college experience a memorable one.

After much debate, I decided to attend graduate school at the University of Texas at Austin where I met Dr. C. Grant Willson. After speaking with him and his team of excellent graduate students, I decided that this was the right group for me. Dr. Willson was very supportive of me and only saw my potential, even when I myself could not. Not enough can be said about his long-time assistant Kathleen Sparks who is the glue that holds the Willson group together. She advised me on numerous occasions when I was struggling in graduate school. I'd like to thank fellow group members Dr. Michael Jacobsson and Ryan Deschner for their excellent career advice as well as their friendship. Dr. Brandon Rawlings, Dr. Xinyu Gu, Dr. Siddharth Chauhan, William Durand, Christopher Chen, Ryan Mesch, and Chris Bates have also been good friends to me in my tenure at UT. Visiting scientists Toshiyuki Ogata, Takanori Kawakami, Yuji Hagiwara, and Takehiro Seshimo have been great golfing partners. Dr. Younjin Cho, William Bell, and Hao Tang frequently gave me help when I needed it. I occasionally needed expertise from outside the group, and people like Gary Doyle, Dr. Dwight Romanovicz, and Dr. Damon Smith all rose to the occasion. Many on-campus employees have aided me in teaching, enrollment, and construction including: Dr. Keith Freidman, Mrs. T. Stockman, Mr. Butch Cunningham, Mr. Jim Smitherman, Mr. Randy Rife, Mr. Eddie Ibarra, Mr. Kevin Haynes, Mrs. Donna Martin, Mrs. Kay Costales-Swift, Mr. Patrick Danielewski, Mr. Terry Watts, and Mr. Mike Ronalter. Finally, I got to know and could not have accomplished all that I did without the help of some very talented undergraduates: Jeffrey Ting, Leon Dean, Wade Wang, Jacob Adams, Alejandro Maurer, and Benjamin Bamgbade.

My former roommate and fellow Aggie Steven Fulk also gave me constant support in graduate school. I also met my first special lady during my tenure at UT. Kriti Dhaubhadel brought me much joy at a time when I needed it most.

Abstract

Solvent Annealing and Thickness Control for the Orientation of Silicon-containing Block Copolymers for Nanolithographic Applications

Logan Joseph Santos, M.S.E.

The University of Texas at Austin, 2012

Supervisor: C. Grant Willson

Block copolymers are an ideal solution for a wide variety of nanolithographic opportunities due to their tendency to self-assemble on nanoscopic length scales[1]. High etch selectivity and thin-film orientation are crucial to the success of this technology. Most conventional block copolymers have poor etch selectivity[2]; however, incorporating silicon into one block produces the desired etch selectivity[3-4]. A positive side effect of the silicon addition is that the χ value (a block-to-block interaction parameter) of the block copolymer increases[5-6]. This decreases the critical dimension of potential features[7]. Unfortunately, one negative side effect is the increase in the surface energy difference between the blocks[8]. Incorporating silicon decreases the surface energy of that block. Typically, annealing is used to induce the chain mobility that is required for the block copolymer to reach its minimum thermodynamic energy state[9]. Thermal annealing is the easiest annealing technique; however, if the glass transition temperature (T_g) of one block is above the thermal decomposition temperature of the other block, the latter will degrade

before the former can reorient[4, 10-12]. In addition, annealing silicon-containing block copolymers usually results in a wetting layer and parallel orientation since the lower surface energy block favors the air interface, minimizing the free energy[2, 13-15]. Solvent annealing replaces the air interface with a solvent, thereby changing the surface energy. The solvent plasticizes the block copolymer, effectively decreasing the T_gs of both blocks[16]. Another benefit is the ability to reversibly alter the orientation by changing the solvent or solvent concentration[5, 10, 15-18]. The challenge with solvent annealing is that it depends on a number of parameters including: solvent selection, annealing time, and vapor concentration[9, 19], which generate a very large variable space that must be searched to find optimum screening conditions.

Table of Contents

List of Tables

List of Figures

Chapter 1: A History of Hard Disk Drives and Customer Demand

In 1965, co-founder of Intel Gordon Moore predicted with only four data points that the number-density of transistors would double every 18-24 months for about the same cost. This statement has held true to this day and become known as Moore's Law[20]. In 1971, the Intel 4004 CPU had 2300 transistors on it. In 2011, the Core i7 Extreme Edition processor contained 1.3 billion transistors[21]. To put this feat in perspective, image a small town that started with a little over 2000 people, grow to the population of China in just 40 years!

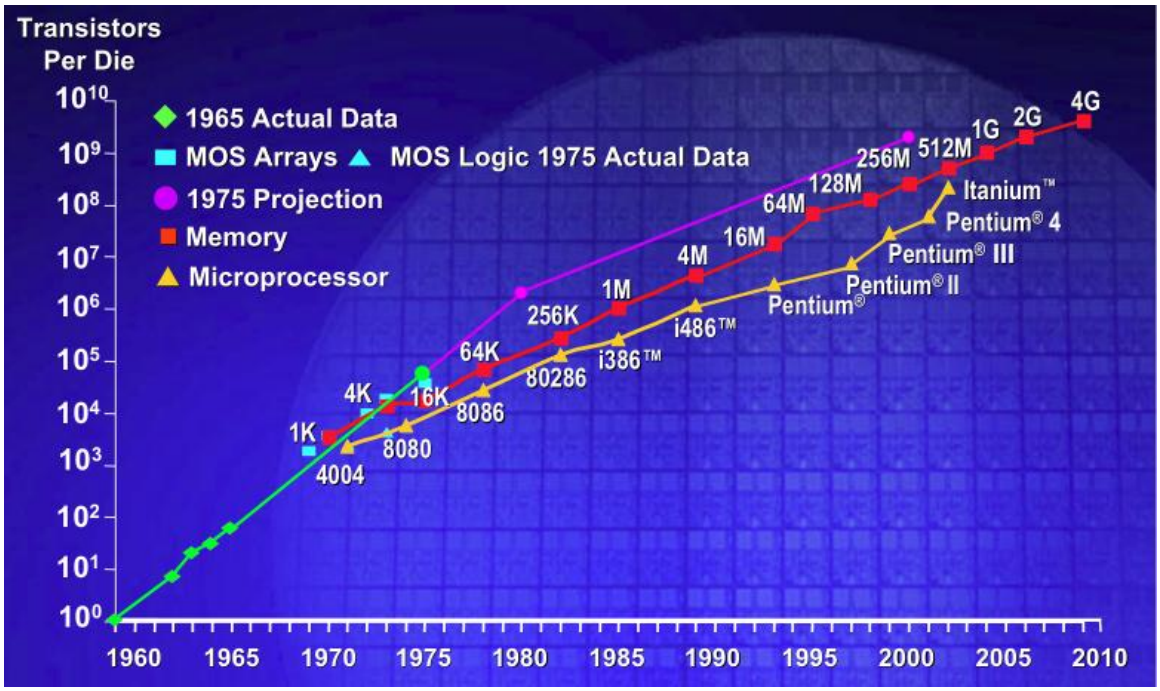

Figure 1: Moore's Law Compared with Actual Data[22]

While Moore's Law was originally directed toward transistors, it has proven true for the price and number-density of data storage as well. In 1981, a 5 MB hard drive cost

about $3500 or $700/MB[20]. In 2012, terabyte hard drives sell for about $100, which corresponds to $0.0001/MB.

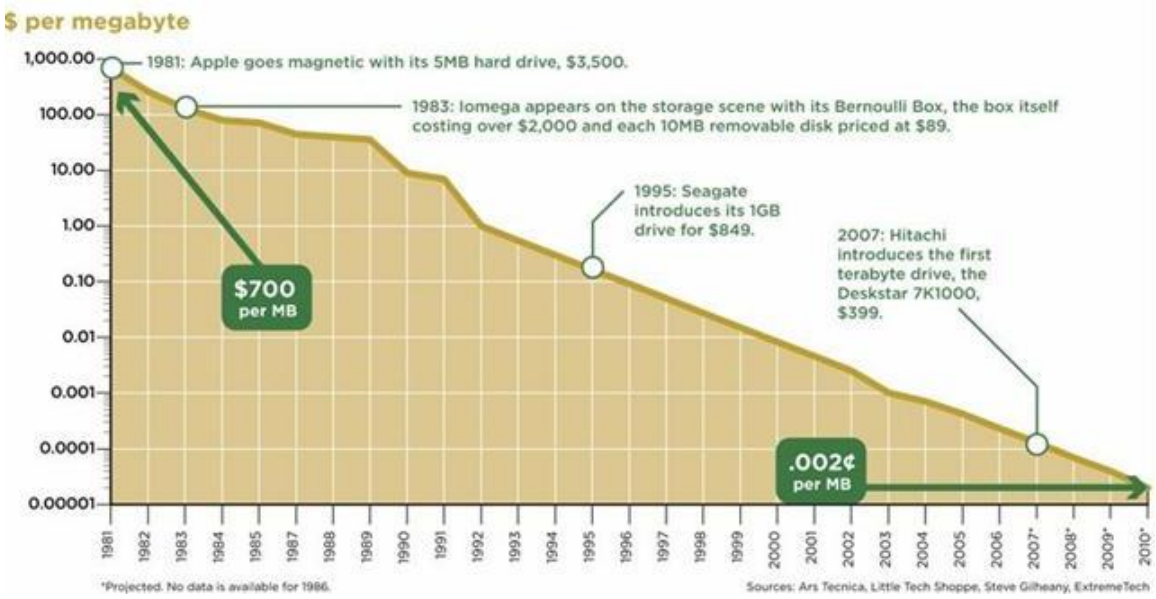

Figure 2: The Cost Decrease per MB of Storage[20]

The areal density of hard drives has also increased greatly over the past two decades.

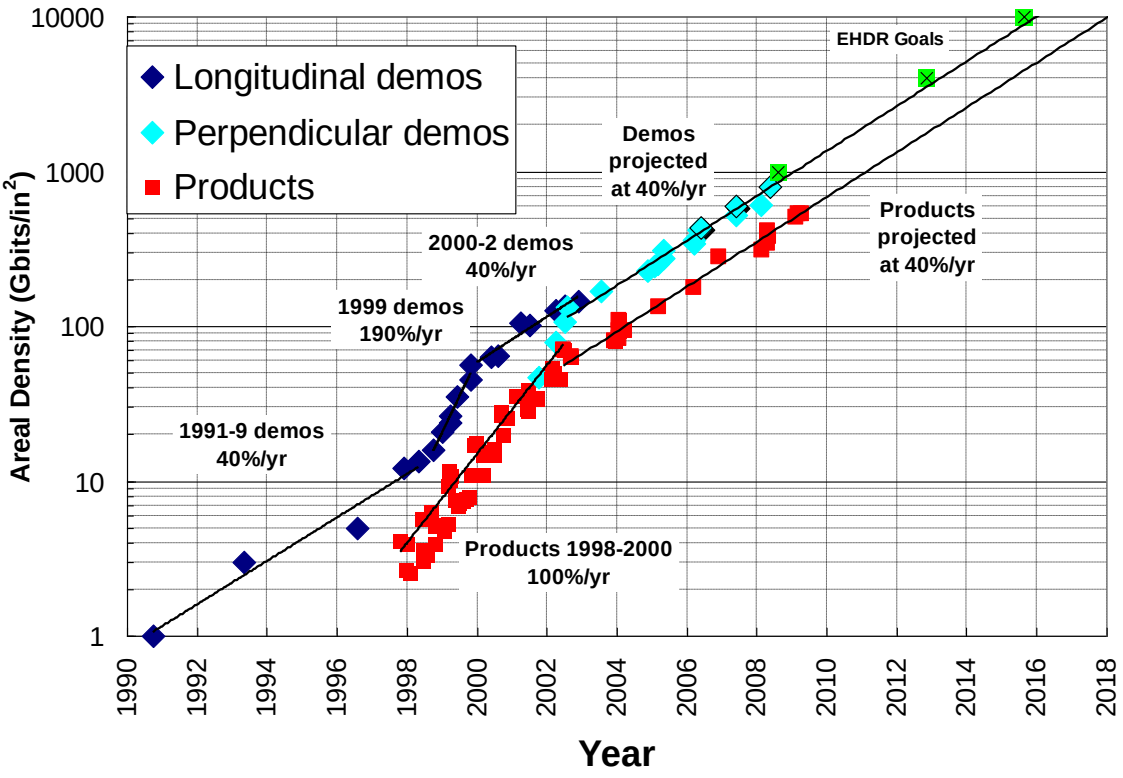

Figure 3: The Increase of Areal Density in Hard Drives[23]

A hard drive is similar to a record player that has the ability to stack multiple disks. These disks are coated with a magnetic media containing tiny particles called grains. Clusters of these grains in different states of magnetization make up bits. A read-write head (analogous to the needle on a record player) passes over the media and either records information by altering the magnetization state of the clusters or simply reads previously stored information. The data are stored in concentric, circular tracks, each of which contain a row of bits. A digital '1' is processed when the boundary between the two bits in a bit cell are of opposite magnetization. This is defined as a "magnetic transition." Alternatively, a '0' is processed when no such magnetic transition occurs in a bit cell (the two bits have the same magnetization)[24]. These data can be strung together to construct

the binary code that computers convert to text. The disks rotate at thousands of revolutions per minute while read-write heads scan both sides[25].

Customers are constantly demanding smaller, more powerful electronics while maintaining near constant or lower purchasing costs. In addition, companies have started to compile massive quantities of consumer data in remote storage facilities. A prime example is Apple's Cloud. Millions of consumers are uploading data to these servers with the number increasing every day. As the amount of data increases, so must the number of hard drives and therefore the size of these facilities, which leads to a rise in operating costs. These are the two main driving forces for miniaturization of electronics. If it were possible to fit more data on the same disk area, more data could be stored in the same space with lower operating costs. In addition, more information could be stored on individual electronic devices. Therefore, companies are constantly trying to increase the areal density of hard drives.

The two greatest challenges designers face are signal-to-noise issues and superparamagnetism. Logically, in order to increase the data-storage areal density, it is necessary to shrink the size of the bit cells. Bit boundaries must adhere to the random clustering of grains. Therefore, instead of ideal, straight lines, magnetic transition boundaries between bits are not smooth and are difficult for the read-write head to interpret. In large bit cells, it is easy to detect magnetic transitions. However, the signal-to-noise factor decreases proportionally with decreasing bit cell size. Ultimately, the read-write head will not be able to properly interpret/alter data. It has been stated that a minimum of roughly 50-100 grains per bit cell is necessary for reliable data detection[24].

Another route to increased areal density would be to shrink the size of the grains themselves. However, this is limited by superparamagnetism. In layman's terms, superparamagnetism is when a bit spontaneously "flips" magnetization due to thermal

effects, resulting in a loss of data. A smaller volume makes a grain increasingly susceptible to thermal fluctuations; therefore, small grains can change magnetization spontaneously at low temperatures. This effectively decreases the read-write head's ability to sense magnetic signals. After a certain point, as the volume of the grains are decreased further, the signal reduction becomes great enough so that data can no longer be read[25].

In the early 1990s, longitudinal recording technology yielded a 1 Gbit/in^2 hard drive. Bits are arranged horizontally while the read-write head scans the surface. Steady improvements over the next decade produced approximately 100 Gbit/in^2 hard drives. Eventually, this technology reached its limits due to the superparamagnetic effect. Therefore, a new technology was needed to replace longitudinal recording media to further increase areal density.

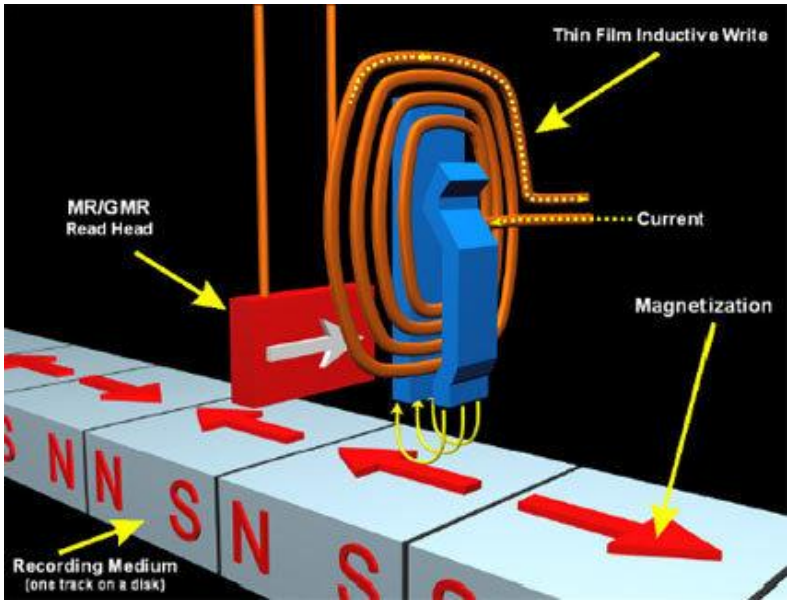

Figure 4: Longitudinal Magnetic Recording Diagram[26]

Perpendicular magnetic recording (PMR) tripled the storage density by aligning the bits perpendicular to the disk. By the end of the 2000s, companies were producing 667 Gbit/in^2 hard drives for consumers; however, it has not been possible to reach PMR's 1000 Gbit/in^2 limit even with tricks like discrete patterned media (rows of grains are separated from each other in an attempt to increase signal-to-noise), once again due to the superparamagnetic effect.

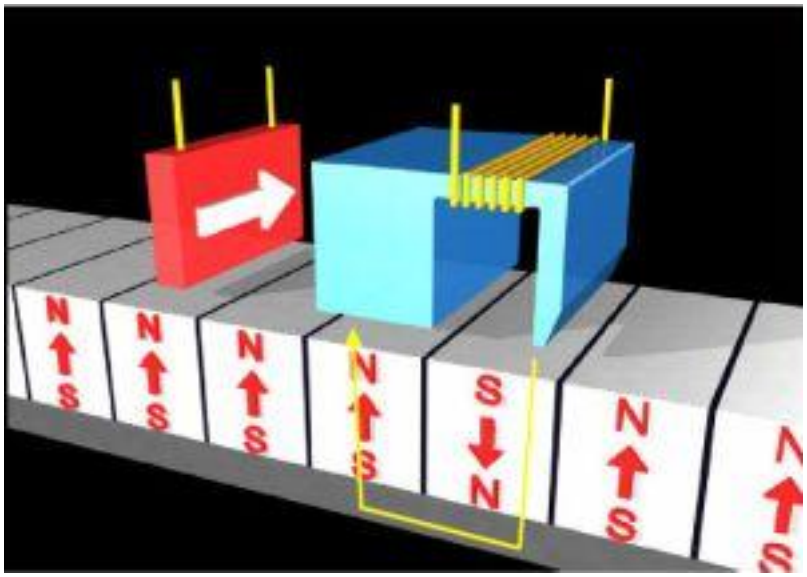

Figure 5: Perpendicular Magnetic Recording Diagram[26]

A new technology is necessary to break the 1 Tbit/in^2 mark. One proposed solution is bit patterned media (BPM). Unlike PMR, BPM has discrete domains, eliminating signal-to-noise issues amongst neighboring bits of different magnetization. In addition, the grains in each bit have a strong magnetic coupling, which increases thermal stability, thereby eliminating the superparamagnetic effect.

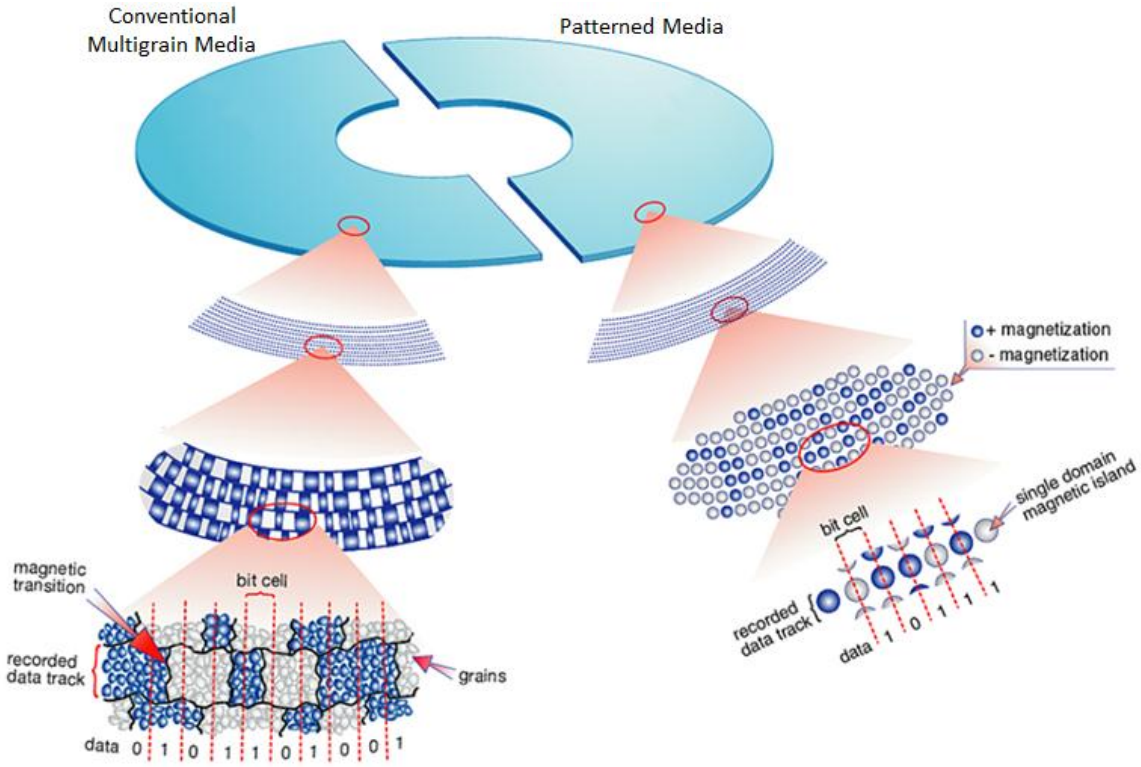

Figure 6: Conventional Media vs Bit Patterned Media[24]

Chapter 2: Optical and Imprint Lithography

A feature center-to-center distance of approximately 27 nm is required to reach the 1 Tbit/in^2 mark. In conventional optical lithography, a light source is shown through a mask with the desired patternable features. A series of lenses shrinks the pattern down to the actual size to be printed on the substrate. The substrate is coated with a photoresist that is either positive tone (exposed areas become more soluble) or negative tone (exposed areas become less soluble). After exposure, the more soluble material is removed so the pattern can now be transferred into the substrate. A final strip removes any remaining photoresist.

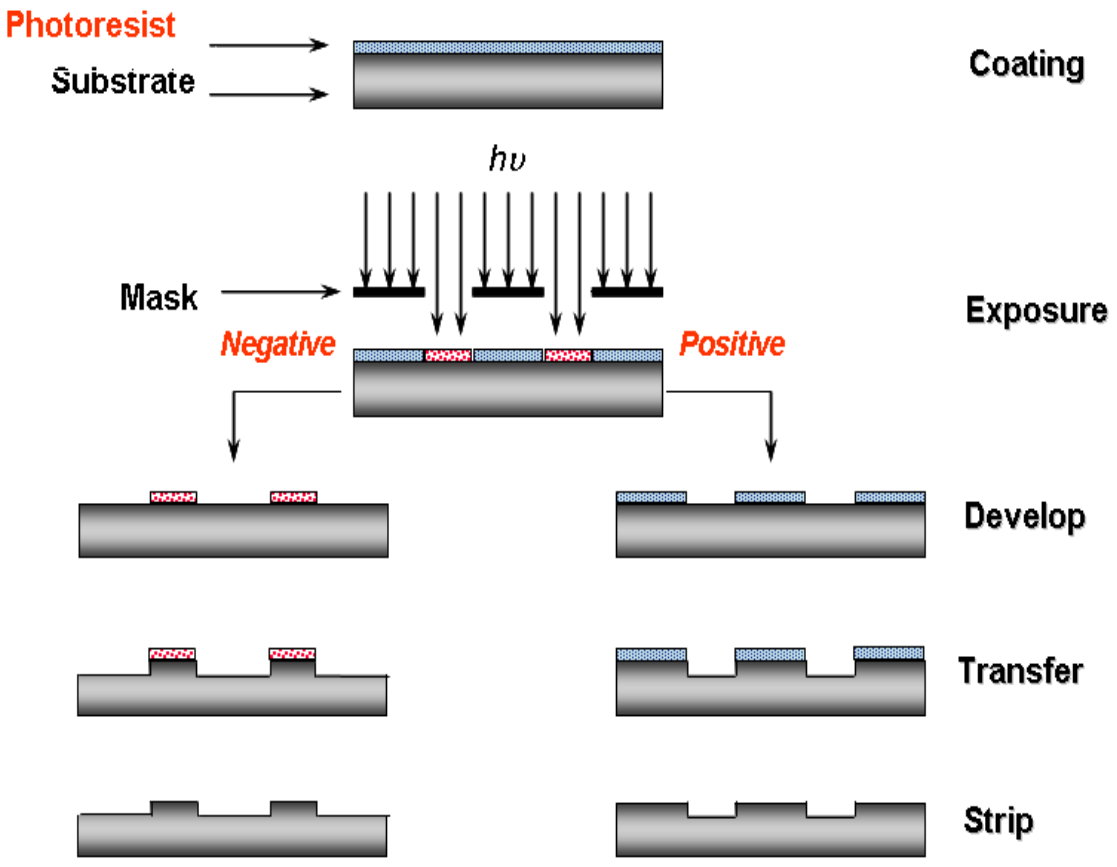

Figure 7: Optical Lithography Exposure[27]

Conventional optical lithography has reached its limits in its current form; it cannot achieve spacing this small. Photolithography resolution is governed by Rayleigh's equation:

$$R = \frac{k_1 \cdot \lambda}{NA}$$

where R is the critical dimension half-pitch resolution of a feature, k_1 is a dimensionless resolution "constant," λ is the wavelength of the exposure source, and NA is the numerical aperture of the lens[27]. The numerical aperture is related to the refractive index of the material between the lens and the substrate (n) and to the acceptance angle of the lens (θ) by the following equation:

$$NA = n \cdot \sin(\theta)$$

Resolution can be decreased using an exposure source with a lower wavelength, decreasing k_1 by altering operating conditions, or increasing the numerical aperture. Historically, the easiest factor to alter was the exposure wavelength. From the early 1960s through the mid-1980s, exposure tools used 436 nm g-line and then 365 nm i-line light from a mercury lamp source. Then, excimer lasers replaced the mercury lamps yielding 248 nm (KrF) and 193 nm (ArF) light. Further decreasing the wavelength of light is difficult since the light goes from being in the vacuum ultraviolet (UV) region of the electromagnetic spectrum to X-ray. Unlike UV light, X-rays cannot be refracted through lenses. Therefore, it is necessary to design a completely new exposure apparatus as well as new exposure materials[27]. This is very expensive, time-consuming, and difficult. Extreme ultraviolet (EUV) has promised exposure wavelengths as small as 13.5 nm[28]. However, the delay in production coupled with the high price tag of the equipment has led many to search for other solutions. As a result, more attention was focused on increasing k_1 by using techniques like double-patterning (exposing once, shifting the

mask, and exposing again) or increasing *NA* by using immersion lithography (replacing the material between the lens and substrate with a higher refractive index material). These add time-consuming process steps or have reached the limits of improvement. Using 193 nm light, the theoretical limit of 0.25 for k_1, and 1.44 for *NA* (the refractive index of water), optical lithography has a resolution limit of about 34 nm. Therefore, 1 Tb/in^2 (27 nm half-pitch) cannot be achieved with optical lithography.

An alternative to optical lithography is nanoimprint lithography (NIL). Unlike optical lithography, nanoimprint lithography does not require an expensive light source or lenses. Instead, a master template is directly contacted with an imprint fluid, which is then cured with UV light before lifting the template off leaving a replica of the mold. However, it is now necessary to create a 1:1 template.

One proposed method is to use electron beam lithography (EBL). The idea is simple: a stamper substrate is coated with an e-beam resist. The exposed regions can now be dissolved away in a developer solution, exposing the stamper substrate. After a reactive ion etch (RIE) into the stamper substrate where it is not protected by the e-beam resist, the template is formed. Finally, the e-beam resist is stripped away.

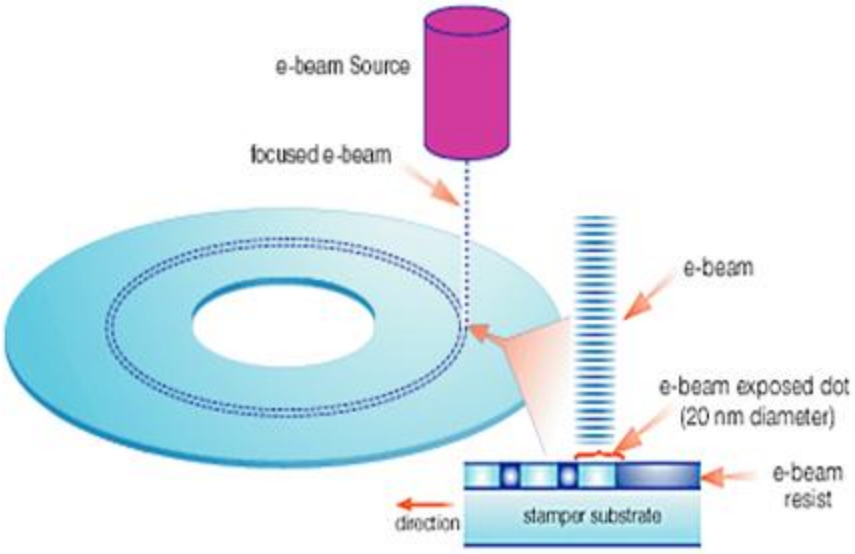

Figure 8: E-beam for Creating a Bit Patterned Media Template[24]

Next, a nanoimprint resist is coated onto a disk substrate. The inverted template is pressed into the nanoimprint resist. After the resist conforms to the shape of the template, it is cured with UV light. The template is then lifted off the hardened resist layer containing the opposite image. Following another RIE into the disk substrate, the resist is once again stripped away. Finally, a magnetic recording layer is coated over the patterned disk. Only the material on top of the pillars is read since it is closest to the read-write head[24].

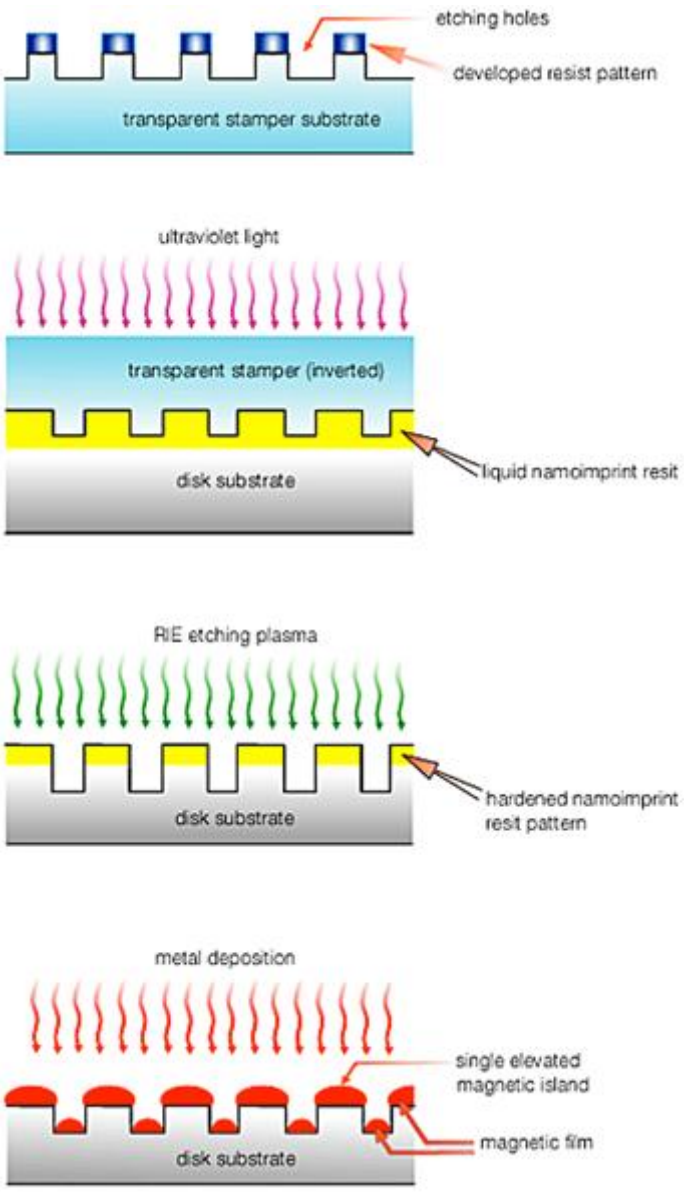

Figure 9: Pattern Transfer from Template to Disk[24]

The problem with this method is that it takes a long time to pattern a substrate with an e-beam tool. It can take several weeks to write a 2.5 inch disk-sized template with a 1 Tb/in^2 pattern density using a high-resolution e-beam resist[29]. This is significantly longer than what is acceptable by industry standards.

Chapter 3: Block Copolymer Directed Self Assembly

An alternative approach to e-beam lithography employs materials which self-assemble. One such material of particular interest is block copolymers (BC), which self-assemble on nanoscopic length scales into various features depending on the relative volume fraction (f), the chi interaction parameter (χ), and the degree of polymerization (N)[1]. This makes them ideal for a wide variety of nano-scale applications including nanoimprinting[30-33], nanoporous membranes[9, 34-36], and bit patterned media[37-41].

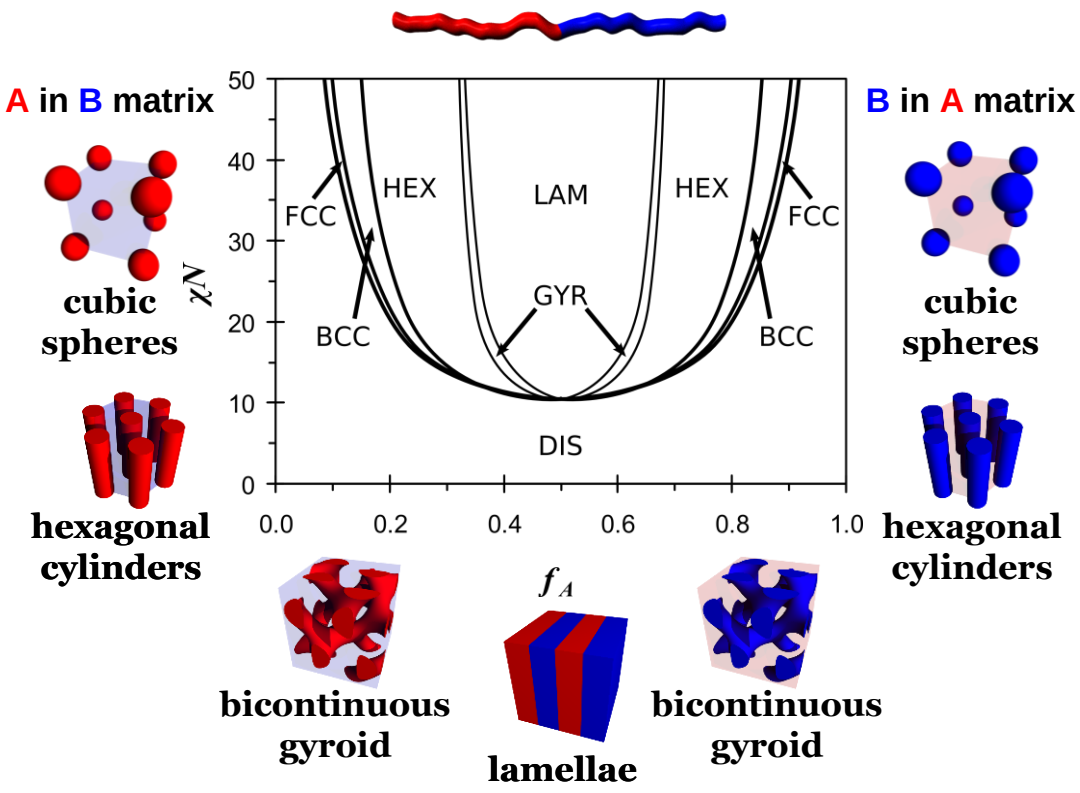

Figure 10: Block Copolymer Self Assembly Phase Diagram[42]

A block copolymer is two homopolymers (polymers comprised of only one type of repeat monomer) that are covalently bonded together[7]. Block copolymers can be

synthesized using various techniques including: living cationic or anionic polymerization, atom transfer free radical polymerization (ATRP), reversible addition fragmentation chain transfer (RAFT), and ring-opening metathesis polymerization (ROMP)[43]. By varying the volume fractions of each polymer, different microdomain features can be formed including: lamellae, bicontinuous gyroids, cylinders, and spheres[1]. χ is a block-block interaction parameter that can be viewed as a measure of how strongly one block favors itself or, alternatively, of how much one block disfavors the other. A higher χ indicates a greater incompatibility which translates to greater separation of the blocks. N is the degree of polymerization which is directly related to the molecular weight which is in turn related to the feature size. Since the periodicity (d) is proportional to the degree of polymerization as $d \propto N^{\frac{2}{3}} \cdot \chi^{\frac{1}{6}}$ in the strong-segregation limit[7], smaller molecular weights give smaller feature sizes so it is desired to make small molecular weight polymers[5]. However, the vertical axis of the plot shown above is "χN". If the product of χ and N falls below a value of 10.5 at 50/50 volume fraction for example, the block copolymer becomes disordered and no features exist. Therefore, in order to get smaller features, a higher χ material is necessary.

3.1 SPIN-COATING PROCEDURE

A polymer is coated onto a substrate (typically a silicon wafer) by first dissolving the polymer in a good casting solvent. The spin-coating apparatus consists of a chuck that rotates at a range of speeds. A variety of chuck sizes is available; however, it is important to select a chuck that is smaller than the substrate. If not, solvent can potentially be sucked into the vacuum lines and cause clogging or worse an explosion. Typical spin speeds are 1000-5500 rpm. Uneven coatings result at spin speeds below around 1000 rpm while there is a danger of the substrate flying off the chuck above about 5500 rpm. The

substrate is held on the chuck with negative pressure from a vacuum pump. The substrate is first blown clean with either a nitrogen or air source to remove large particles like dust and placed onto the spin-coater with a spin speed selected. Next, three washes of acetone and isopropyl alcohol (while the substrate is rotating), respectively, clean the substrate of organic matter. When the solvents evaporate, a color change is observed indicating the substrate is dry. After cleaning and drying, a small amount of the polymer solution, which has been filtered to remove any particulates, is dripped onto the substrate. Activating the spin-coater spreads the solution horizontally across the entire substrate. As the solvent evaporates, a uniformly-thin layer of the polymer remains[44]. The following equation relates spin speed to layer thickness:

$$t \cdot \omega^{\frac{1}{2}} = \text{constant}$$

where ω is the spin speed and t is the film thickness[45]. Since the product of the two terms is constant, it is possible to estimate the spin speed required to get a specific thickness given another thickness and its corresponding spin speed with the following equation:

$$\omega_2 = \omega_1 \cdot \left(\frac{t_1}{t_2} \right)^2$$

Typically, polymer solutions are 1 wt% which yield thicknesses around 100 nm in the spin speed range of 1000-5500 rpm.

The goal is to spin a hexagonally-packed cylinder-forming block copolymer on top of a silicon wafer, align the cylinders normal (perpendicular) to the wafer surface, and etch away one of the blocks.

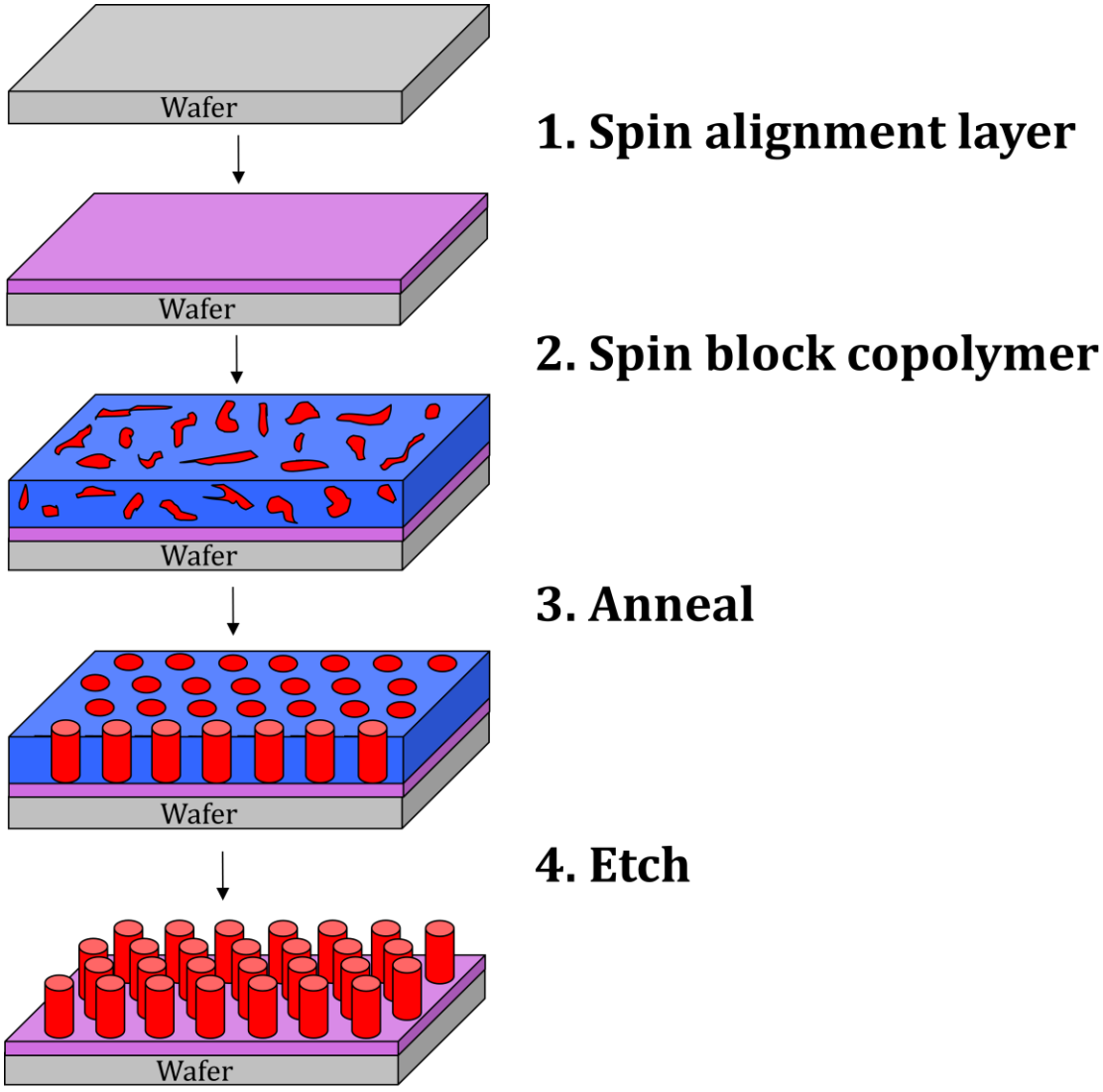

Figure 11: Directed Self Assembly Process

3.2 THERMAL ANNEALING AND SILICON INCORPORATION

A wide variety of block copolymers have been synthesized including: PS-*b*-PDMS[2, 5, 8, 46-48], PS-*b*-PEO[17, 49-50], and PS-*b*-PFS[5, 51] where PS is polystyrene, PDMS is polydimethylsiloxane, PEO is poly(ethylene oxide), and PFS is polyferrocenylsilane. One of the most popular block copolymer candidates is polystyrene-*block*-poly(methyl methacrylate) [PS-*b*-PMMA or P(S-*b*-MMA)][4, 12, 14-15, 29, 40, 52-54]. The idea was to spin-

coat the block copolymer onto a silicon wafer and thermal anneal to induce perpendicular orientation of the cylinders. Thermal annealing is heating a polymer above its glass transition temperature (T_g) in order to impart sufficient mobility for the chains to rearrange and assume mesostable morphology.

Some polymers degrade when heated in the presence of oxygen so thermal annealing must be done in a vacuum oven. However, after the annealing process was finished, the ovens in the Willson group took a very long time to cool down, putting a bottleneck on the testing. A custom oven was designed that would heat to 250 ^{o}C, have the ability to operate under tight vacuum, and cool down quickly. The new oven design will be discussed in greater detail later.

The thermal annealing procedure worked well for PS-*b*-PMMA. However, PS and PMMA have similar etch rates so no or low-aspect ratio features would be left after etching. Also, the χ value of PS-*b*-PMMA is too small to achieve the desired feature sizes.

Silicon incorporation into one of the blocks greatly increases etch selectivity[3-4]. While an oxygen etch volatilizes organic components, the oxygen reacts with the silicon to form SiO_2, which does not etch in oxygen. PS-*b*-PEO produces smaller features than PS-*b*-PMMA[36], and PS-*b*-PDMS has a higher χ than PS-*b*-PMMA[5] in addition to silicon atoms; however, poly(ethylene oxide) and polydimethylsiloxane have low glass transition temperatures[55], making them liquids at room temperatures. This is not a desirable quality for template formation. Therefore, the Willson group synthesized a block copolymer similar to PS-*b*-PMMA with the addition of silicon in the form of a trimethylsilyl (TMS) group[6].

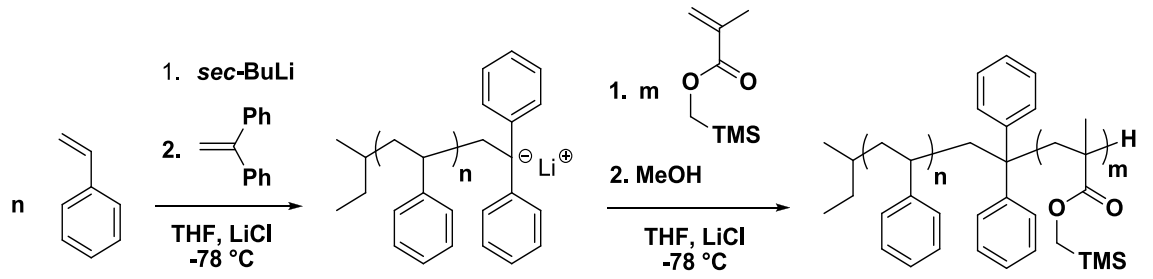

Figure 12: Synthesis Scheme for PS-*b*-PMTMSMA

However, after thermally annealing the new block copolymer, PS-*b*-PMTMSMA, it did not readily orient perpendicular to the wafer substrate like PS-*b*-PMMA. In addition, the block copolymer formed a wetting layer of PMTMSMA on the top so no features could be viewed with scanning electron microscopy (SEM), as seen in previous silicon-containing block copolymers[2, 13].

Silicon-containing polymers have very low surface energies. As a result, it was postulated that incorporating silicon atoms into the polymer would increase the χ interaction parameter as well as the etch selectivity. Both of these advantageous results were accompanied with a side effect. PS and PMMA have both similar surface energies and T_gs, which makes achieving vertical alignment with simple thermal annealing easy. Incorporating silicon atoms into a block greatly decreases the surface energy of that block. Upon thermal annealing, the block copolymer reorients itself to minimize the free energy at both the air and substrate interfaces. The non-polar TMS group prefers to wet the air interface since air also has a low dielectric constant. Both of these wetting preferences drive parallel orientation[14-15] (which is undesirable for the bit pattern media application) and a PMTMSMA wetting layer is produced that is impervious to oxygen etching.

3.3 SUBSTRATE SURFACE NEUTRALIZATION LAYER

It became clear that neutralization of both interfaces is paramount to achieving vertical orientation. The substrate interface can be neutralized by spin-coating a mat which has a surface energy equally favorable to both blocks[9, 56]. This should result in the desired perpendicular orientation; however, a preferential mat would lead to parallel orientation.

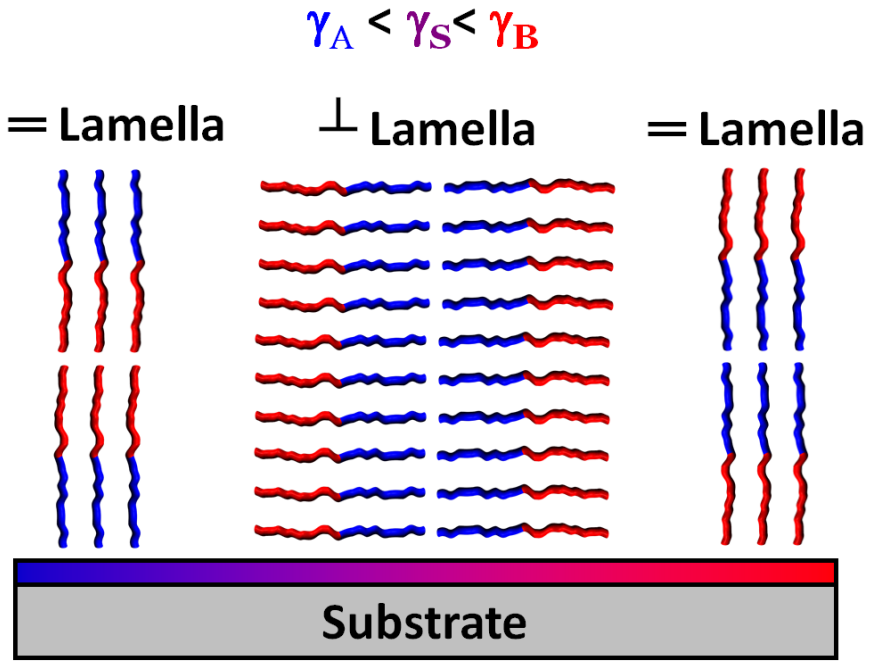

Figure 13: Surface Alignment Theory

The mat must be cross-linked so it does not dissolve or diffuse into the block copolymer when the block copolymer is spin-coated on top of the mat. Two mat structures were proposed to serve as effective neutralization layers: a series of polymers with the same backbone structure but a single varying substituent[44] and a random copolymer of the same materials as the block[9, 41, 57]. All of these polymers have a small amount of cross-linking agent incorporated into them. By varying the substituent on the first class of polymers, the surface energy of the polymer may be altered until it is ideal for a given

block copolymer. The random copolymer contains the same materials as the block copolymer so the surface energy should be similar. The specific block copolymer studied in this research is 67% PS and 33% PMTMSMA by mole. Therefore, a random copolymer was synthesized with approximately the same molar composition together with a small amount of the cross-linker poly-4-vinylbenzyl azide (PVBzAz).

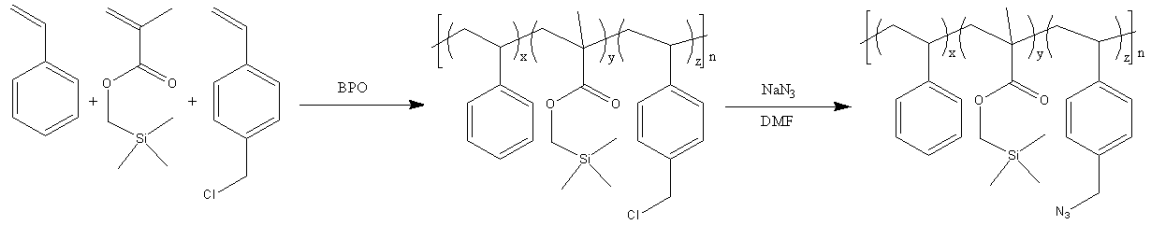

Figure 14: Random Copolymer Synthesis Scheme

Unfortunately, the relative amounts of the monomers added together for polymerization are rarely the relative amounts that end up in the polymer. This is a phenomenon known as "composition drift." Simply stated, a monomer unit at the end of an active polymer chain does not have an equal probability of reacting with all unreacted monomers. However, reaction rate constants (and therefore reactivity ratios) can be determined experimentally or found in the literature that enable the prediction of how much of each starting material (monomers) must be added to a mixture in order to produce the desired ratios in the polymer using correlations like the Mayo-Lewis Equation (two components) or the Alfred-Goldfinger Equation (three components). Since the desired random copolymer is PS-*r*-PMTMSMA-*r*-PVBzCl (the chloride will be converted to the azide in a second reaction), it is necessary to get all of the reactivity ratios for this system and use the Alfred-Goldfinger Equation.

$$\frac{M_1}{M_2} = \frac{m_1 \cdot \left(\frac{m_1}{r_{12} r_{31}} + \frac{m_2}{r_{21} r_{32}} + \frac{m_3}{r_{23} r_{31}} \right) \cdot \left(m_1 + \frac{m_2}{r_{12}} + \frac{m_3}{r_{13}} \right)}{m_2 \cdot \left(\frac{m_1}{r_{12} r_{31}} + \frac{m_2}{r_{12} r_{32}} + \frac{m_3}{r_{13} r_{32}} \right) \cdot \left(m_2 + \frac{m_1}{r_{21}} + \frac{m_3}{r_{23}} \right)}$$

$$\frac{M_1}{M_3} = \frac{m_1 \cdot \left(\frac{m_1}{r_{12} r_{31}} + \frac{m_2}{r_{21} r_{32}} + \frac{m_3}{r_{23} r_{31}} \right) \cdot \left(m_1 + \frac{m_2}{r_{12}} + \frac{m_3}{r_{13}} \right)}{m_3 \cdot \left(\frac{m_1}{r_{13} r_{21}} + \frac{m_2}{r_{12} r_{23}} + \frac{m_3}{r_{13} r_{23}} \right) \cdot \left(m_3 + \frac{m_1}{r_{31}} + \frac{m_2}{r_{32}} \right)}$$

Figure 15: Alfred-Goldfinger Equation

Through a series of experiments, a very talented undergraduate (who is now a graduate student at the University of Minnesota working with Dr. Frank Bates) named Jeffrey Ting calculated these values. The reactivity ratios are $r_{12} = 0.766$, $r_{13} = 0.284$, $r_{21} = 0.402$, $r_{23} = 0.191$, $r_{31} = 0.886$, and $r_{32} = 2.523$ where PS = *1*, PMTMSMA = *2*, and PVBzCl = *3*. A Mathematica® code was used to calculate the monomer values (m_i) for the desired polymer values (M_i) with the given reactivity ratios (r_{jk}).

All monomers were stirred with a 1 g of purifier to 10 g of monomer ratio with both calcium hydride (CaH_2) and basic aluminum oxide (AlO_2) purifiers for one hour. The simplest method to synthesize a random copolymer is with free radical polymerization. An initiator was added to the monomer mixture in order to start the polymerization. Initiators form radicals when heated, which start polymerization via the following general mechanism:

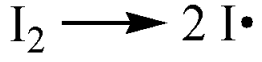

Figure 16: Initiator Mechanism

The initiator for this experiment was benzoyl peroxide (BPO). The amount of initiator added affects the average molecular weight of the polymer chains. For example, adding more initiator will decrease the molecular weight since more sites are available to react with the same amount of monomers, leaving fewer monomers to add to a polymer chain. The kinetic chain length υ (the average number of monomer units reacting with an active radical site) during chain growth polymerization can be calculated with the following equation[43]:

$$\upsilon = \frac{k_p \cdot [M]}{2 \cdot (\eta \cdot k_d \cdot k_t \cdot [I])^{\frac{1}{2}}}$$

where k_p is the polymer propagation constant, k_d is the initiator disassociation constant, k_t is the polymer termination constant, η is the initiator efficiency, [M] is the total concentration of all monomers, and [I] is the initiator concentration. If all reactions end by disproportionation (a radical terminates the living polymer chain), $N = \upsilon$ where N is the degree of polymerization (the number of monomers in a polymer unit or the total molecular weight of a polymer chain divided by the molecular weight of the repeat unit). If all reactions end by coupling (polymer chains terminate by combing), $N = 2 \cdot \upsilon$. Usually, there are both types of terminations so the true value of N is between υ and $2 \cdot \upsilon$. If all of the reaction constants and the efficiency are known, it would be easy to calculate N from the desired polymer chain molecular weight. However, it is difficult to calculate all of these values, and they are only known for very well-studied reactions so no values exist yet in the literature for most new random copolymers. However, the rate constants are a function of temperature only so (assuming the efficiency stays the same) the equation can be arranged to yield:

$$\frac{N \cdot [I]^{\frac{1}{2}}}{[M]} = \text{constant}$$

Note that this works no matter if it assumed that all reactions end is disproportionation ($N = \upsilon$), coupling ($N = 2 \cdot \upsilon$), or something in between as N is always proportional to υ. Therefore, by running a test reaction at a given temperature with a known amount of initiator and monomer and then calculating the degree of polymerization (via the molecular weight from a GPC), it will be easy to calculate the amount of initiator needed to achieve a specific molecular weight in another reaction at the same temperature from the following equation:

$$[I]_2 = [I]_1 \cdot \left(\frac{[M]_2}{[M]_1} \cdot \frac{N_1}{N_2} \right)^2$$

After filtering the purifiers, the monomers are poured into a round-bottom flask with the appropriate amount of initiator and a stir bar. The presence of oxygen would act as an additional catalyst (resulting in a lower the molecular weight) so the solution is either freeze-pump-thawed three times or degased by argon for twenty minutes. Freeze-pump-thawing involves freezing the solution in liquid nitrogen, pumping out all of the oxygen, and then thawing the frozen solution. Doing this three times effectively removes all of the oxygen from the sealed flask. However, by simply placing a needle through the septa and bubbling argon through the solution, the same result may be accomplished faster. The half-life of benzoyl peroxide is one hour at 92 ^{o}C[58]. Therefore, the reaction was run in an oil bath for one hour at 90 ^{o}C. The conversion for the reaction was very low under these conditions (indicated by the solution being mostly liquid at the end). This is done intentionally since during long reaction times, the monomer concentrations will change (due to the composition drift as discussed earlier) leading to polymers with varying compositions.

The polymer is soluble in the monomers so the reaction was run neat (no solvents). Once the reaction is complete, the solution is immediately quenched in an ice

bath to stop further polymerization. The polymer was precipitated from the monomer solution into ten times its volume of methanol. The polymer solution was added drop-wise near the glass of the beaker (where the fluid-flow forces are greatest) containing the non-solvent while stirring vigorously. Next, the polymer was re-dissolved in THF. The polymer is re-precipitated twice more to get rid of any remaining monomer. Finally, the polymer was placed into a small round-bottom flask, dissolved (10 wt% by mass) in benzene, and frozen in liquid nitrogen. The solid solution is quickly placed into a vacuum chamber where the benzene sublimes and is pumped out of the chamber continuously. This process is called lyophilization or "freeze drying." The product is a fluffy, pure solid. NMR and GPC confirm monomer percentages and molecular weight, respectively. To calculate the mole percentages, four equations are needed. Although there are multiple possibilities based on hydrogen positions, four of the easiest formulas are

$$5 \cdot x + 4 \cdot z = a$$
$$9 \cdot y = b$$
$$2 \cdot z = c$$
$$x + y + z = 1$$

where x, y, and z indicate the relative percentages of PS, PMTMSMA, and PVBzCl (respectively) in the random copolymer, and a, b, and c are values obtained from the NMR. The first equation is related to the total number of hydrogens on the carbons in the benzene rings in the compounds. The second equation accounts for the number of hydrogens on the carbons in the trimethylsilyl group. The third equation accounts for the two hydrogens on the benzyl carbon of the PVBzCl. Finally, the fourth equation simply states that all mole fractions must sum to unity. a, b, and c are calculated relative to each other so one value must be specified in the program. Typically, a is equated to nine since there are nine total hydrogens on the benzene rings. However, now the equations must be altered by using ratios to get three new linearly independent equations. The following is

one example of a typical rearrangement; however, as before there are multiple possibilities.

$$\frac{5 \cdot x + 4 \cdot z}{9 \cdot y} = \frac{a}{b}$$
$$\frac{9 \cdot y}{2 \cdot z} = \frac{b}{c}$$
$$x + y + z = 1$$

Now, three linearly independent equations contain three unknowns and may easily be solved.

The next step was to convert the PVBzCl to PVBzAz by reacting the random copolymer with sodium azide (NaN_3) overnight in DMF solution. An important safety note: NaN_3 readily reacts with metals resulting in a violent explosion. Never work alone and use a plastic spatula to scoop out the NaN_3. A six times molar excess NaN_3 was suggested for complete conversion. The final product was precipitated and purified using the same methods as before. A final NMR showed a peak shift form chloride to azide at around 4.3 ppm.

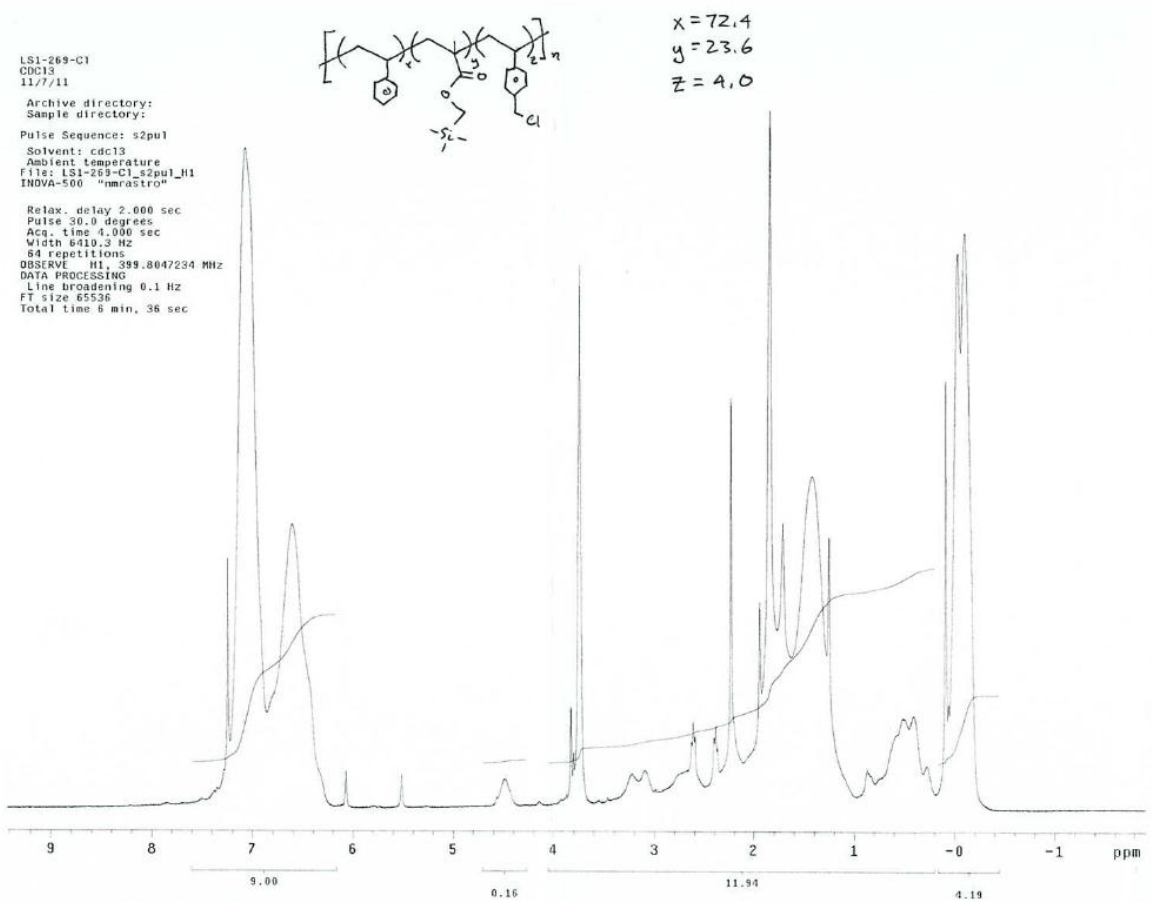

Figure 17: NMR of P(S-*r*-MTMSMA-*r*-VBzCl)

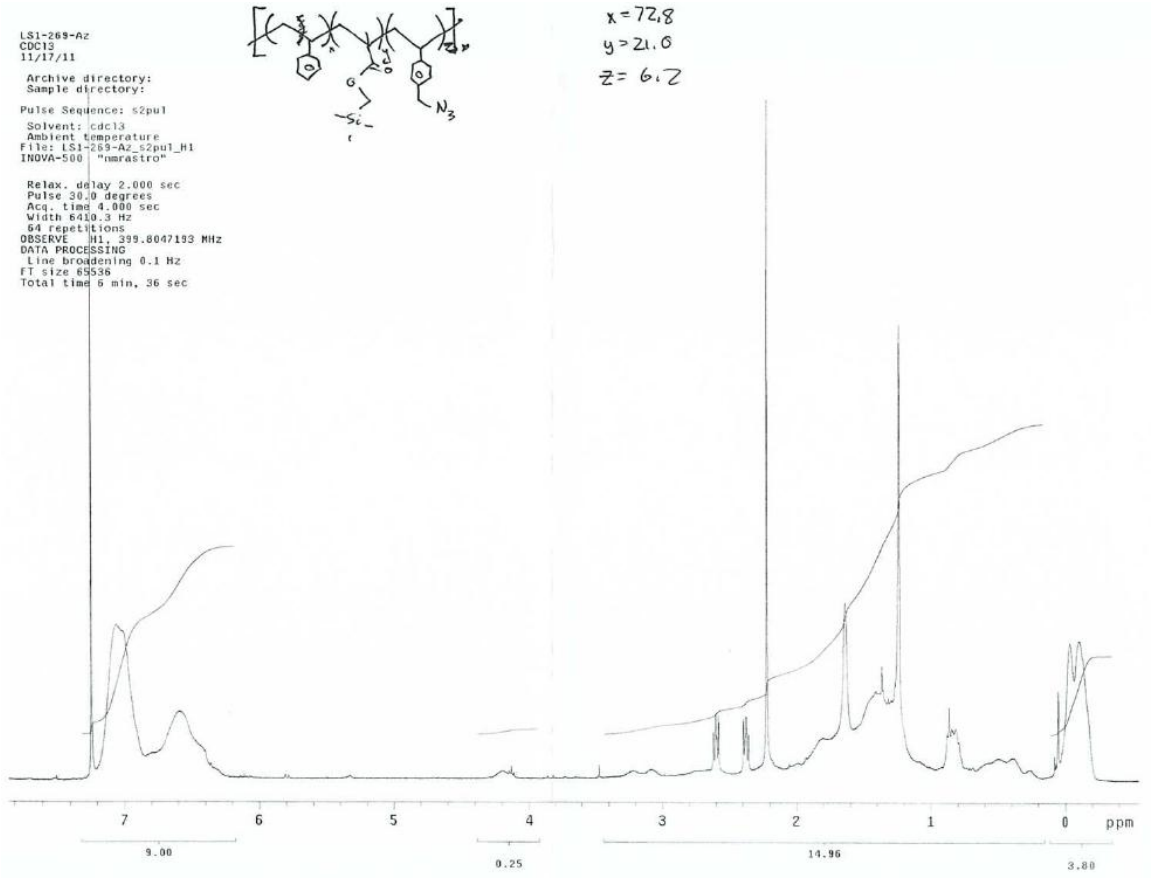

Figure 18: NMR of P(S-*r*-MTMSMA-*r*-VBzAz)

For this polymer, $a = 9.00$, $b = 0.25$, and $c = 3.80$ since the peaks on the left are characteristic of benzene rings, the peak around 4.2 ppm is consistent with benzylic hydrogens, and the peaks near zero are for the trimethylsilyl group which makes sense as tetramethylsilane is a common NMR standard which is set to zero; therefore, $x = 0.728$, $y = 0.210$, and $z = 0.062$. The peaks between zero and 4 ppm are all the rest of the hydrogens not already assigned. This region is typically messy for polymers. The solvent used to dissolve the polymer for the NMR is $CDCl_3$ so a reference peak is at 7.24 ppm.

Once a random copolymer was synthesized with acceptable mole percentages and enough cross-linking agent, it was possible to coat a silicon wafer with the neutralization

layer to provide a coating that was no longer soluble in casting solvents. The random copolymer was cross-linked thermally at 250 ^{o}C for five minutes on a hot plate and then washed twice for two minutes in toluene to remove any non-cross-linked polymer.

3.4 ETCHING

Etching the samples was challenging. It appeared that there was always a wetting layer of what was assumed to be PMTMSMA. In addition, etchers have relatively high etch rates (on the order of nanometers per second). For samples just tens of nanometers thick, a few seconds of etching would etch the entire sample away. In addition, in the first few seconds of etching, there is always a start-up transition which can lead to inconsistent results. Therefore, it was necessary to construct new formulas with much slower etch rates (on the order of nanometers per minute). Etching with oxygen gas volatilizes organic material which is pumped away. However, any silicon is oxidized to silicon dioxide, which forms an impervious layer that does not etch in the oxygen etch process[59].

$$n \cdot (CH_2)_{(s)} + \frac{3}{2} \cdot n \cdot O_{2(g)} \rightarrow n \cdot CO_{2(g)} + n \cdot H_2O_{(g)}$$

$$Si_{(s)} + O_{2(g)} \rightarrow SiO_{2(s)}$$

This leads to very high etch selectivity as predicted earlier. However, if a wetting layer exists, it is necessary to use a fluorine-containing gas, which etches both polymers at about the same rate but has the ability to etch silicon-containing materials.

$$x \cdot (CH_2)_{(s)} + y \cdot F\bullet \rightarrow w \cdot CH_xF_{y(g)} + z \cdot CH_xF_{y(s)}$$

$$Si_{(s)} + n \cdot F\bullet \rightarrow SiF_{n(g)}$$

Therefore, two formulas were required, each with very low etch rates and one with high etch selectivity. There are several etching parameters including: ICP power, RF power, etch gas pressure, temperature, relative gas flow rates, and reactive gas dilution. The dissertation of Dr. Matthew Colburn[59] and the interpretation of Dr. Brandon Rawlings brought great insight into how etchers operate. First, the vacuum chamber

containing the sample is emptied of all gases (Figure 19 - a). After the pressure is low enough, the desired etching gas is introduced into the chamber to the desired pressure (Figure 19 - b). Continuous vacuum is pulled so it takes a few seconds for the pressure and flow rates to equilibrate. Once this is achieved, an alternating potential difference is applied between the upper and lower plates (Figure 19 – c,d). This splits gas molecules into electrons and their corresponding positively-charged ions (Figure 19 - e). The top plate of the etching chamber is connected to a ground. Therefore, its voltage is always zero. However, the bottom plate is connected to the AC source so its voltage oscillates between a positive and a negative value. Therefore, the potential difference between the plates also oscillates between a positive and negative value. The electrons move much faster than the ions and are directed toward the plate that has a more positive charge at the time. Since the voltage oscillations are rapid, the electrons move toward both plates equally (Figure 19 - f); however, the bottom plate has a capacitor which collects the electrons and builds up a negative charge (Figure 19 - g). The positive ions, which move relatively slower, now are attracted to the negatively-charged bottom plate where the sample is located (Figure 19 - h). As the ions are directed downward, they etch the sample.

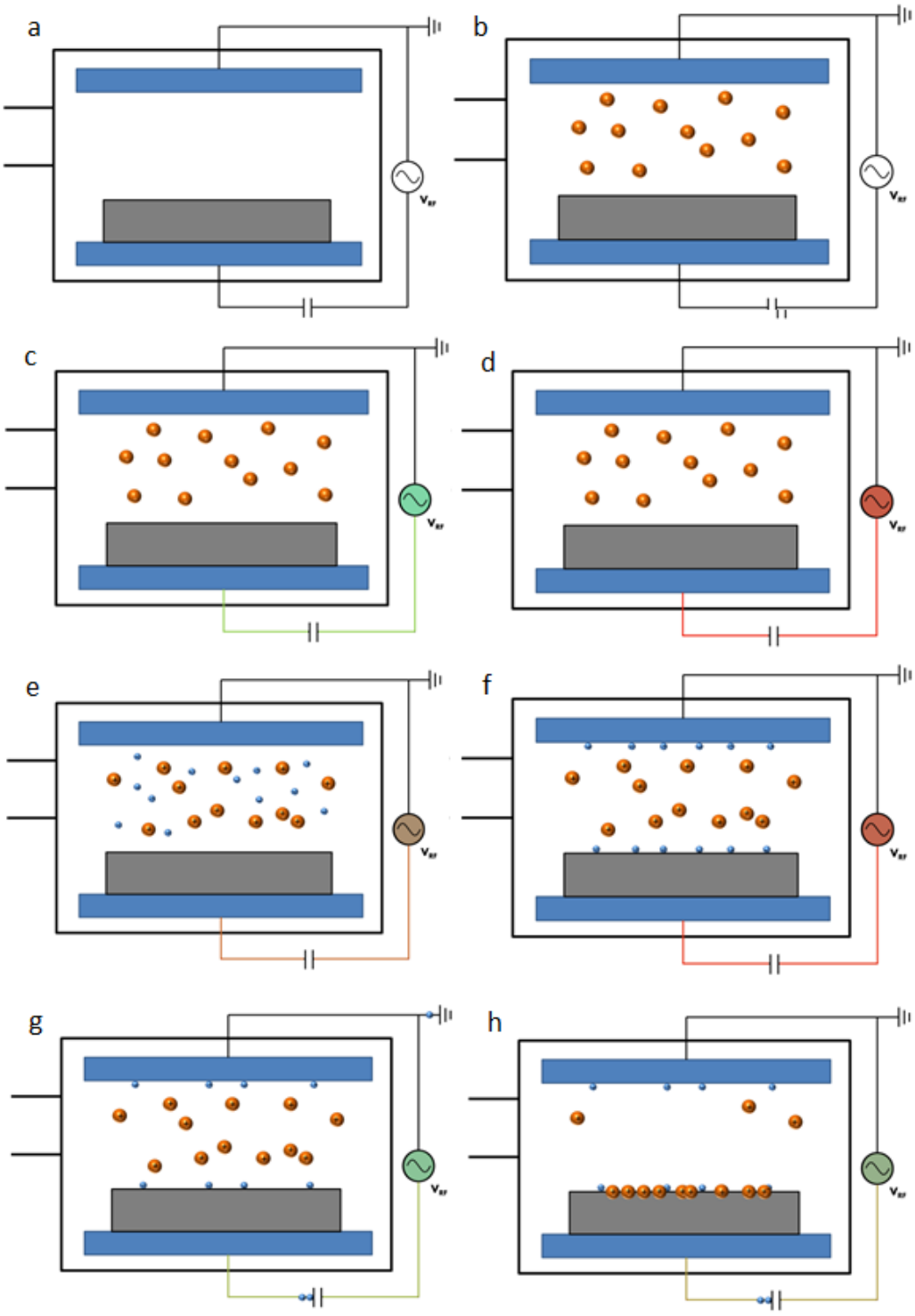

Figure 19: Reactive Ion Etch (RIE) Mechanism

Etching expert Gary Doyle of Molecular Imprints, Inc. provided valuable information on adjusting etching parameters to accomplish the desired goals. He explained that at low pressures, there is not enough gas to etch the sample at a fast rate. At high pressures, there are so many molecules that the mean free path is very small (lots of collisions) so the etch rate is also slow. Etching samples results in the sample becoming hotter. As the sample gets hotter, the etch rates change (usually increase). This leads to etch rates that are not constant with time as well as high etch rates. If it is desired to use a higher pressure with a low flow rate of the reactive gas, it may be difficult to ignite the plasma. By using a diluting gas (like argon or helium), it is possible to decrease the mean free path (slow etch rates) while still igniting the plasma. After receiving this valuable information, several formulas were tested with low and high reactive gas pressures, low plate temperatures, and different dilution percentages.

Table 1: Trion Etcher Formulas

#	**Reactive Gas**	**Flow Rate (sccm)**	**Flow Rate He (sccm)**	**Power (W)**	**Pressure (mtorr)**
1	O_2	5	45	20	50
2	O_2	5	45	20	100
3	O_2	5	45	20	150
4	CF_4	5	45	20	50
5	CF_4	5	45	20	100
6	CF_4	5	45	20	150
7	O_2	5	45	50	50
8	O_2	5	45	50	100
9	O_2	5	45	50	150
10	CF_4	5	45	50	50
11	CF_4	5	45	50	100
12	CF_4	5	45	50	150

The two homopolymers of PS and PMTMSMA were etched in each of the previous etching conditions on the Trion Oracle Etcher at Pickle Research Center. The following charts contain the results of the etching experiments.

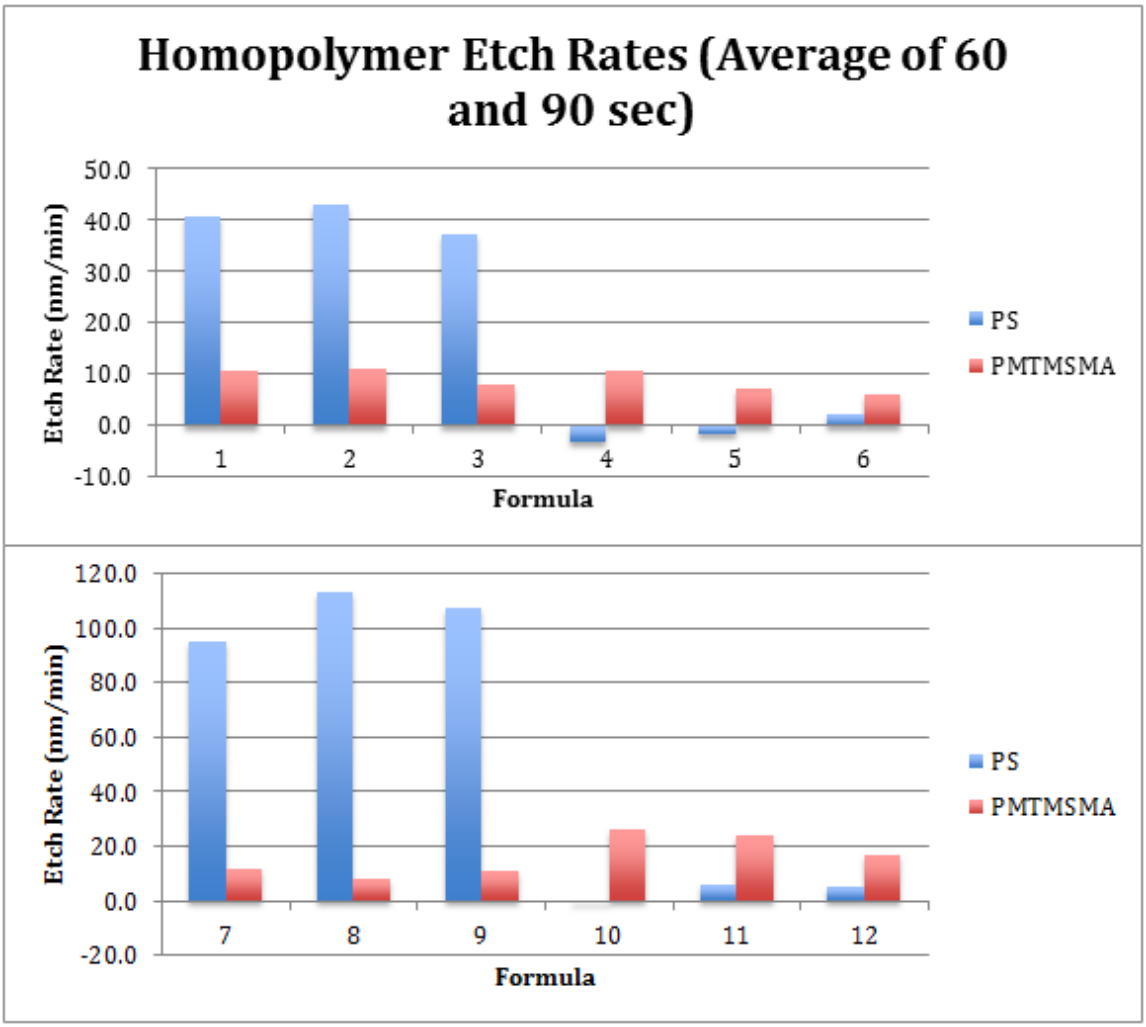

Figure 20: Trion Etcher Etch Rates for Homopolymers

Formulas of oxygen etches #1-3 had much slower flow rates than the oxygen etches #7-9. Of those, the best oxygen etch formula appeared to be formula #2 since it had the highest

selectivity. CF_4 etch #10 was used since, even though it had a higher flow rate, it was still low enough for the present application and had reproducible results. Three thickness measurements on different parts of each sample were averaged when calculating etch rates. Etch rates were also calculated and averaged at sixty and ninety seconds to make sure the etch rates did not change with time.

These studies provided a process that successfully removed the wetting layer and etched away the styrene block as shown below in Figure 21. Please note: the magnification is only pertinent to the screen on which the image was taken. It is no longer valid.

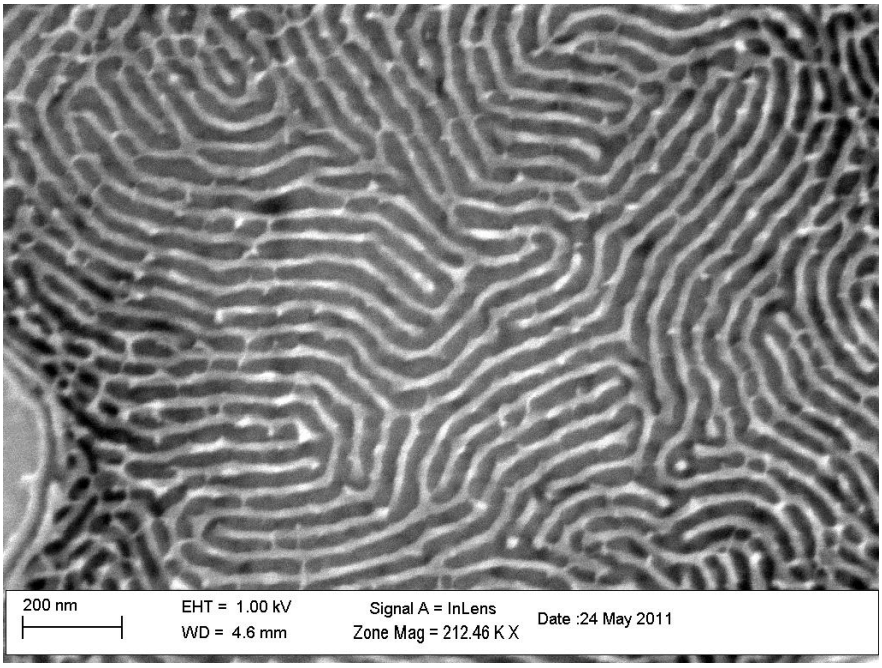

Figure 21: 15 nm CF_4 Etch #10 Followed by 40 nm O_2 Etch #2 of PS-*b*-PMTMSMA

SEMs produce an image from the backscattered electrons from the electron beam striking the sample. Polymers are difficult to image since they are not very conductive. As a result, very few electrons are transferred to the ground so charge builds up across the

sample. This is known as charging and leads to images which are very bright and hard to interpret. Thanks to advice from SEM expert Dr. Dwight Romanovicz, the SEM conditions were optimized for polymer imaging. First, in-lens detection is imperative. Instead of measuring side-scattered electrons, this detection methods records electrons reflected directly back toward the beam. This allows the use of much lower beam voltages (typically less than 1 kV) which means less charging. However, the sample must be very close to the beam (typically working distances less than 5 mm). The polymer samples are held to the metal sample holders with conductive copper tape. This aids in grounding electrons. When taking an image, the best results come by focusing on a dust particle or feature over a smaller area than desired in the final image. After focusing, zoom out, pause the scanning, re-locate to an area that has not been imaged, and do a quick scan. This greatly reduces charging. A typical area size is 2 μm x 2 μm.

3.4 SOLVENT ANNEALING

A solvent annealing study was carried out. The first step was to choose an optimal solvent. The best-known approach is to use solubility parameters to calculate $\chi_{P\text{-}S}$ using the following formula:

$$\chi_{P-S} = \frac{\hat{V}_S \cdot (\delta_S - \delta_P)^2}{\mathrm{R} \cdot T} + 0.34$$

for non-polar systems where $\chi_{P\text{-}S}$ is the polymer-solvent interaction parameter, $\hat{V}_S$ is the molar volume of the solvent, $\delta_{S,P}$ is the solubility parameter of the solvent and polymer respectively, R is the ideal gas constant, and T is the absolute temperature. If $\chi_{P\text{-}S}$ is less than 0.5, the solvent will swell the polymer[35, 54]. Molar volumes of most solvents as well as solvent and polymer solubility parameters can be found in the Polymer Handbook[55]. However, for the new polymer PMTMSMA, not much information is known. In order to

find the solubility parameter, the group contribution method gives a good estimate. According to the following equation:

$$\delta = \frac{\Sigma(F_i)}{\hat{V}_{PMTMSMA}} = \frac{\Sigma(F_i)}{\frac{MW_{PMTMSMA}}{\rho_{PMTMSMA}}} \approx \frac{\Sigma(F_i)}{\frac{MW_{PMTMSMA}}{\rho_{PMMA}}}$$

where F_i is the contribution of group i associated with the PMTMSMA molecule, ρ is the density of the polymer, and MW is the molecular weight of the polymer. Since the density of the new polymer is unknown, it can be approximated using the Fetters[60] value for PMMA. The individual group contribution values are from Small[61] as reported in the Polymer Handbook[55]. This gives an approximate PMTMSMA solubility parameter of 17.4 $MPa^{1/2}$.

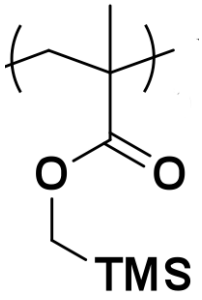

Figure 22: PMTMSMA Molecule

Table 2: Solubility Parameter Estimation with Group Contribution Method

Group	**F ($MPa^{1/2}*cm^3/mol$)**	**# of Groups per Molecule**	**Total F ($MPa^{1/2}*cm^3/mol$)**
-CH3	437	4	1748
-CH2-	272	2	544
=C=	-190	1	-190
=Si=	-77	1	-77
-COO-	634	1	634
		Total F (ΣF_i)	2659

$$\delta = \frac{\Sigma(F_i)}{\frac{MW_{PMTMSMA}}{\rho_{PMMA}}} = \frac{2659 \frac{\mathrm{MPa}^{\frac{1}{2}} \cdot \mathrm{cm}^3}{\mathrm{mol}}}{\frac{172.37 \frac{\mathrm{g}}{\mathrm{mol}}}{1.13 \frac{\mathrm{g}}{\mathrm{cm}^3}}} = 17.4\,\mathrm{MPa}^{\frac{1}{2}}$$

At the time, it was reported that some groups achieved different features using selective and non-selective solvents[4, 10, 12, 15-16, 54]. A perfectly selective solvent swells one block while not swelling another block. A perfectly non-selective solvent swells both blocks equally. In the Schwartz case, perpendicular features resulted from selective solvent annealing while parallel features formed during non-selective solvent annealing[4]. Therefore, a solvent was selected with $\chi_{A\text{-}S} > 0.5$ (polymer *A* does not swell in the presence of solvent *S*), $\chi_{B\text{-}S} < 0.5$ (polymer *B* swells in the presence of solvent *S*), and a big $\Delta\chi_{P\text{-}S} = \chi_{A\text{-}S} - \chi_{B\text{-}S}$ (very selective toward block B). Using the predicted solubility parameter for PMTMSMA and the literature value for PS (18.6 $MPa^{1/2}$), the table below lists these values for many common solvents[55]. The two solvents that fit the criterion are acetone and diethyl ether. These results will be discussed later.

Table 3: Optimal Solvent Selection

Solvent	δ **(MPa$^{1/2}$)**	$\hat{V}_S$ **(cm^3/mol)**	$\chi_{PS\text{-}S}$	$\chi_{PMTMSMA\text{-}S}$	$\Delta\chi$
acetone	20.3	74.1	0.427	0.594	0.167
tetrahydrofuran (THF)	18.6	81.9	0.340	0.388	0.048
cyclohexane	16.8	108.7	0.484	0.356	0.128
toluene	18.2	106.9	0.347	0.368	0.021
methanol	29.7	40.7	2.385	2.851	0.466
benzene	18.8	89.4	0.341	0.411	0.070
ethyl acetate	18.6	98.5	0.340	0.398	0.058
hexane	14.9	131.6	1.075	0.675	0.399
heptane	15.1	146.5	1.072	0.656	0.416
ethylene glycol	29.9	55.8	3.245	3.895	0.650
2-propanol (IPA)	23.5	76.8	1.092	1.505	0.413
diethyl ether	15.8	104.8	0.675	0.449	0.226
dimethyl sulfoxide (DMSO)	26.6	71.3	2.201	2.801	0.600
N,N-dimethylformamide (DMF)	22.7	92.5	0.974	1.399	0.425
2-butanone (MEK)	19.0	90.1	0.346	0.434	0.088
acetonitrile	24.3	52.6	1.037	1.361	0.324
pyridine	21.9	80.9	0.699	1.008	0.309

Over time, confidence in the polymer solvent interaction parameter method began to wane. It is stated that materials with similar solubility parameters will be soluble. Therefore, if a polymer's solubility parameter is similar to that of a solvent, the polymer will swell in the presence of the solvent vapor. However, this is not always the case as some other factors like polarity also affect swelling. It is this researcher's opinion that the best method is to simply swell a polymer in many solvents to develop a profile. Usually, the solubility parameter is a good point around which to select solvents (ones with similar

solubility parameters). This method was tested on the literature value for polystyrene. Several solvents did swell the polymer around 18.6 $MPa^{1/2}$ as predicted; however, some solvents did not swell the polymer even though their solubility parameters were similar to that of polystyrene. Armed with this knowledge, it is now possible to get a better estimate of the solubility parameter of PMTMSMA. The group contribution method's predicted value is 17.4 $MPa^{1/2}$. The swelling apparatus used for these experiments is a simple Teflon chamber with quartz windows that can be placed on an ellipsometer stage. Please see the appendix for a picture.

After correcting for strain-induced birefringence from the windows, aligning the sample, and getting an initial thickness, solvent was dripped around the sample (although the solvent did not contact the sample as it was raised on top of metal washers) and the chamber top was sealed with a glass slide. The swelling could be recorded *in situ* as a function of time. The following are plots of maximum swelling percentage for a polymer in different solvents.

Table 4: Homopolymer Swelling in Various Solvents[55]

PS		
Solvent	**Max Swelling %**	**δ ($MPa^{1/2}$)**
diethyl ether	200	15.1
cyclohexane	190	16.8
cyclopentane	200	17.8
p-xylene	185	18
toluene	170	18.2
tetrahydrofuran	180	18.6
benzene	220	18.8
chloroform	220	19
chlorobenzene	170	19.4
acetone	145	20.3

PMTMSMA		
Solvent	**Max Swelling %**	**δ ($MPa^{1/2}$)**
pentane	220	14.3
hexane	230	14.9
diethyl ether	330	15.1
dodecane	135	16.2
cyclohexane	260	16.8
benzene	235	18.8
acetone	220	20.3

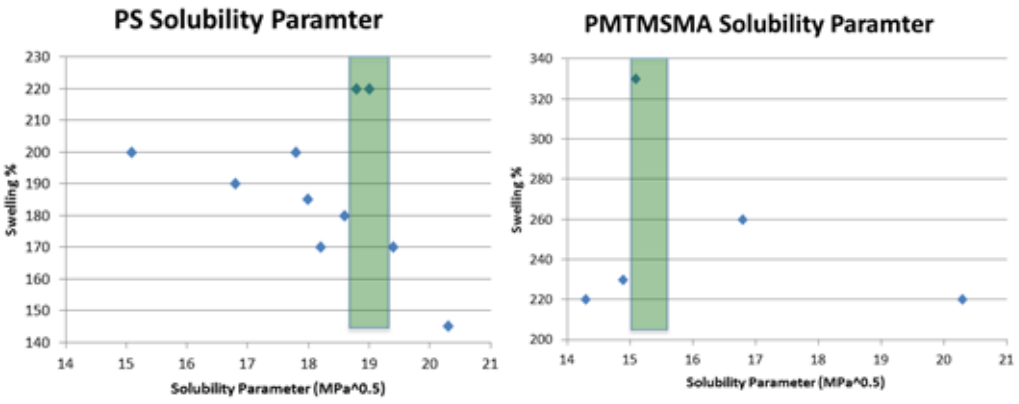

Figure 23: Solubility Parameter Calculation for Homopolymers

This indicates that the solubility parameter of PMTMSMA is closer to 15.3 $MPa^{1/2}$, but the original estimate of 17.4 $MPa^{1/2}$ derived from the group contribution method with approximated values from PMMA was a good estimate.

Neutralizing the air interface is a bit more challenging. Another mat cannot be spin-coated on top of the block copolymer since the casting solvent would wash away the block or allow for inter-diffusion of the mat into the block. The block copolymer cannot be cross-linked before spin-coating like the substrate-interface mat since it would no longer be able to realign. Instead, air can be replaced with another substance to contact the top interface. Solvent annealing utilizes a solvent vapor instead of heat (as in thermal annealing) to effectively plasticize the polymer, which imparts mobility on the polymer chains allowing them to rearrange[16]. Since all compounds have different surface energies, different solvents or combinations of solvents can be tested to find one with a favorable surface energy match.

Solvent annealing actually changes the polymer's location on the phase diagram in two ways. First, by swelling both blocks, the volume fraction of the blocks is likely to change. This is particularly true when using a selective solvent. This will shift the block copolymer horizontally on the phase diagram. As a result, a wide variety of structures can be obtained from the same starting sample[5, 10, 15-18]. Swelling the different blocks with the same solvent results in the blocks becoming more and more similar to each other. This should decrease χ resulting in a downward shift on the phase diagram[62]. If this is the case, there is a danger that too much solvent swelling could result in the polymer becoming disordered as rapid solvent evaporation would result in a disordered, undesirable sample.

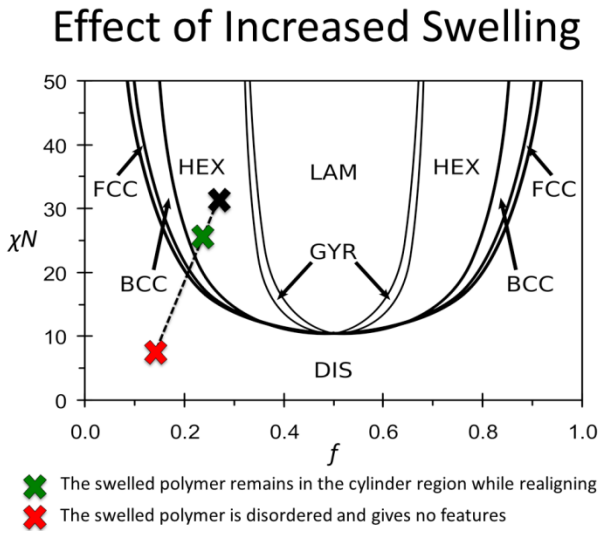

Figure 24: Swelling of an Ordered Block Copolymer

However, there is a threshold value to which a polymer must be sufficiently swelled to achieve a T_g below room temperature. This means that there is a set range of swelling percentages in which to operate. For this, an apparatus is required that can control the vapor pressure of the solvent in its chamber. Therefore, the design for the custom oven (introduced earlier) was altered to include an input port for a solvent flask. By controlling the temperature of the liquid in the flask, the vapor pressure in the annealing chamber could be altered resulting in different swelling thicknesses. The vapor pressures of solvents can be predicted using the Clausius-Clapeyron Equation:

$$\ln\left(\frac{P_2}{P_1}\right) = \frac{-\Delta H_V}{\mathrm{R}} \cdot \left(\frac{1}{T_2} - \frac{1}{T_1}\right)$$

where P is the vapor pressure, ΔH_v is the latent heat of vaporization of the substance, R is the ideal gas constant, and T is the absolute temperature. By simply looking up the latent heat of vaporization for the solvent and a known pressure at a respective temperature (usually room temperature), it is possible to calculate the vapor pressure at any other

temperature. This information is usually found on a material safety data sheet (MSDS). Figure 25 below is an example of typical vapor pressure curves.

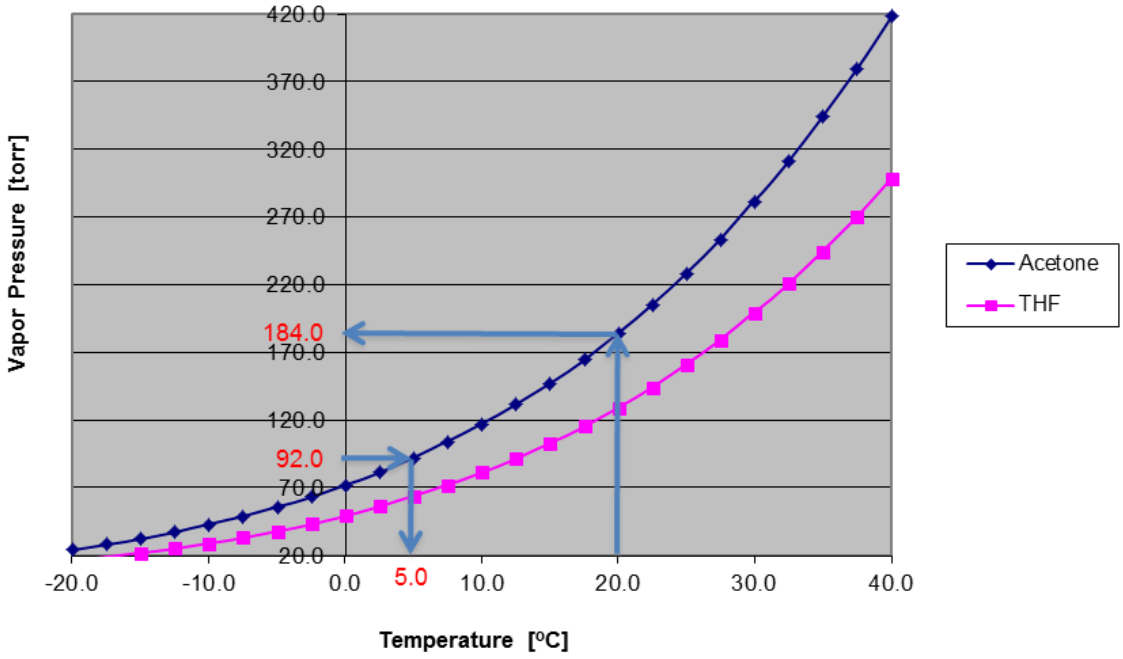

Figure 25: Clausius-Clapeyron Demonstration

In Figure 25, the vapor pressure of acetone at room temperature (20 ^{o}C) is 184 torr. To get half that vapor pressure, it is necessary to cool the system to 5 ^{o}C. At this lower temperature, it is more difficult for the fluid particles to gather the energy to enter the vapor phase; therefore, the vapor pressure is less.

Since the process would involve flammable solvents and altering vapor pressures, it was necessary to do some safety calculations. Taking out one leg of the "fire triangle" can eliminate the potential for fires and explosions. In order for such disasters to occur, three things must be present: fuel (the solvent vapor), oxygen, and an ignition source. A slightly less known term is "flammability limits." If the volumetric percentage of gas is below the lower flammability limit (LFL), there is not enough fuel present to ignite the

gas. If the volumetric percentage of gas is above the upper flammability limit (UFL), there is not enough oxygen present to ignite the gas. Between these two values, the gas may readily ignite. These values are also easily accessible in a MSDS. Therefore, by approximating that any gases act as ideal gases at these lower pressures, an equation was created for quick pressure limits for the system. $P_{tot} \cdot V_{tot} = n_{tot} \cdot \mathrm{R} \cdot T$ for an ideal gas where "*tot*" indicates a total value, and $P_i \cdot V_{tot} = n_i \cdot \mathrm{R} \cdot T \approx P_{tot} \cdot V_i = P_{tot} \cdot \left(z_i \cdot V_{tot}\right)$ where "*i*" indicates a partial value so V_i is the "partial volume" of a gas in the solvent/air mixture and z_i is the volume fraction of that gas. Therefore, $P_i \approx z_i \cdot P_{tot}$. The worry is that after the solvent vapor is introduced into the system, air might leak in and put the solvent in the flammable range. This limit is the upper flammability limit. Therefore, by rearranging the last equation:

$$P_{tot} \approx \frac{P_i}{z_i} = \frac{P^{vap}(T)}{UFL}$$

where P_{tot} is the maximum pressure that can be read from the pressure transducer before the solvent-air mixture is flammable, P_i is the vapor pressure of the solvent at the operating temperature T [aka $P^{vap}(T)$], and z_i is the upper flammability limit (UFL). The following table gives critical values for some common solvents using the formula.

Table 5: Sample Critical Pressure Calculations

Solvent	**UFL (vol %)**	**P^{vap}(20°C) (torr)**	**P_{tot} (torr)**	**Risk**
acetone	12.8	184	1440	Very Low
tetrahydrofuran	11.8	129	1090	Very Low
cyclohexane	8.0	95	1190	Very Low
toluene	7.1	22	310	Mild

With these design criteria in mind, the oven was designed and built. In order to make sure the oven would reach the desired 250 °C, a simple heat balance was performed to see

how many and what power cartridge heaters were needed. Please see the appendix for pictures and the design plans.

The general heat equation derived from Fourier's Law is

$$q = -k \cdot \nabla T = \frac{\dot{Q}}{A}$$

for conductive heat flow where q is the heat flux (energy per time per area) across a boundary, k is the thermal conductivity, ∇T is the gradient of the temperature, $\dot{Q}$ is the heat flow, and A is the cross-sectional area across which heat flows.

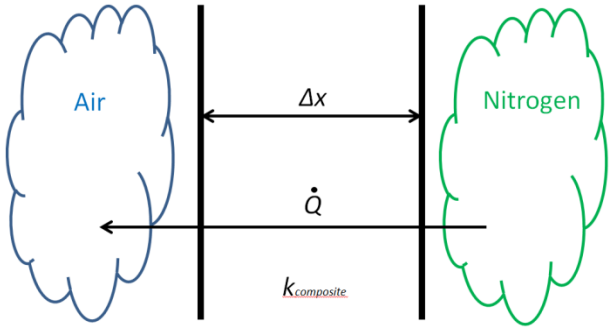

Figure 26: Conduction Approximation

By rearranging the previous equation, approximating the total k of the insulation and metal walls, and approximating with one-dimensional heat flow:

$$\dot{Q} = A \cdot k \cdot \frac{T_{oven} - T_{air}}{\Delta x} = \left[2 \cdot (10 \cdot 10) + 4 \cdot (10 \cdot 4.75)\right] \text{in}^2 \cdot \left(0.1 \frac{\text{W}}{\text{m} \cdot \text{K}}\right) \cdot \left(\frac{(250 - 25)\,\text{K}}{1\,\text{in} \cdot \frac{1\,\text{m}}{39.37\,\text{in}}}\right) = 225\,\text{W}$$

Finally, it was assumed that approximately half the heat would be lost through the aluminum block which served as the base of the oven. This means the total power required is 450 W; therefore, three 200 W cartridge heaters were required.

In order to reduce the cooling time after thermal annealing, the material of the base plate containing the cartridge heaters was made of aluminum, which has a high heat

transfer coefficient so it cools much more quickly. This reduced cooling time from seven or eight hours to about an hour. For example, the oven cooled from 250 ^{o}C to room temperature in 83 minutes. The base plate also contains the thermocouple so it was necessary to calibrate the oven to get the temperature of the top of the plate where the samples would rest. The walls are padded with glass wool insulation. The gasket on the door is a silicon rubber which can withstand temperatures up to 260 ^{o}C but deforms in some solvents making it difficult to hold vacuum. There are four essential and one backup ports: one for pulling vacuum, one for connecting the solvent flask, one for the pressure transducer, and one for a purge line. The purge line performs the dual tasks of diluting the oxygen in the chamber before annealing and re-pressurizing the chamber after the annealing process is complete. A typical solvent annealing procedure consists of the following steps:

1) Freeze-pump-thaw a solvent three times in a flask to remove air.
2) Put the flask in the temperature bath and connect the flask to the chamber via Swagelok fittings.
3) Prepare a solvent trap to collect the solvent after the experiment is over.
4) Insert the samples, close the door, tighten the lock, and pull vacuum on the system.
5) Purge the chamber with nitrogen gas three times to remove oxygen.
6) After the final purge, open the solvent flask to the chamber and anneal.
7) After annealing, close the flask and pump out the solvent.
8) Re-pressurize the chamber in order to open the door.

It is very important for safety to have a solvent trap. If solvent enters the pump, it could result in pump damage or an explosion.

The first solvent for testing in the new oven was tetrahydrofuran (THF) at room temperature on the silicon-containing block copolymer PS-*b*-PMTMSMA at various thicknesses for four hours. The following are height, amplitude, and phase (respectively) atomic force microscopy (AFM) images of the first samples.

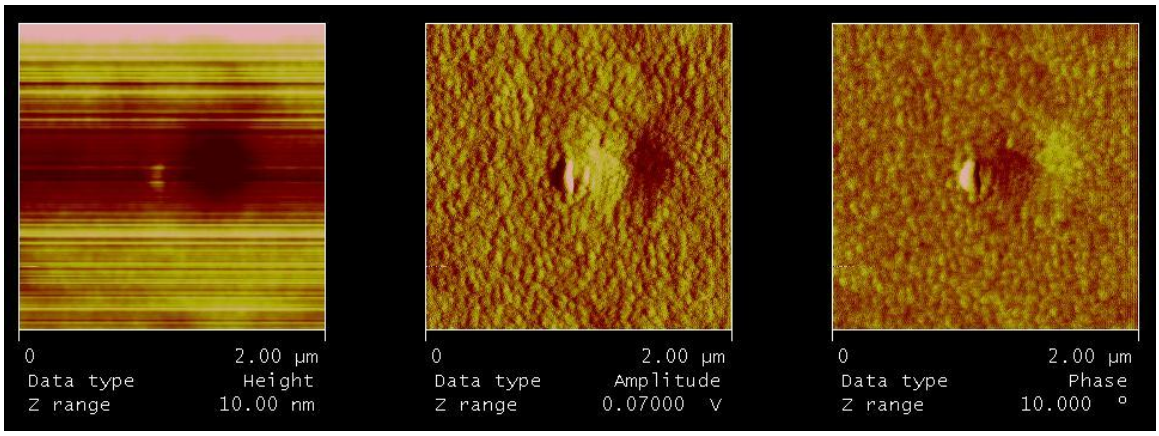

Figure 27: PS-*b*-PMTMSMA which is 20 nm thick in THF for Four Hours at Room Temperature in Solvent Annealing Oven

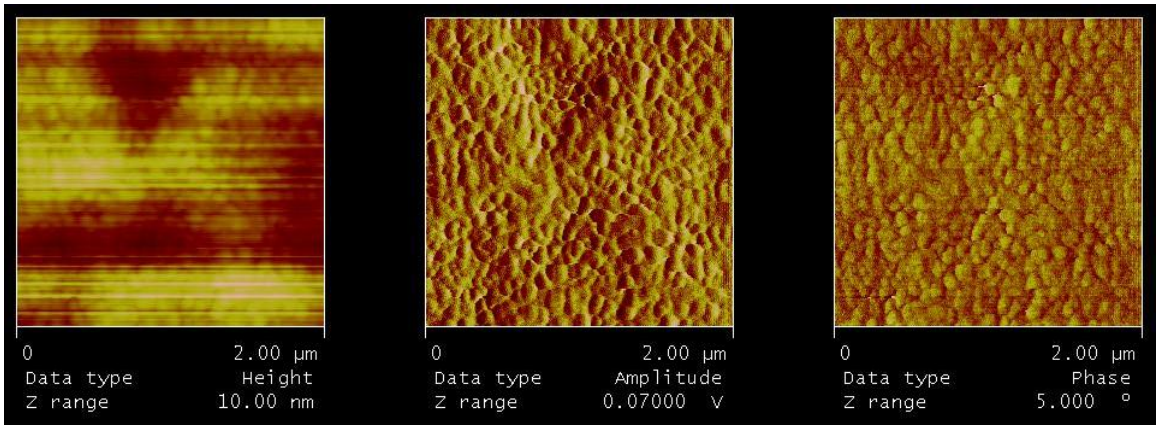

Figure 28: PS-*b*-PMTMSMA which is 30 nm thick in THF for Four Hours at Room Temperature in Solvent Annealing Oven

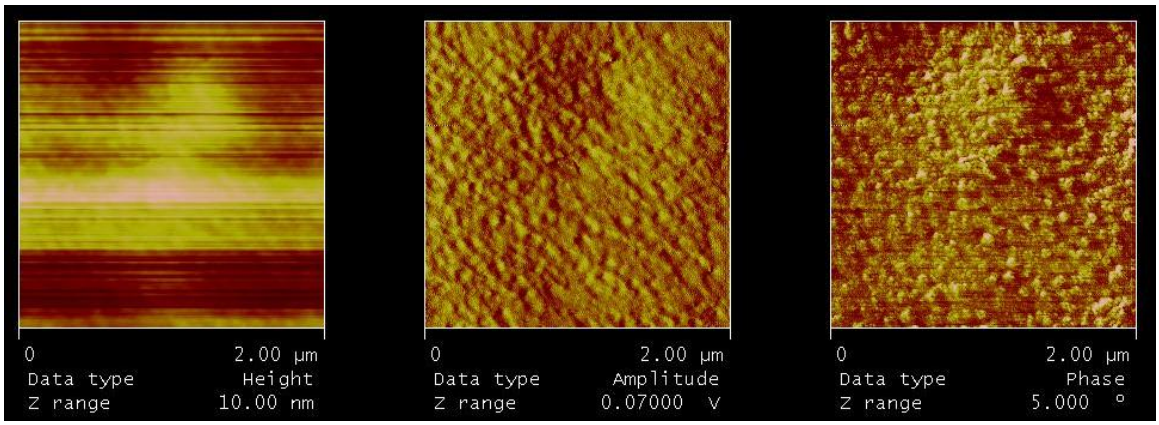

Figure 29: PS-*b*-PMTMSMA which is 40 nm thick in THF for Four Hours at Room Temperature in Solvent Annealing Oven

It is difficult to tell if any features have formed. One possible interpretation is that the cylinder domains are swollen. In addition, most of the sample dewet from the wafer. Both of these observations supported swelling at a lower vapor pressure.

Another common solvent used in the literature is acetone. For the second set of experiments, acetone was used to swell the block copolymer to various thicknesses at room temperature for around one hour. The following are height, amplitude, and phase (respectively) AFM images of those samples.

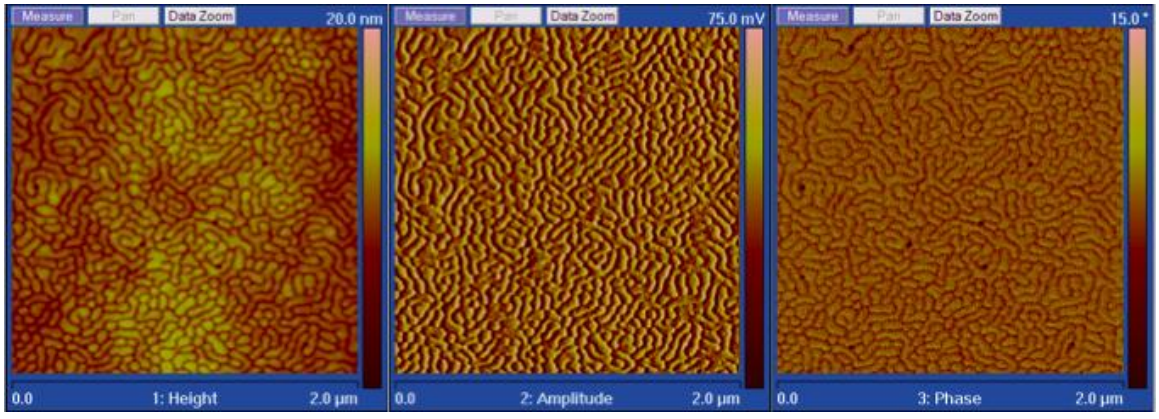

Figure 30: PS-*b*-PMTMSMA which is 30 nm thick in Acetone for One Hour at Room Temperature in Solvent Annealing Oven

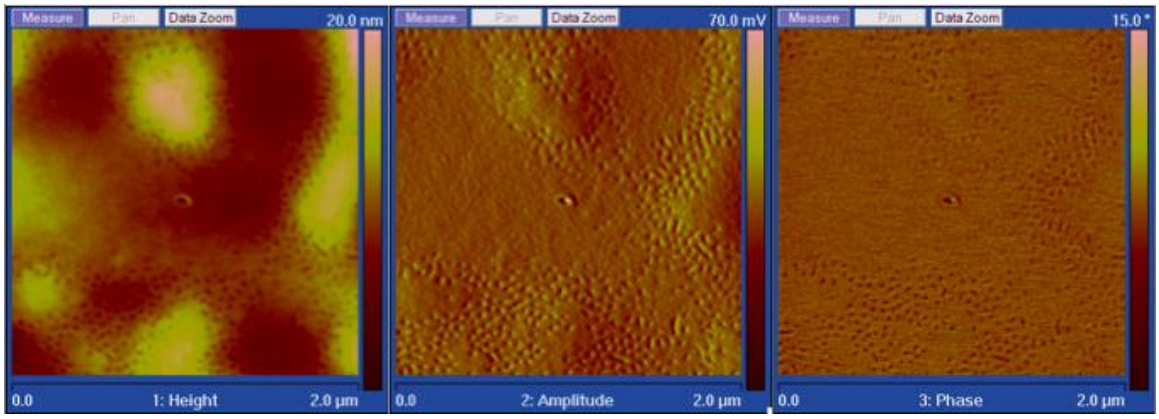

Figure 31: PS-*b*-PMTMSMA which is 46.5 nm thick in Acetone for 0.75 Hour at Room Temperature in Solvent Annealing Oven

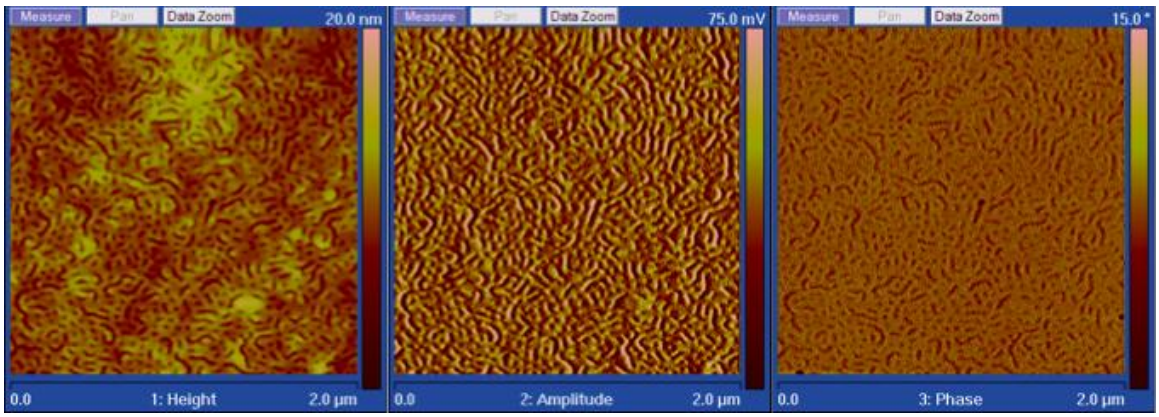

Figure 32: PS-*b*-PMTMSMA which is 70 nm thick in Acetone for One Hour at Room Temperature in Solvent Annealing Oven

Clear ordering is evident in all three AFM images. In Figure 30, PMTMSMA cylinders (darker color) are laying parallel to the substrate. In Figure 31, dark spots can be seen indicating that the cylinders are starting to align perpendicular to the substrate which is the ultimate goal. However, the dots do not appear to be hexagonally packed and only appear at scattered patches. Finally, in Figure 32, a mixture of parallel and perpendicular cylinders is observed. Interestingly, the only major difference in annealing

conditions was the thickness to which the block copolymer was spun-coat. This would indicate that thickness may be a factor in achieving different orientations.

Acetone annealing under these conditions gave alignment but also had significant dewetting. These AFM images were collected from a few select spots. According to the $\chi_{P\text{-}S}$ studies mentioned earlier, the two solvents that would theoretically work best were acetone and diethyl ether. Therefore, a series of studies were conducted with diethyl ether. The following are height, amplitude, and phase (respectively) AFM images of those samples.

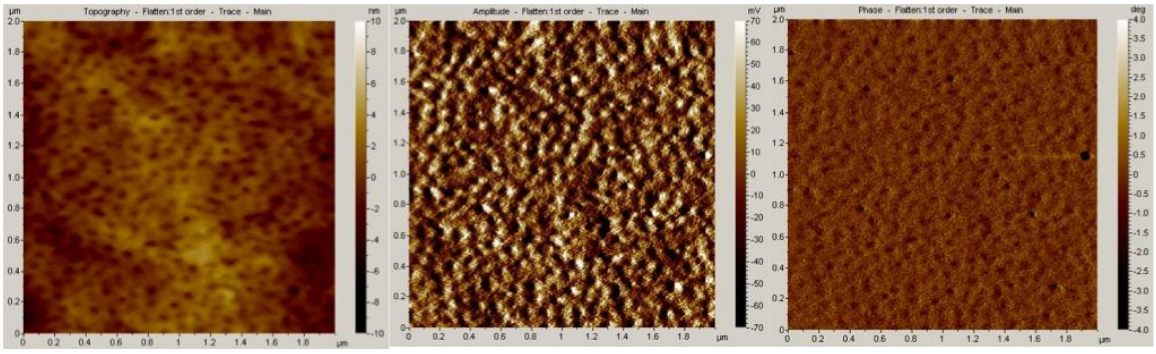

Figure 33: PS-*b*-PMTMSMA which is 20 nm thick in Diethyl Ether for 0.5 h at Room Temperature in Solvent Annealing Oven

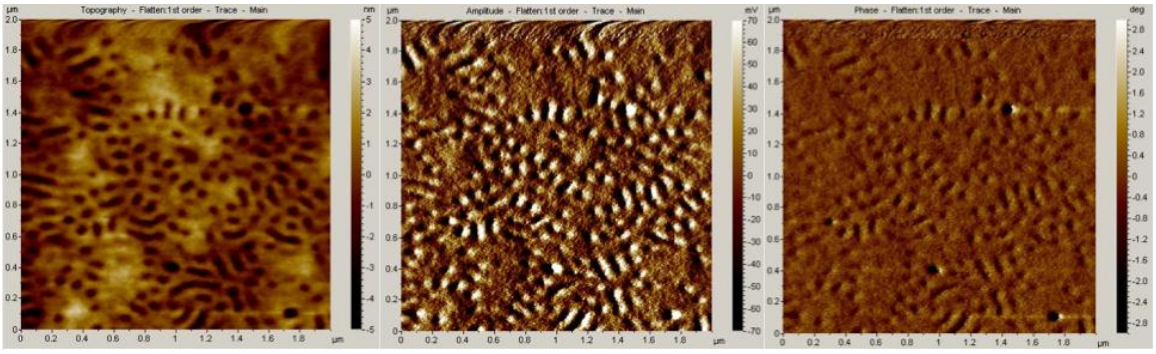

Figure 34: PS-*b*-PMTMSMA which is 30 nm thick in Diethyl Ether for 0.5 h at Room Temperature in Solvent Annealing Oven

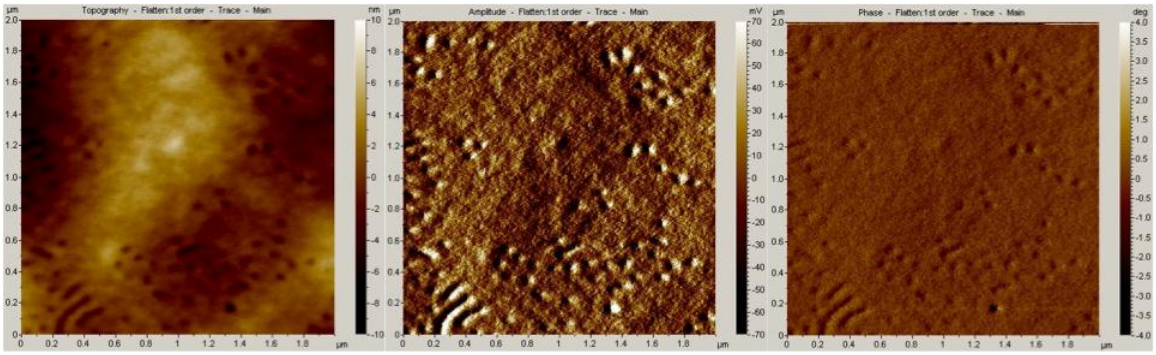

Figure 35: PS-*b*-PMTMSMA which is 40 nm thick in Diethyl Ether for 0.5 h at Room Temperature in Solvent Annealing Oven

Ordering is observed at all three thicknesses. At 20 nm in Figure 33, it appears to be mostly cylinders of PMTMSMA (dark spots) aligned perpendicular to the surface. For Figure 34 and Figure 35, both parallel (dark lines) and perpendicular orientations exist. Once again, thickness is the only varying factor.

With these results in hand, the two solvents acetone and diethyl ether were tested to see if the results agree with the $\chi_{P\text{-}S}$ prediction. According to the predictions, acetone should swell PS more than PMTMSMA ($\chi_{PS\text{-}S} < 0.5 < \chi_{PMTMSMA\text{-}S}$) while diethyl ether should swell PMTMSMA more ($\chi_{PMTMSMA\text{-}S} < 0.5 < \chi_{PS\text{-}S}$). The following graphs are the homopolymer swelling studies performed in the crude Teflon swelling apparatus.

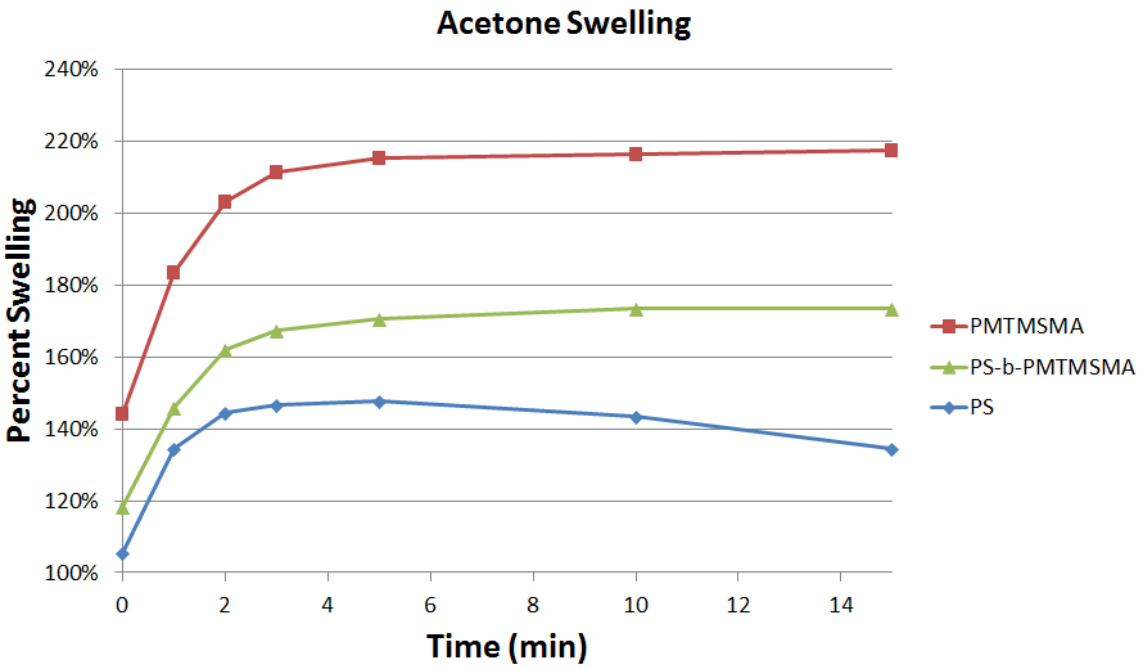

Figure 36: Homopolymer Swelling in Acetone

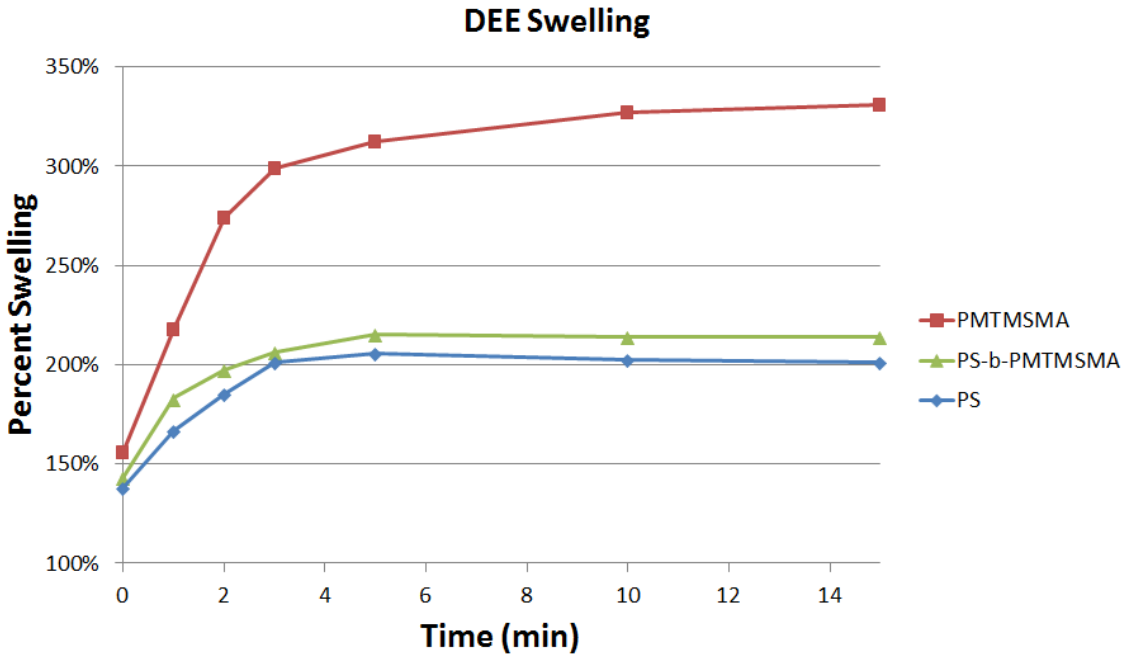

Figure 37: Homopolymer Swelling in Diethyl Ether

As predicted, the diethyl ether swelled PMTMSMA much more than PS. However, acetone showed the same trend. In both solvents, the PMTMSMA swelled to a much greater percentage of its original thickness than did the PS. As a result, confidence in the $\chi_{P\text{-}S}$ method began to wane. On a side note, most of the swelling occurred within the first five minutes of exposure. Also, the polymers returned to their original thicknesses within a second of removing the glass slide, destroying the saturated environment.

3.5 TARGETING SWELLING THICKNESSES

Dewetting was always discouraging, especially in the longer runs, as a lot of time was consumed and no useful data resulted. It would be advantageous if the sample were visible during the run. In addition, papers were starting to report that swelling thickness is key to achieving alignment[2, 15, 29, 40, 63-65]. The equilibrium period of a block copolymer (L_o) is the length of two block copolymer chains back-to-back in the ordered state[35].

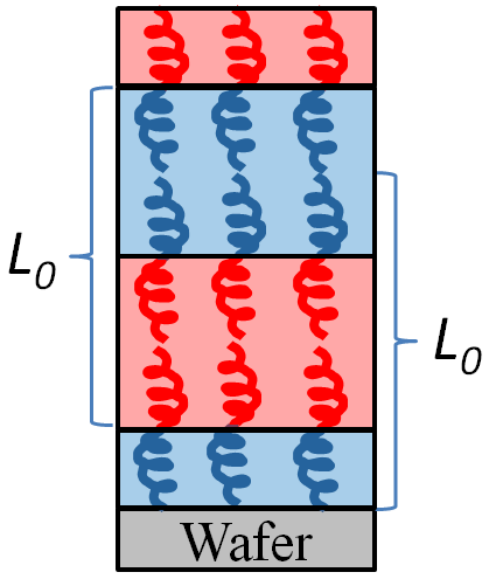

Figure 38: Definition of the Equilibrium Period

Different conformations can be achieved by swelling the block copolymer to multiple values of the equilibrium period. Of particular interest are commensurate ($D = n \cdot L_0$) and incommensurate $\left[D = \left(n + \frac{1}{2} \right) \cdot L_0 \right]$ thicknesses. Some papers had reported vertical alignment at commensurate values while others argued in favor of incommensurate values. To understand the possible cases, a model was studied.

In 1976, Helfand[66] postulated that the free energy of an unconfined block copolymer in the bulk is a balance between enthalpic and entropic components. Enthalpically, the two blocks do not want to be in contact with each other so they phase-separate to minimize the contact area between the blocks. As this occurs, there is an entropic penalty as the structure is becoming more ordered. At equilibrium, the forces balance at a minimum free energy.

$$\Delta G = \Delta H - T \cdot \Delta S$$

Helfand suspected that the equation for free energy in the bulk of a lamellar structure in the strong-segregation limit would be a function of both the degree of polymerization (N) and the lamellae period (L) of the following form:

$$F = \mathrm{c}_1 \cdot \left(\frac{N}{L} \right) + \mathrm{c}_2 \cdot \left(\frac{L}{N^{\frac{1}{2}}} \right)^{\omega}$$

where F is the bulk free energy and c_1, c_2, and ω are constants.

In 1986, Ohta[67] confirmed Helfand's predictions by solving for the constants. For the enthalpic term, the excess energy per molecule is

$$E_H = \frac{\sigma \cdot D^2 \cdot \frac{2 \cdot D}{L}}{\zeta}$$

where E_H is the enthalpic contribution to the free energy per molecule, σ is the interfacial energy per area of interface, D is the length of the block copolymer segment, and ζ is the

number of molecules. This only applies to a cubic structure of length D so the area is D^2 and the number of interfaces is 2*D/L.

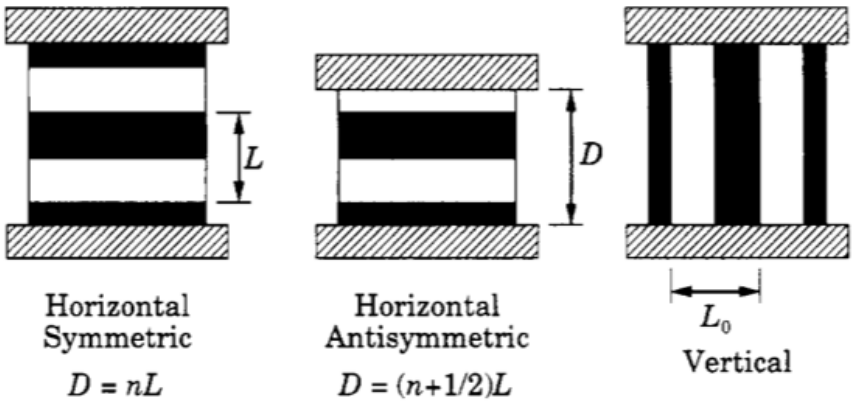

Figure 39: Defining D, L, and L_o[68]

For the entropic term, the end-to-end distribution for a Gaussian chain is

$$Q(r,N) = e^{-\frac{3 \cdot r^2}{2 \cdot N \cdot a^2}}$$

where r is the distance between two endpoints and a is the Kuhn statistical length. For the lamellar structure, $r = \frac{L}{2}$ and $E_S = \ln[Q(r,N)]$ therefore

$$E_S = -\frac{3 \cdot L^2}{8 \cdot N \cdot a^2}$$

In 1994, Walton[68] related the interfacial energy per area of interface (σ) to the Flory-Huggins interaction parameter (χ) so

$$\frac{F}{k \cdot T} = E_H + E_S = 2 \cdot \zeta \cdot a \cdot \sqrt{\frac{\chi}{6}} \cdot \left(\frac{N}{L}\right) + \frac{3 \cdot \zeta}{8 \cdot a^2}\left(\frac{L}{N^{\frac{1}{2}}}\right)^2$$

which is indeed the form predicted by Helfand. The equilibrium free energy (F_o) is obtained simply by taking the derivative of the free energy with respect to L to solve for the equilibrium lamellae period (L_o).

$$\frac{dF}{dL} = -2 \cdot \zeta \cdot a \cdot \sqrt{\frac{\chi}{6}} \cdot \left(\frac{N}{L_0^{\,2}} \right) + \frac{3 \cdot \zeta}{4 \cdot a^2} \cdot \frac{L_0}{N} = 0$$

$$\Rightarrow L_0 = 2 \cdot a \cdot N^{\frac{2}{3}} \cdot \left(\frac{1}{3} \cdot \sqrt{\frac{\chi}{6}} \right)^{\frac{1}{3}}$$

$$\Rightarrow \frac{F_0}{k \cdot T} = \frac{3}{2} \cdot \zeta \cdot N^{\frac{1}{3}} \cdot \left(\frac{\chi}{2} \right)^{\frac{1}{3}}$$

In 1992, Turner[69] developed a model to predict how the free energy would change when the block copolymer was confined between two parallel plates. Turner stated that

$$\frac{F_h}{F_0} = \frac{1}{3} \left\{ \lambda^2 + \frac{2}{\lambda} + \frac{1}{n \cdot \lambda} \left[2 \cdot \Gamma + \delta \cdot \left(\frac{1 - (-1)^{2n}}{2} \right) \right] \right\}$$

where F_h is the free energy of the block copolymer horizontally aligned, $\lambda = L/L_o$, n is the integer number of domain spacings, Γ is the interfacial tension between block A and the substrate (γ_{AS}) / interfacial tension between block A and block B (γ_{AB}), and $\delta = (\gamma_{BS} - \gamma_{AS}) / \gamma_{AB}$ where γ_{BS} is the interfacial tension between block B and the substrate. Turner's model assumes $\gamma_{BS} > \gamma_{AS}$, the block is symmetric in A (A wets both surfaces), the volume fractions of A and B block are equal (50/50), and both plates are the same material. Walton expanded Turner's model to include the cases of asymmetric wetting and plates of different material.

$$\frac{F_h}{F_0} = \frac{1}{3} \left\{ \lambda^2 + \frac{2}{\lambda} + \frac{1}{m \cdot \lambda} \left[\Gamma_1 + \Gamma_2 + \delta_k \cdot \left(\frac{1 - (-1)^{2m}}{2} \right) \right] \right\}$$

Here, $m = n$ for symmetric or m = n + ½ for asymmetric, subscripts *1* and *2* denote the different surface layers, and k is the index of the substrate adjacent to the B block for the asymmetric case. The λ terms account for when the block is stretched or compressed away from its equilibrium value, as this will change the enthalpic and entropic

contributions from their equilibrium values as accounted for in F_o. The Γ terms describe how the plate-block surface interactions affect the free energy. The δ_k term is a way to account for the different symmetries. For a symmetric block copolymer, $m = n$ so the exponent "$2m$" must always be an even number; therefore the δ_k term vanishes. This indicates that either γ_{AS} or γ_{BS} is not a factor in the calculations. This makes sense as the same block is in contact with both interfaces. For the asymmetric case, $m = n + ½$ so the exponent "$2m$" must be an odd number; therefore, the constant term of δ_k reduces to unity. This makes sense as now both γ_{AS} and γ_{BS} play a roll.

Walton further altered Turner's equation to account for vertical alignment of the lamellae. For vertical alignment, the equilibrium length of the block copolymer segment is not perturbed much from its equilibrium position as long as D is not less than $L_o/2$. Therefore, $L \approx L_o$ so $\lambda \approx 1$. Also, both blocks are now touching both substrates (equally for a 50/50 volume fraction) so the δ_k term can be altered to yield

$$\frac{F_v}{F_0} = \frac{1}{3}\left\{3 + \frac{1}{m \cdot \lambda}\left[\left(\Gamma_1 + \frac{\delta_1}{2}\right) + \left(\Gamma_2 + \frac{\delta_2}{2}\right)\right]\right\}$$

With these equations and known values of surface energies for the polymers, it is possible to tell which orientations and symmetries are favored for various surface treatments. The previous equations were analyzed graphically by plotting the free energy of the polymer systems versus the reduced plate separation (related to λ). In each figure, the preferred orientation is indicated by the curve that corresponds to the lowest free energy. All three geometries are calculated for various surface conditions. The following plots were created in MatLAB® using code written by fellow researcher William Durand.

The first case in question is when the block copolymer is annealed thermally directly onto a silicon wafer. The top and substrate interfaces will act as the "plates" in the model. The silicon wafer actually has a thin layer of native silicon dioxide on its

surface. Therefore, this surface is hydrophilic. The trimethylsilyl groups in the block copolymer make it hydrophobic. Therefore, it will not be favorable to wet the wafer surface. This is visually evident when attempting to spin-coat a layer of PMTMSMA homopolymer directly onto a silicon wafer. The block rarely wets the surface and is very non-uniform when it does. This means that PS is preferential to the substrate interface. On the other hand, the silicon atoms in the PMTMSMA favor the low-surface energy air interface so it wets the top interface. In the following graphics, the red block copolymer is PMTMSMA while the blue is PS.

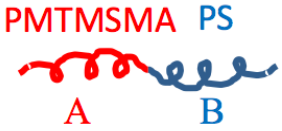

Figure 40: PS-*b*-PMTMSMA Cartoon

The wetting graphics are depicted below.

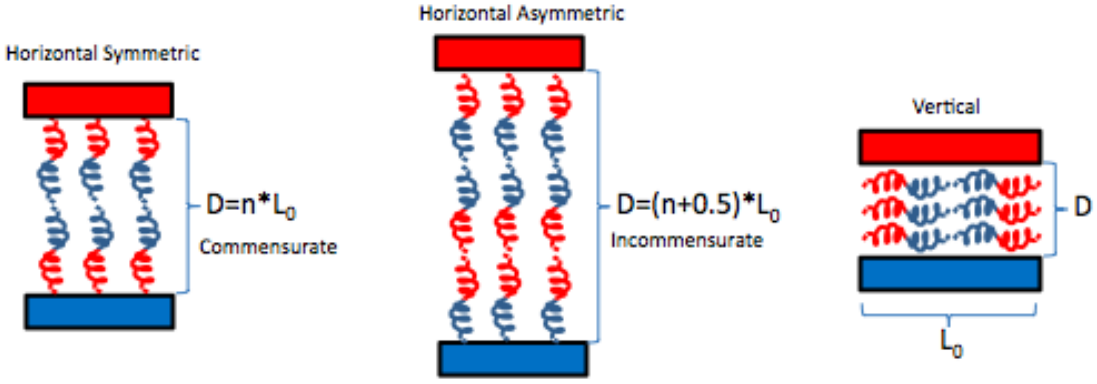

Figure 41: Not Optimized Block Copolymer Wetting Graphics

In the horizontal symmetric case, the top surface is completely satisfied while the bottom is not at all. This can be viewed as only 50% favorable. In the horizontal asymmetric case, both surfaces have favorable interactions. This is equivalent to 100% favorable. In the vertical case, half of both surfaces are satisfied so this is also tantamount

to 50% favorable. Intuitively, it can be guessed that horizontal asymmetry (and therefore incommensurate thicknesses) is preferred. In the following plots, the abscissa is the distance between the plates normalized to the block copolymer period, $d = D/L_o$, while the ordinate is the normalized free energy relative to the bulk free energy, F/F_o. When plotting with γ values that emulate this scenario, the intuition turns out to be correct. The horizontal asymmetric case is almost always preferred as indicated by the blue curves being lower than the other curves, corresponding to the lowest free energy.

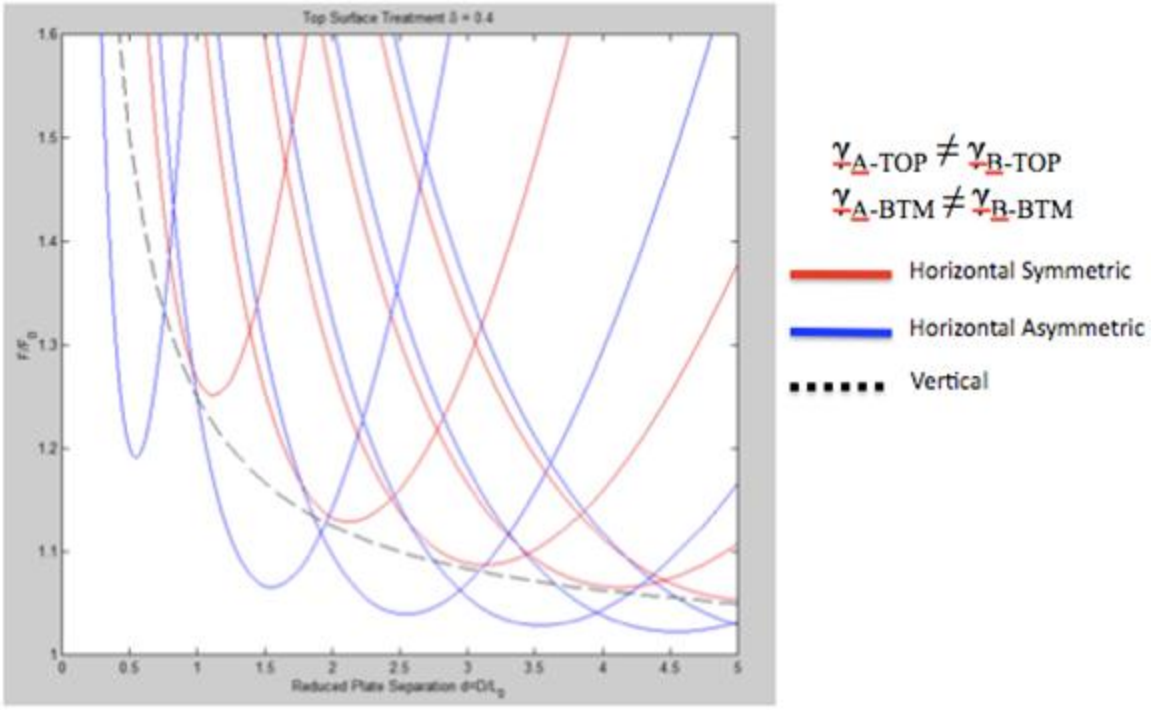

Figure 42: Free Energy when Both Layers Not Optimized

In order to increase the window for vertical (perpendicular) alignment, both interfaces need to be optimized. First, the substrate interface can be replaced with a neutral cross-linkable surface treatment (XST). The wetting graphics are depicted below.

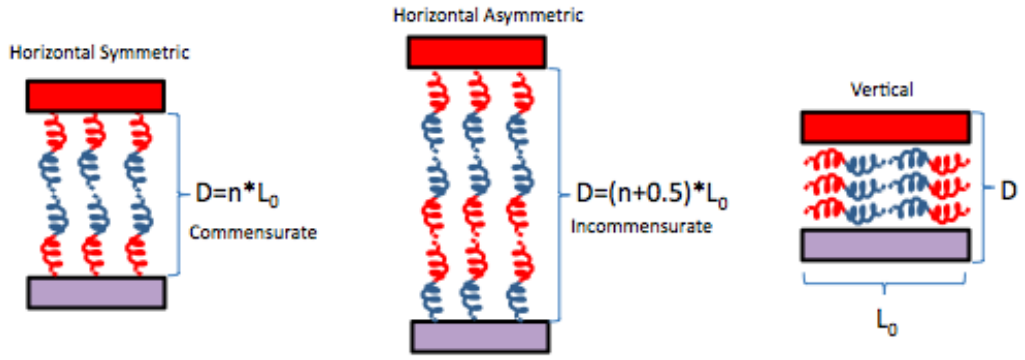

Figure 43: Bottom Surface Optimized Wetting Graphics

In Figure 44, the top layer is assumed to have a very low surface energy, which is commonly found experimentally for block copolymer films exposed to air with only a bottom surface treatment. In this setup, the bottom surface is assumed to be treated (low δ), while the top surface favors the A block (high δ).

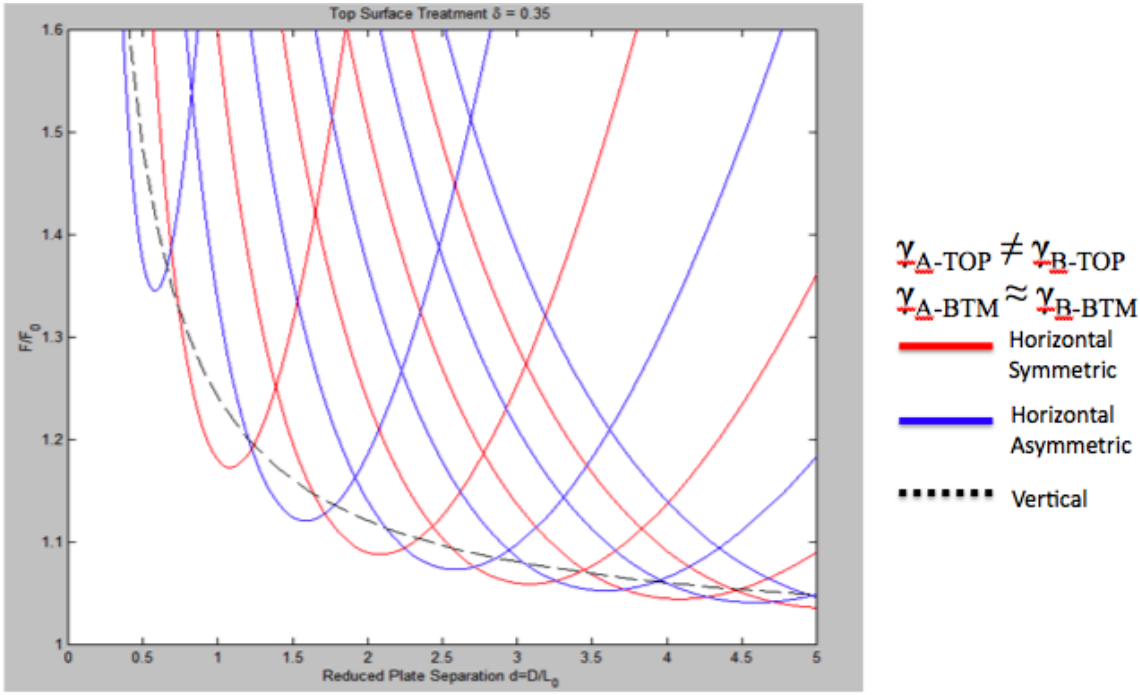

Figure 44: Free Energy of BC with Low-Energy Top Layer

In this scenario, the disparate interfacial energies at the top surface can cause both the symmetric and asymmetric horizontal geometries to be favored. The vertical alignment only exists in a small region, corresponding to $d < 1$. As d increases, the orientation continually alternates between symmetric and asymmetric horizontal. The wetting layer will always be the polymer with the lower surface energy. What changes is the layer that wets the substrate interface. Straying from commensurate/incommensurate values generates a chain stretching (entropic) penalty that is not great enough to induce vertical alignment (enthalpic penalty of unfavorable contacts).

Finally, a case is considered where the top surface is chosen to match closely with the interfacial energies of the two blocks. The wetting graphics are depicted below.

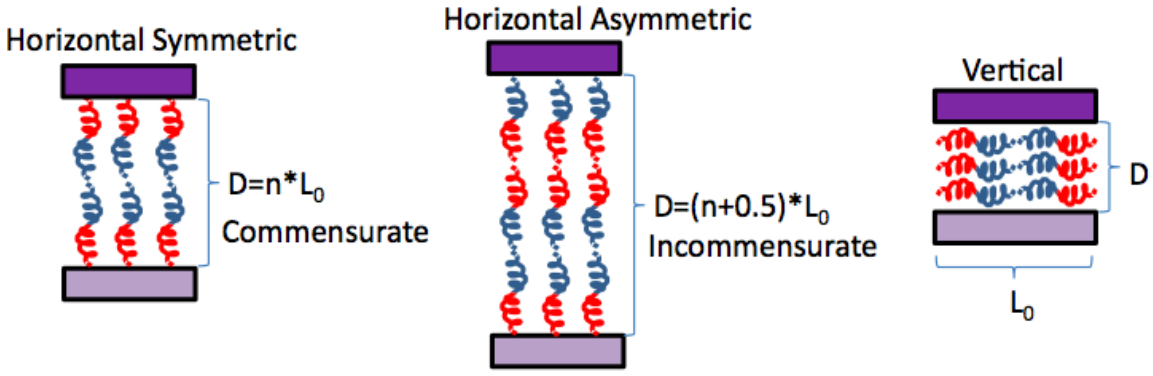

Figure 45: Both Surface Optimized Wetting Graphics

A small disparity between the interfacial energies corresponds to a very low δ.

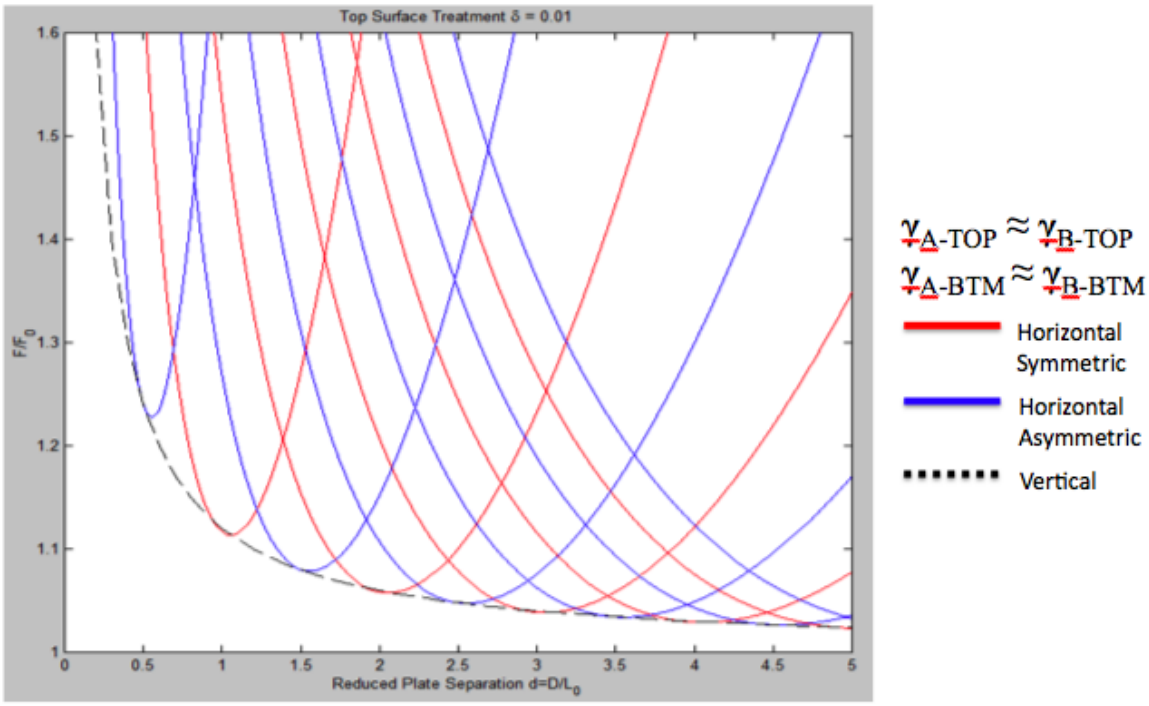

Figure 46: Free Energy of BC with Similar Interfacial Energy Top Layer

Figure 46 shows that the vertical orientation is strongly favored when the top surface treatment matches the interfacial energies of the two blocks. Similar to the identical plate case, the horizontal asymmetric case is never favored. The horizontal symmetric case is only favored in regions close to the equilibrium periodicity. The most important observation, however, is the fact that there are competing orientations to vertical at the commensurate and incommensurate values. At these points, both orientations are equally likely as there is no enthalpic contact penalty (since both surfaces are optimized) and no entropic stretching penalties. However, as *d* deviates from these values, the chains are stretched in the horizontal symmetric and asymmetric cases whereas there is never chain stretching in the vertical case. Therefore, vertical alignment is clearly favored between commensurate and incommensurate values.

This analysis confirmed the need to create an apparatus which could accurately control the swelling thickness of a block copolymer sample introduced to solvent vapor. It is possible to accurately control thickness by splitting an inert carrier gas, having one stream bubble through a solvent before recombining with the other pure stream, and altering the flow rates of the two streams. Ideally, increasing the flow rate of the solvent stream (or alternatively decreasing the flow rate of the pure stream), the solvent would swell more. Such systems have been previously reported[10, 12, 65].

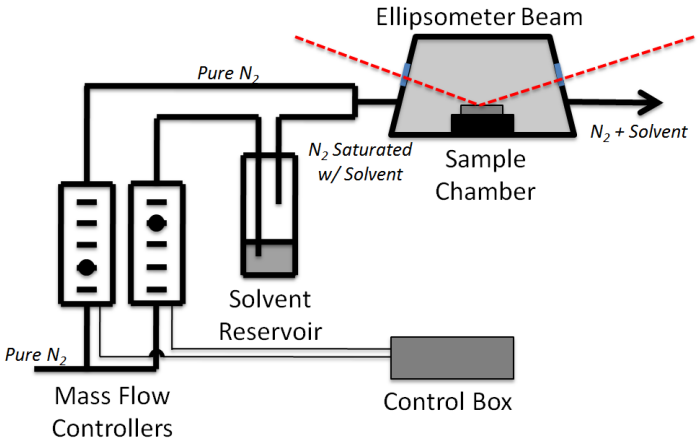

Figure 47: Controlled Swelling Apparatus Schematic

By using a chamber with quartz windows, it is possible to measure the thickness in-situ and make appropriate adjustments on the control box until the desired thickness is achieved. Originally, the polymer would not swell much or slowly with a step change on the control box. Achieving control and reproducibility required several modifications of the chamber to avoid solvent contact with any absorbent materials. The pressure transducer and electric ports were sealed to keep more solvent in while removing cables which may have absorbed some solvent. The heat plate stand was replaced with a custom-built Teflon stand which forced the flow of solvent directly over the sample and

decreased the volume of the chamber. Finally, bolts were put on the door to the chamber (originally held on by vacuum) in order to keep in solvent. Originally, the door was replaced with a light silicon wafer held on by vacuum grease. The grease was actually absorbing solvent, as proved by swelling in the original, simple Teflon chamber. Please see the appendix for pictures of the apparatus.

Once all the modifications were completed, an experiment was conducted which demonstrated that the thickness can be altered quickly by varying the flow rates.

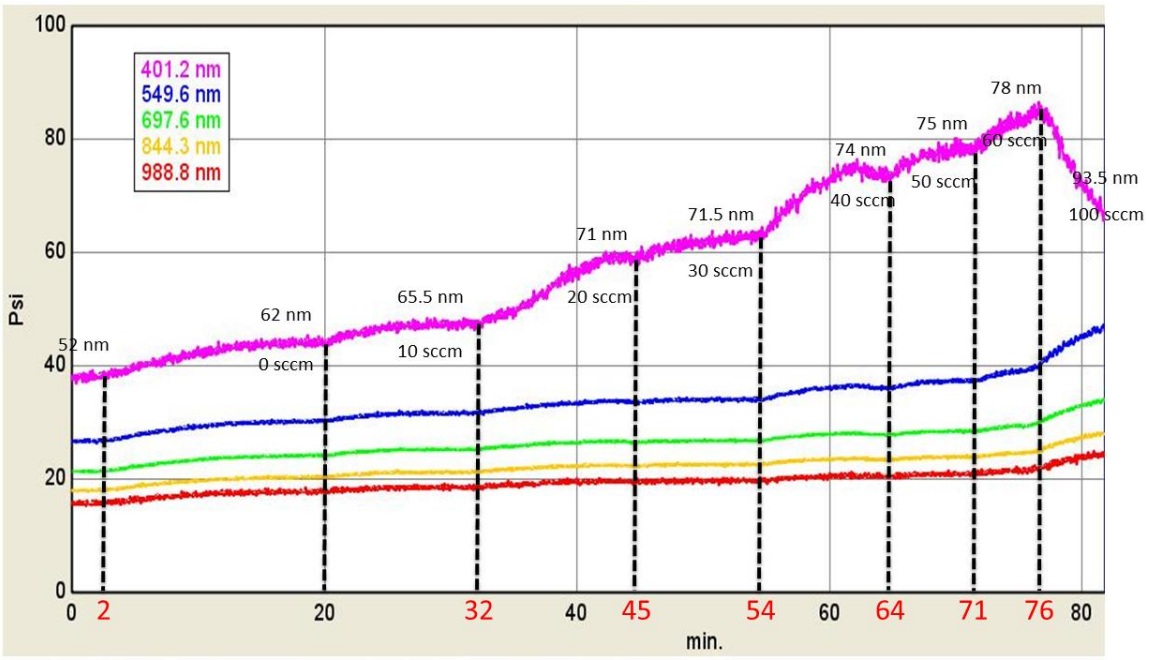

Psi = amplitude ratio of incident beam

Figure 48: Thickness Control on Swelling Apparatus

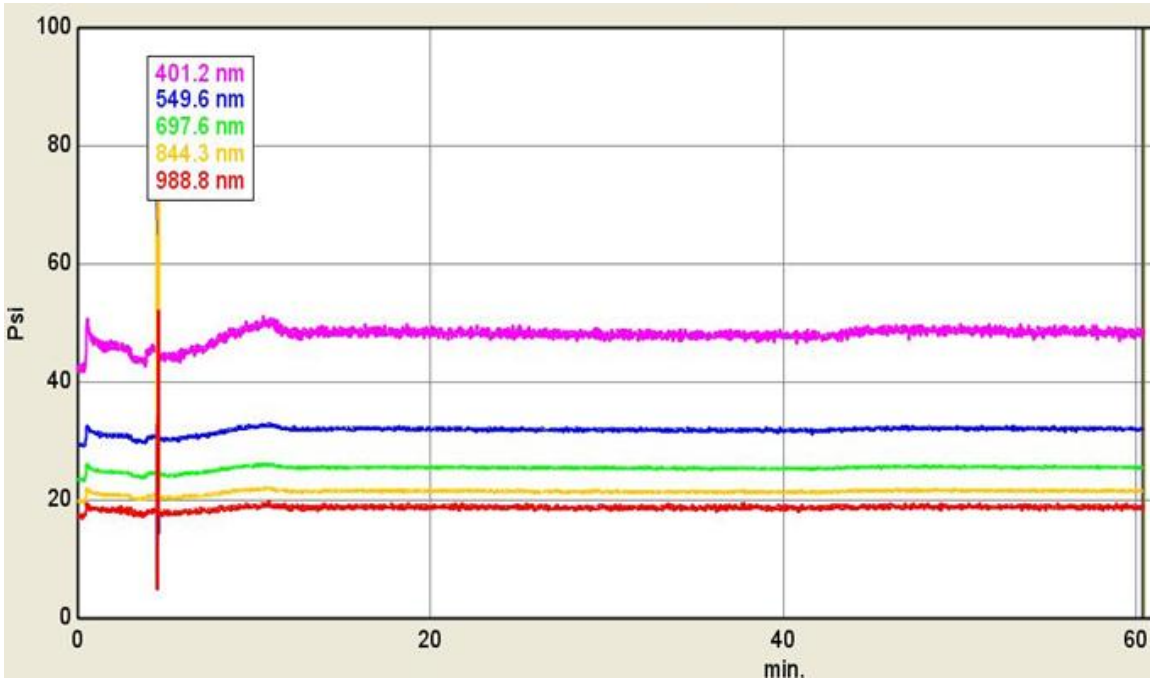

Figure 49: Holding Constant Thickness on Swelling Machine

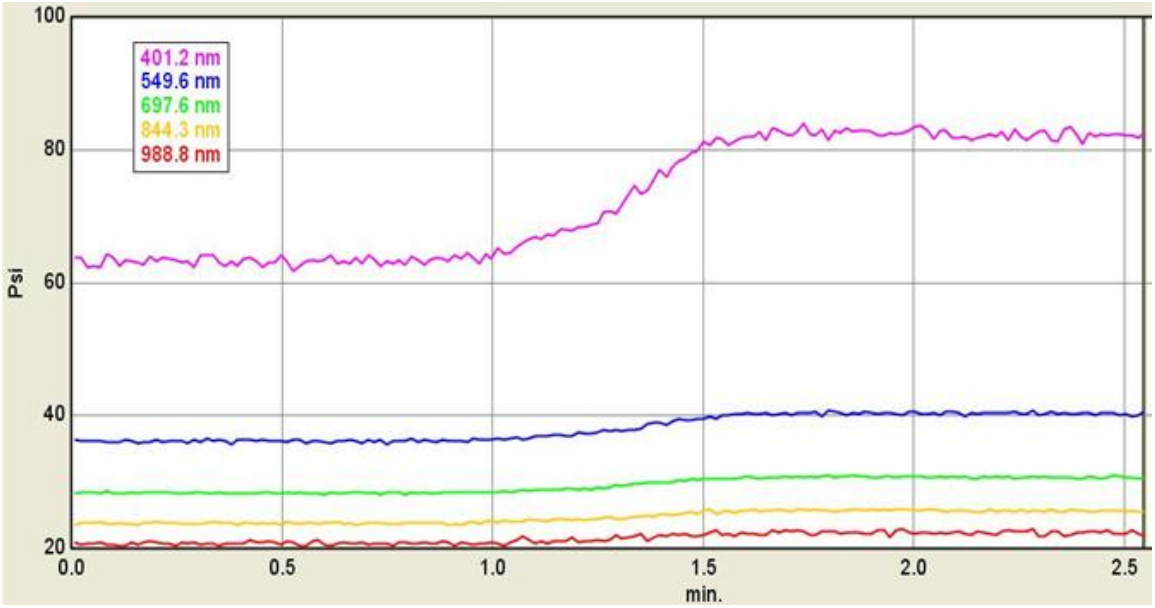

Figure 50: Quick Step Change on Swelling Machine

In Figure 48, the solvent flow rate is varied against a constant pure stream. As predicted, the solvent alters the polymer thickness and equilibrates after each set point change. In Figure 49, the same thickness is easily held without operator interference for about an hour. To date, runs up to 24 hours have been conducted while maintaining constant thickness. Finally, Figure 50 shows the system only takes about 30 seconds to re-equilibrate after a step change.

Once the system was optimized, target thickness were calculated, a cross-linkable random copolymer mat was synthesized, good etch conditions were known, and a firm knowledge of SEM imaging was obtained, it was then possible to run experiments.

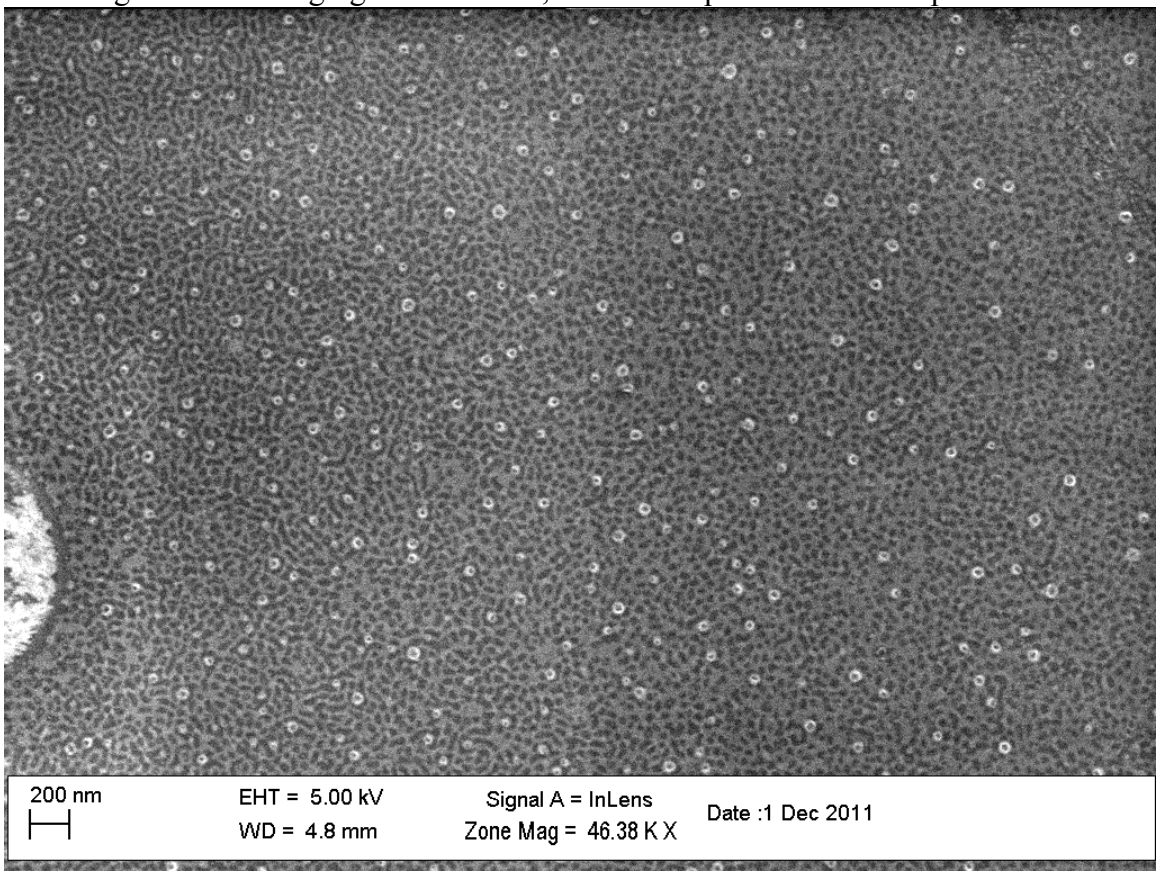

Figure 51: PS-*b*-PMTMSMA on Random Copolymer Mat in Acetone Swelled to 26 nm for One Hour

Figure 51 is PS-*b*-PMTMSMA on a random copolymer mat (composed of approximately the same molar ratio as the block copolymer) annealed in acetone to 26 nm [43% of its bulk equilibrium period (L_o = 61 nm)] for one hour. Acetone had previously dewet the polymer; however, at this reduced swelling ratio, no dewetting occurs and features are seen.

3.6 FUTURE WORK

Although a machine now exists which can accurately control polymer swelling thickness for long periods of time, there is still a large parameter space in which to experiment. There are a wide variety of solvents to try, and the correct solvent will most likely vary from polymer to polymer. Annealing time must be studied in order to give the polymer enough time to re-orient. The polymer must also be swelled to various thicknesses (commensurate, incommensurate, and intermediate values) to test the validity of the theory. Ultimately, the ability to do experiments at different temperatures may become important. The chamber was designed for temperature control so this transition should be possible with a few adaptations. The most promising PS-*b*-PMTMSMA annealing results were seen at 46.5 nm (0.75*L_o) in acetone for 0.75 h at room temperature. The cylinders seem to be aligned perpendicular to the surface and hexagonally packed. This sample was not etched so it would be interesting to see the results of a short etch with the optimized formulas. This validates the thickness model's prediction that the best results exist between commensurate and incommensurate values.

Appendices

A SATURATED TEFLON SWELLING APPARATUS

A. 1 Teflon Apparatus with Quartz Windows

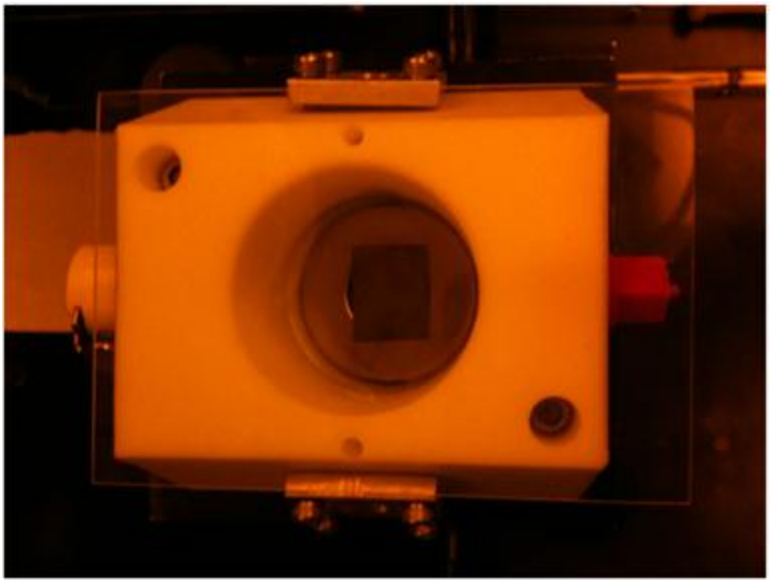

A. 2 Sample on Washer Stand with Solvent Surrounding and Glass Slide Seal

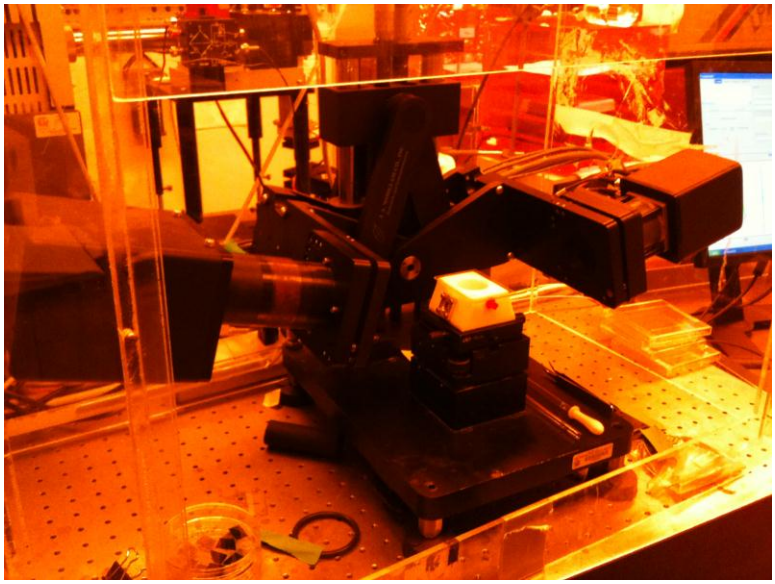

A. 3 Apparatus on Ellipsometer while Taking Measurements

B SOLVENT ANNEALING OVEN

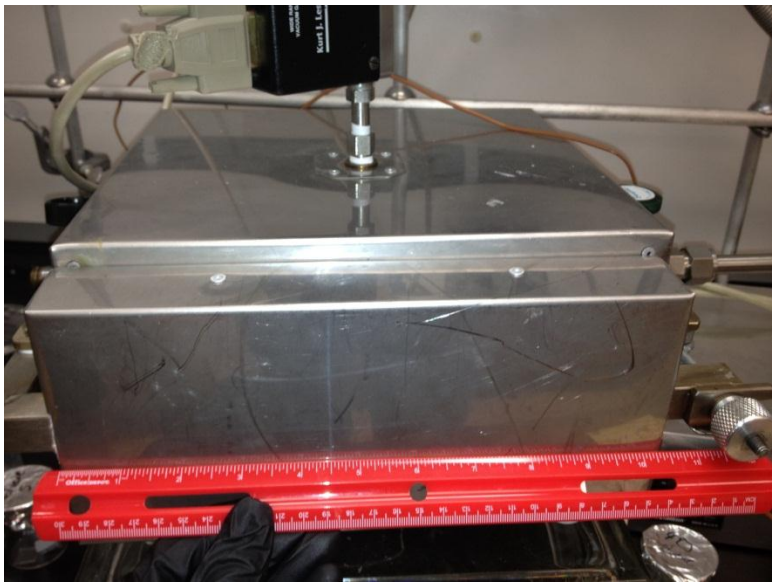

B. 1 Front View of Door and Stainless Steel Outer Coating

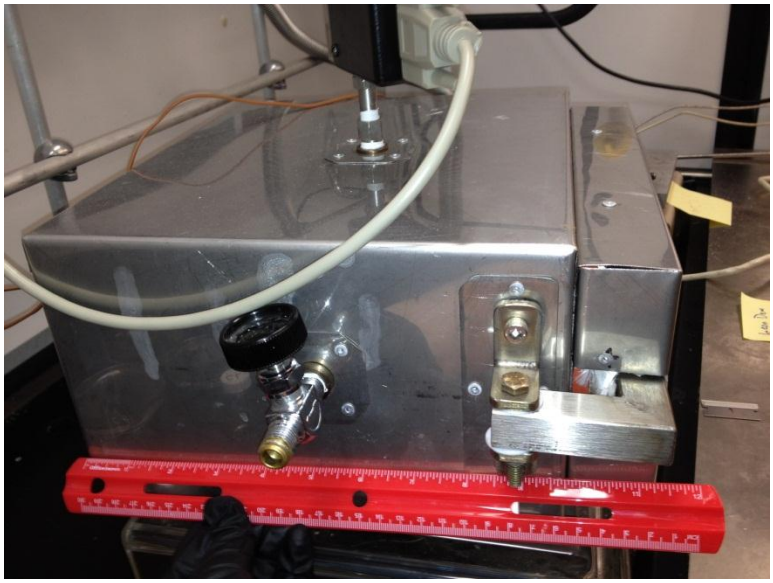

B. 2 Side View with Nitrogen Port and Door Handle

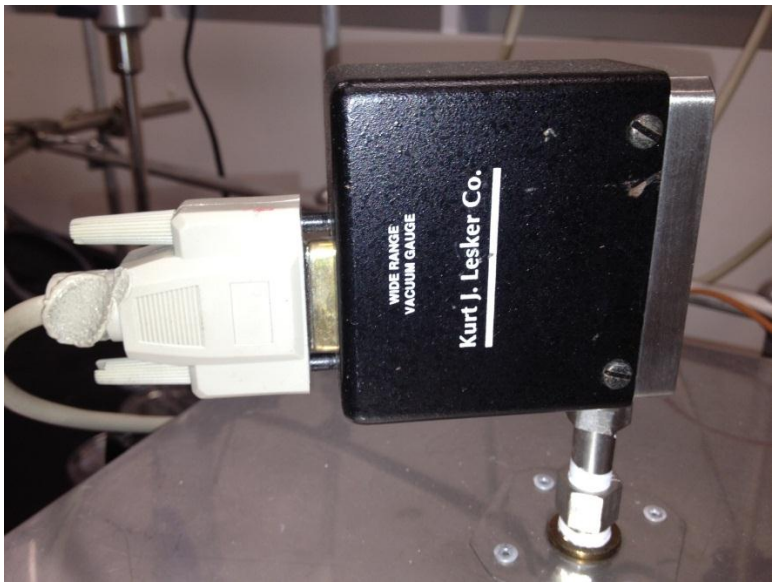

B. 3 Pressure transducer

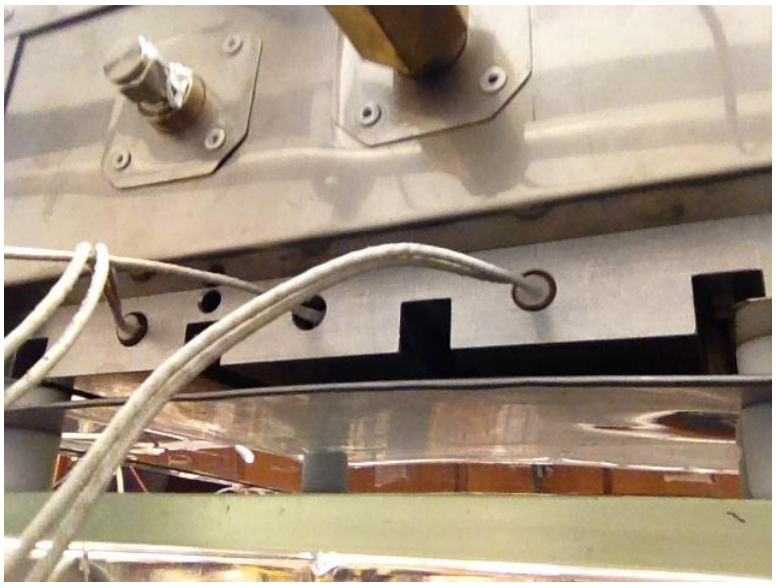

B. 4 Back View of Cartridge Heater Ports, Thermocouple Port, and Solvent Flask Port

B. 5 Pressure Reader

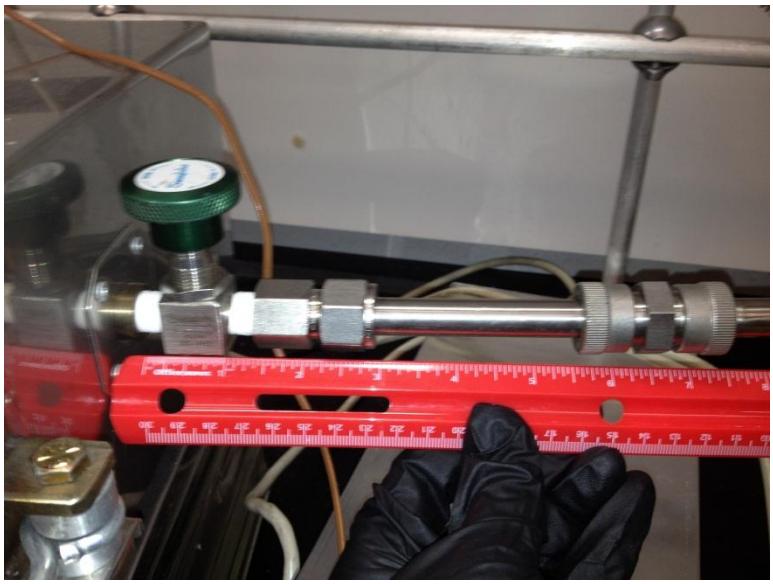

B. 6 Vacuum Port

B. 7 Door Lock

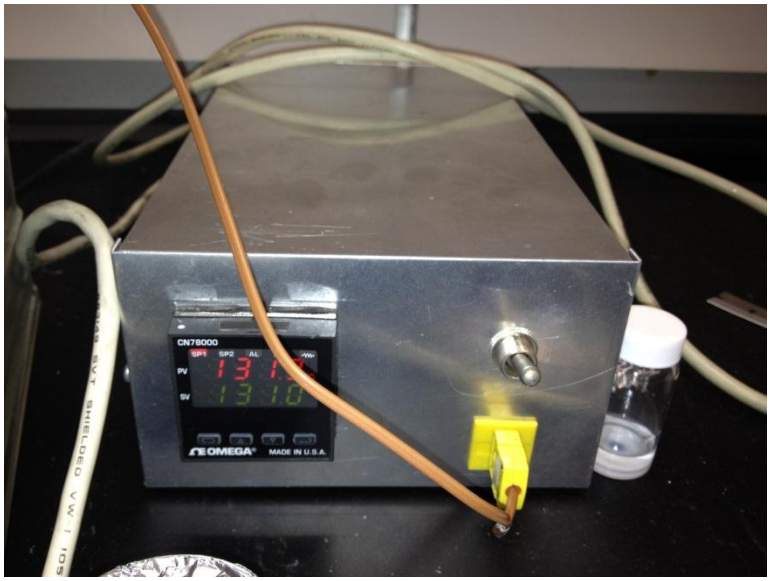

B. 8 Control Box

B. 9 Solvent Trap

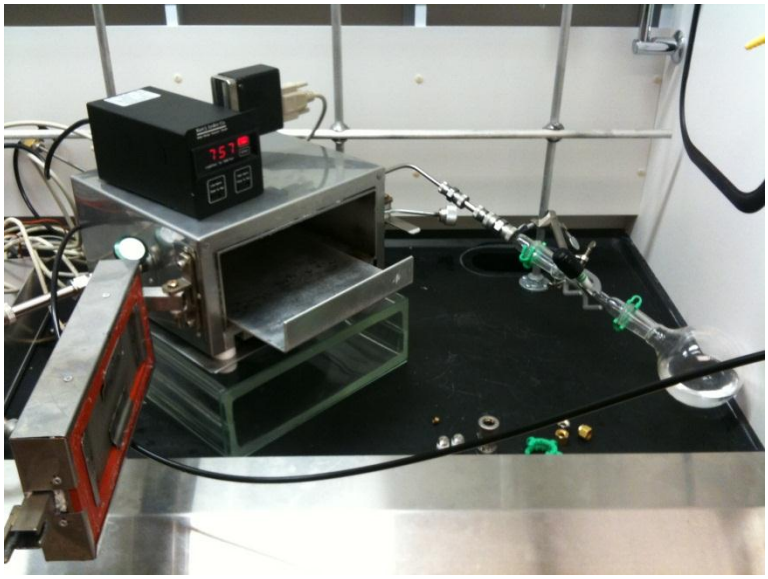

B. 10 Solvent Flask Connected to Oven with View of Silicon Rubber Gasket

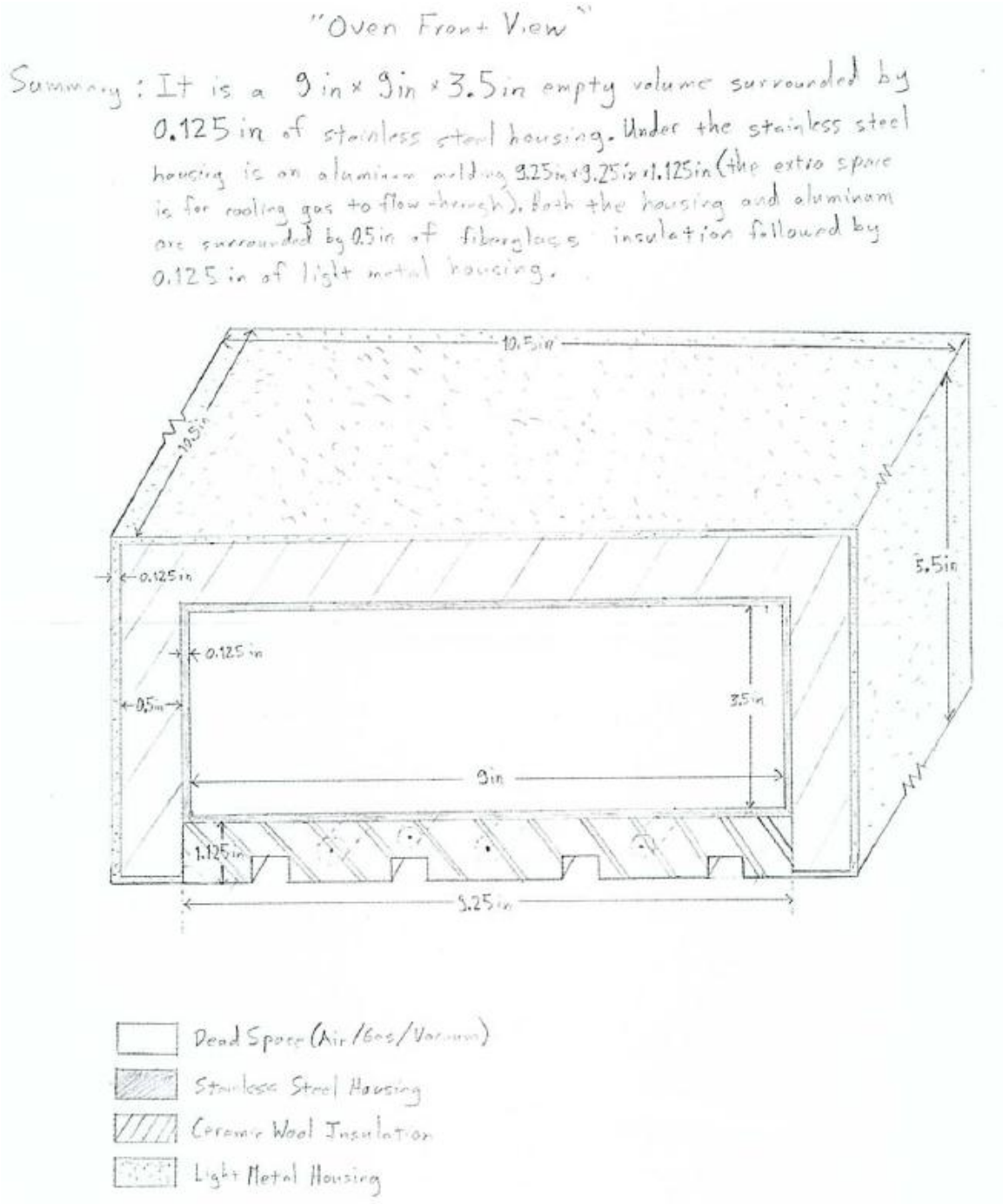

B. 11 Oven Front View Schematic

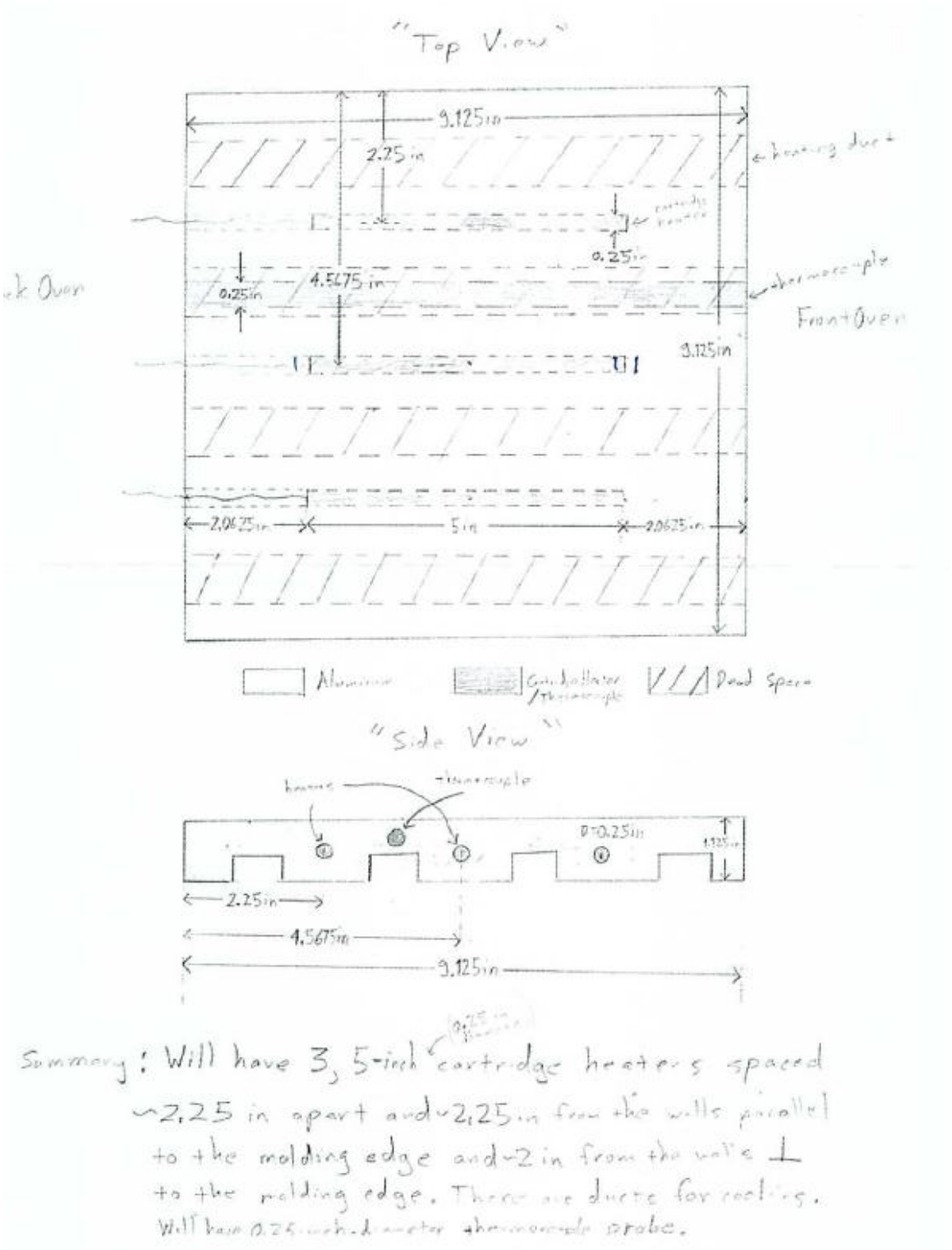

B. 12 Oven Top View Schematic

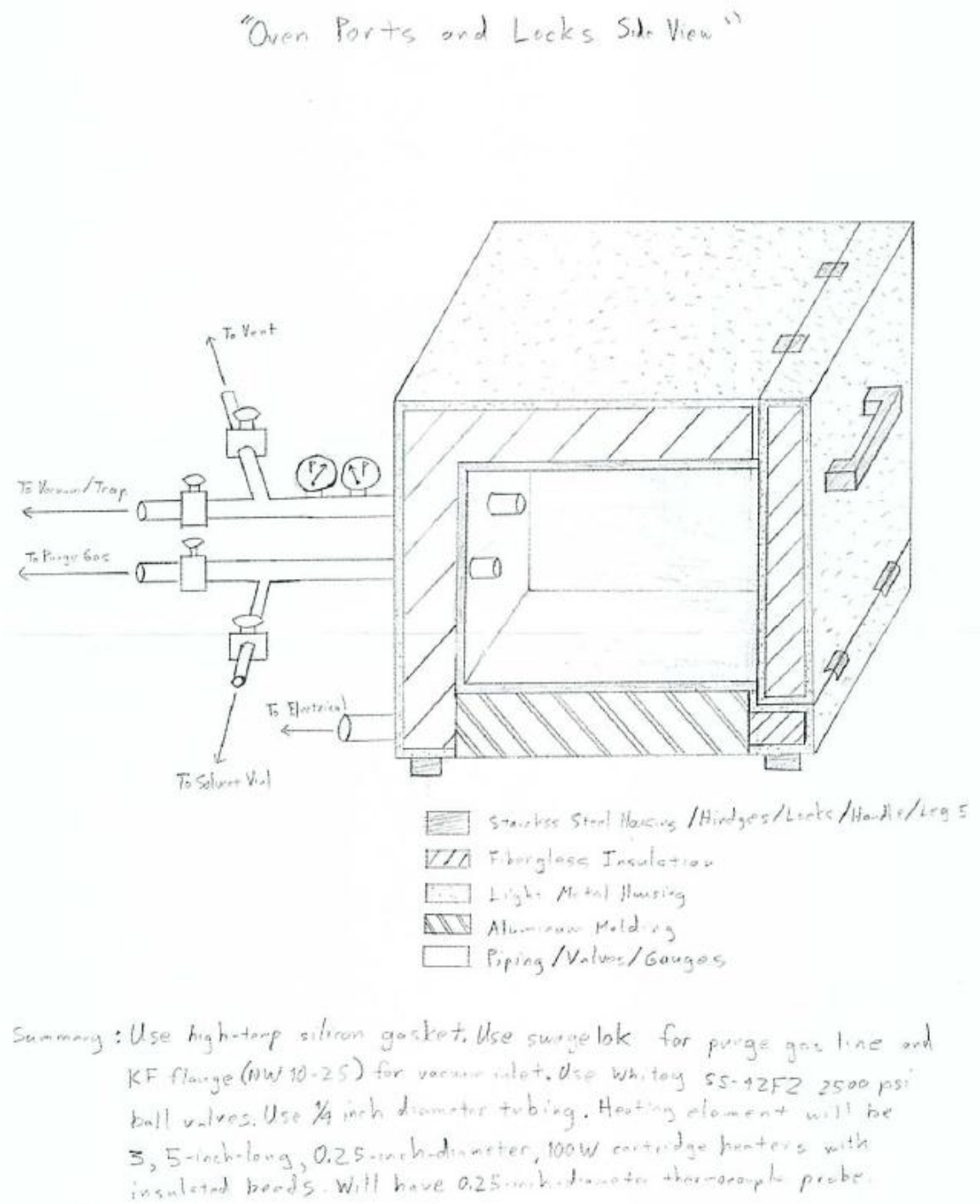

B. 13 Oven Side View Schematic

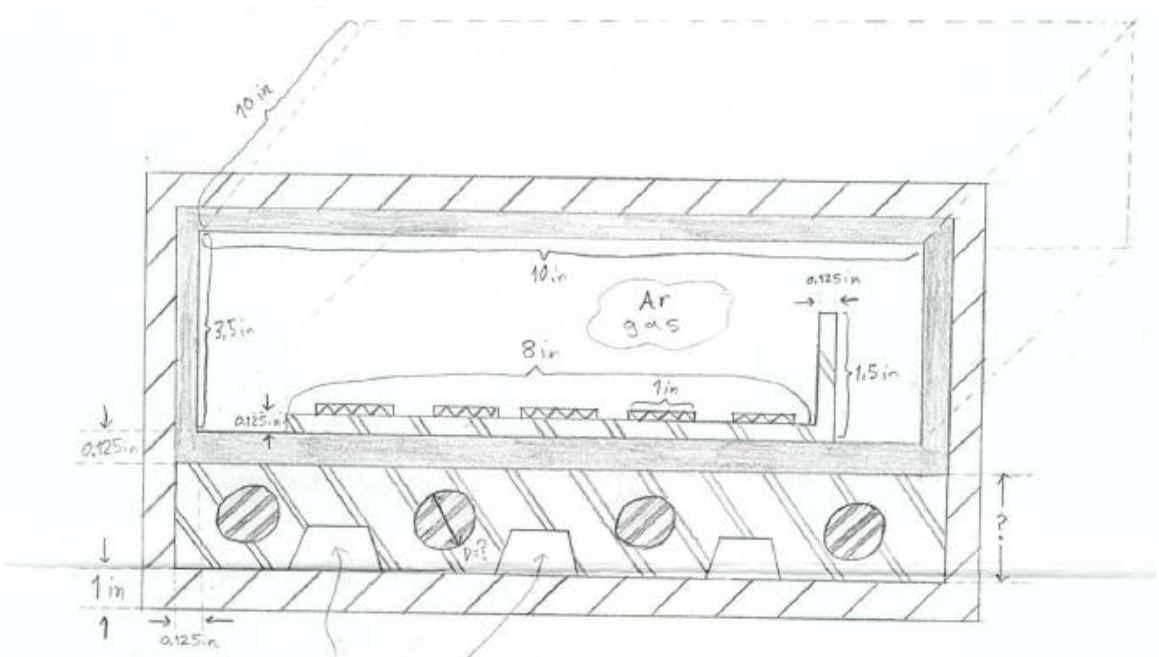

Notes: Inner dimensions of housing will be 10 in x 10 in x 3.5 in.
Sample tray will be 8 in x 8 in with 1.5 in "handle". All thicknesses 0.125 in.
Samples are shards of silicon wafer ~1 in x 1 in and very small thickness.
Insulation will be about 1 in thick.
The housing will be about 0.125 in thick but could be thicker on bottom if needed.
The chamber will be vacuumed void of O_2 and then purged with Argon gas before being heated to temperatures ranging from 150°C - 250°C.
The cartridge mold thickness will depend on the diameter heater you recommend as well as the number of cartridges needed to get even sample heating up to 250°C.

B. 14 Oven Base Plate Schematic

C THICKNESS CONTROL APPARATUS

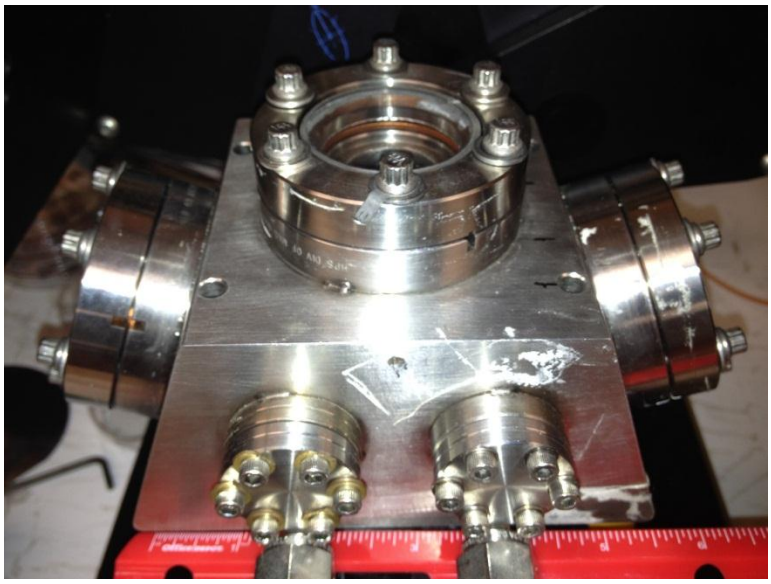

C. 1 Stainless Steel Jamieson Chamber with Quartz Windows

C. 2 Original Heated Sample Platform and Door with Gasket before Bolts Added

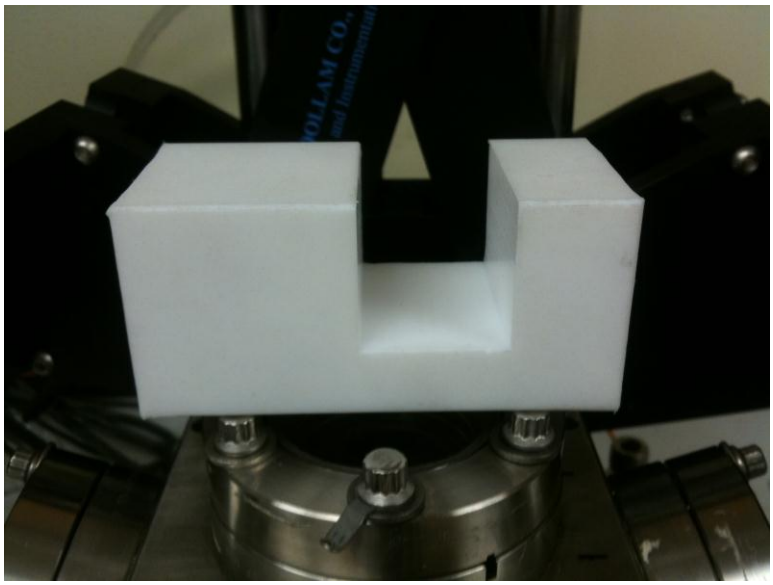

C. 3 New Teflon Platform used to Direct Solvent Flow and Decrease Chamber Volume

C. 4 Door with Bolts Added to Operate without Vacuum

C. 5 View of Entire Apparatus

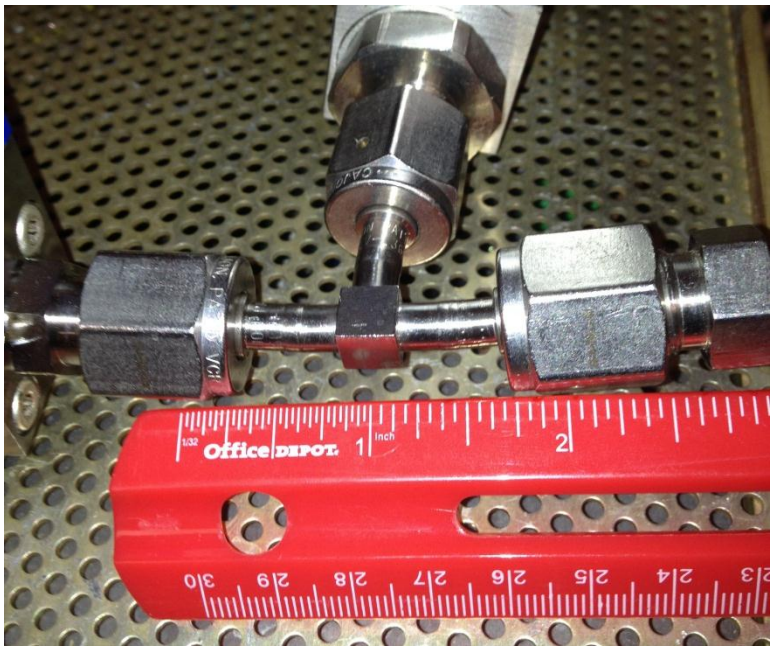

C. 6 Typical Female VCR Three-way Junction used to Split Streams

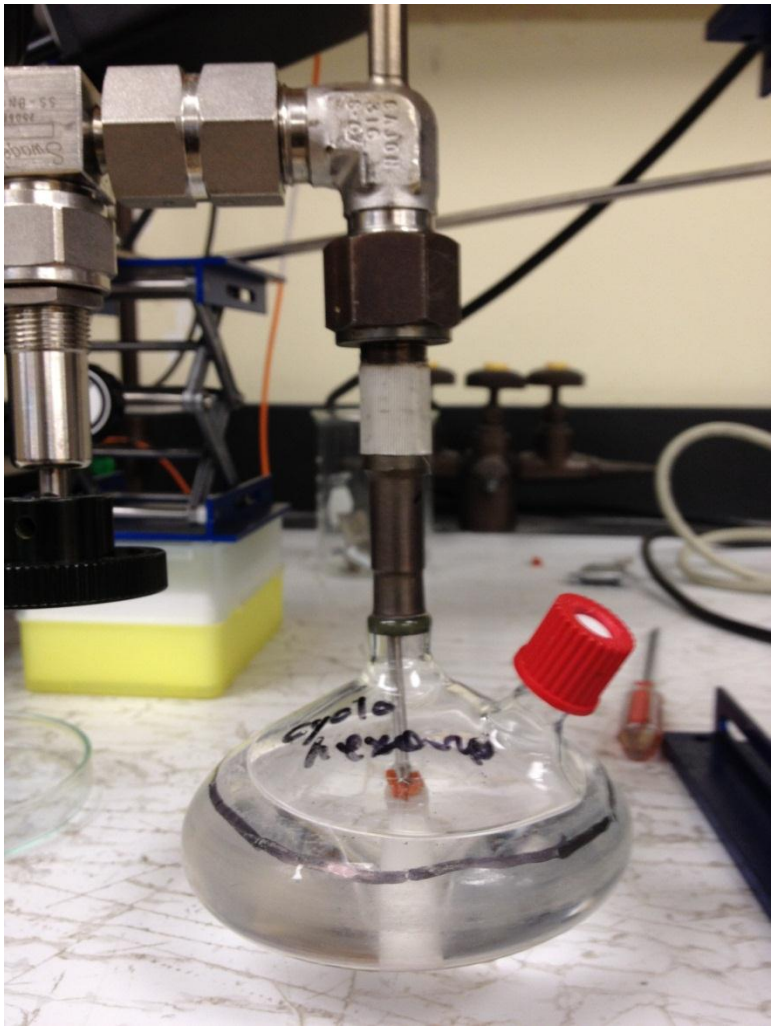

C. 7 Custom Metal-to-glass, Large-area Sparger with Port for Adding more Solvent

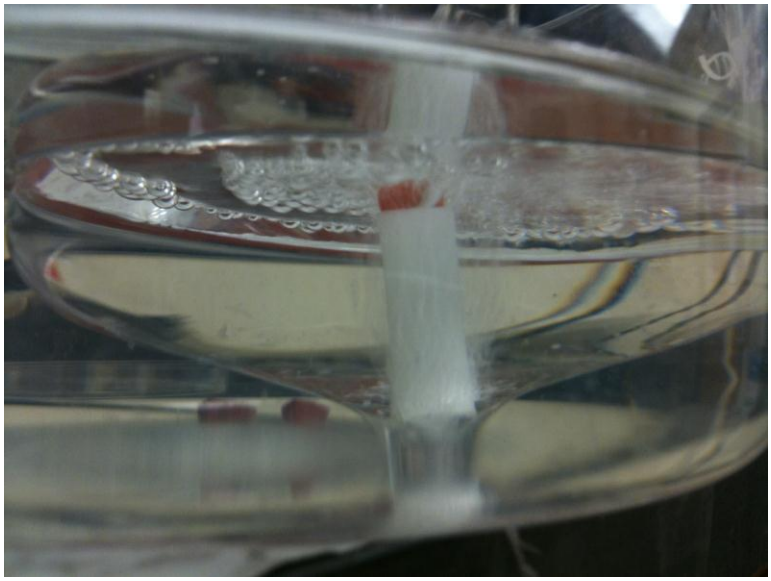

C. 8 Fish Tank Bubbler Added to Increase Saturation

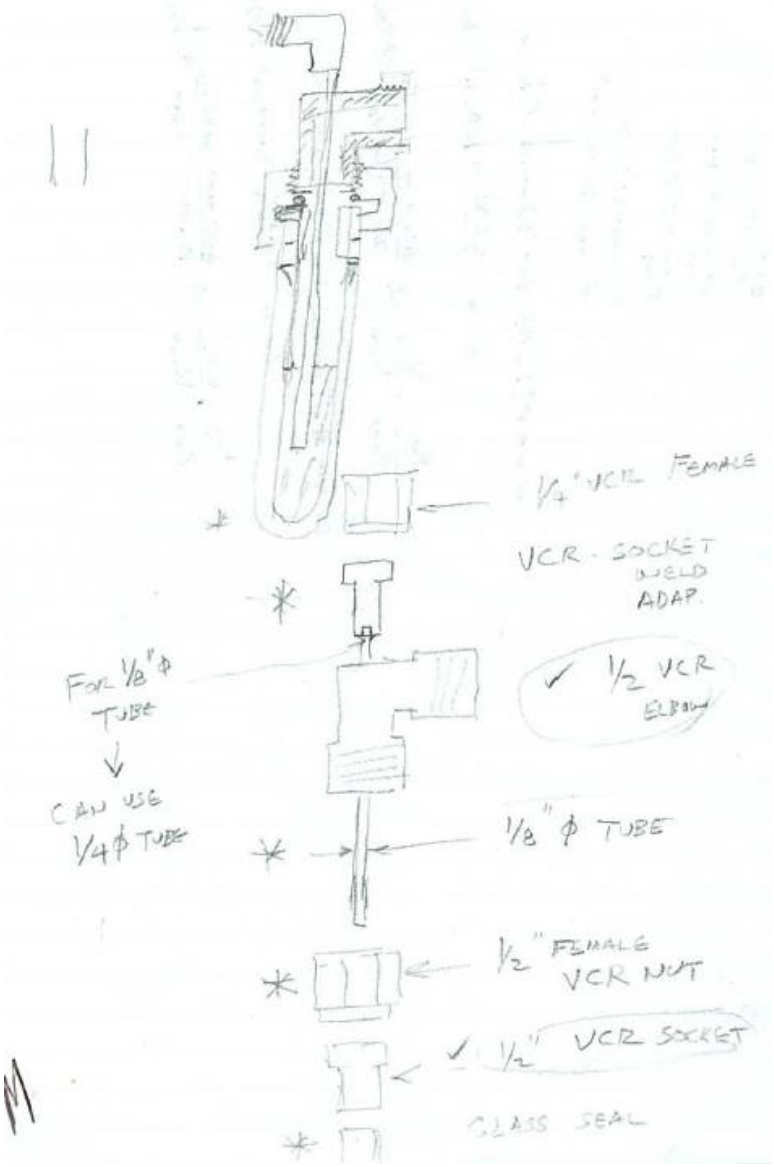

C. 9 Sparger Schematic

D PARTS LIST

Solvent Annealing Oven and Control Box

Item	Number
Stainless steel sheet	400 in^2
Aluminum block (10 in x 10 in x 1 in)	100 in^3
3/8” diameter, 5” long 200 W cartridge heaters	3
Temperature control	1
Solid state relay	1
Finned heat sink	1
¼” diameter, 6” long K-type thermocouple	1
DB15 extension cable, male-female, 6 ft	1
¼” thick, 12”x12”, 40A durometer extreme high-temperature silicon gasket	1
40” wide, 1/8” thick fiberglass insulation	1
Kurt J. Lesker Co. wide range vacuum gauge	1
Valve	4
½” stainless steel tubing	6 ft
Swagelok stainless steel ultra-torr vacuum fittings	2
KF (QF) flange to quick connect fitting adapter	2

Thickness Control Apparatus and Sparger

Item	Number
316 SS VCR face seal fitting, ½” female nut	1
316 SS VCR face seal fitting, reducing socket weld gland, ¼” VCR x 1/8” tube socket	1
316 SS VCR face seal fitting, ¼” silver-plate gasket, non-retained style	25
316 SS VCR face seal fitting, Swagelok tube fitting connector body, ¼” VCR x ¼” tube fitting	6
316 SS WELDED VCR face seal fitting, Swagelok tube fitting connector, ¼” WVCR x ¼” tube fitting	2
316 SS VCR face seal fitting, double female reducing union, ½” female VCR x ¼” female VCR	1
316 SS welded VCR face seal fitting, Swagelok tube fitting connector, ¼” WVCR x 3/8” tube fitting	2
Valve	5
¼” Stainless steel pipe	10
Petco® Discard-a-Stone	1
Mass flow controller	2
MKS PR 4000 control box	1

E MATLAB CODE FOR ALIGNMENT SIMULATION

```
%% Variables
clear all

gam_AS1=24;                    %% top interfacial tension b/w A&S
gam_AS2=39;                    %% bottom interfacial tension b/w A&S
gam_BS1=26;                     %% top interfacial tension b/w B&S
gam_BS2=41;                     %% bottom interfacial tension b/w B&S
gam_AB=100;                       %% polymer interfacial tension b/w A&B
Gam1=gam_AS1/gam_AB;             %% top ratio
Gam2=gam_AS2/gam_AB;              %% bottom ratio
del1=(gam_BS1-gam_AS1)/gam_AB
del2=(gam_BS2-gam_AS2)/gam_AB

D=[0.1:0.1:7];

%% Vertical Surface Free Energy / F0

Fv=1/3*(3+1./D.*((Gam1+del1/2)+(Gam2+del2/2)));

%plot(lam,Fv)

%% Symmetric Horizontal Surface Free Energy / F0

f=5;
d=[0.1:0.001:f];

for m=[1:f];
    lam_s=d/m;
    Fh_s(m,:)=1/3*(lam_s.^2+2./lam_s+1./(m*lam_s).*(Gam1+Gam2));
end

%% Anti-symmetric Horizontal Surface Free Energy / F0

for n=[0.5:1:f+1]
    lam_a=d/n;

Fh_a(n+0.5,:)=1/3*(lam_a.^2+2./lam_a+1./(n*lam_a).*(Gam1+Gam2+del2));
end

%% Plots

plot(d,Fh_s,'r',d,Fh_a,'b',D,Fv,'--k')
axis([0 f 1 1.6])
xlabel('Reduced Plate Separation d=D/L_0','interpreter','tex')
ylabel('F/F_0')
title(['Top Surface Treatment \delta = ',num2str(del1)])
```

F INSTRUMENTATION

Polymer solutions were filtered with 0.20 μm PTFE filters prior to spin coating. Films were spin coated on a Brewer Science, Inc. CEE 100CB Spincoater. Film thicknesses were determined with a J.A. Woollam Co., Inc. VB 400 VASE Ellipsometer using wavelengths from 382 to 984 nm with a 65° angle of incidence. Ellipsometer thickness images were generated with CompletEASE® software. A Digital Instruments Dimension 3100 atomic force microscope and an Agilent Technologies 5500 scanning probe microscope with NCHR Pointprobe® Non-Contact Mode tips with a force constant of 42 N/m were used to collect AFM images. AFM images presented in this thesis are false color phase images. A Zeiss Supra 40 VP Scanning Electron Microscope was used to collect all SEM images presented in this report. SEM mounts and copper tape were purchased from Ted Pella, Inc. All supplies for both annealing apparatuses were ordered from Omega Engineering, Inc.®, Kurt J. Lesker®, and McMaster-Carr®.

Glossary

A	cross-sectional area
a	Kuhn statistical length
AC	alternating current
AFM	atomic force microscopy
ATRP	atom transfer radical polymerization
BC	block copolymer
BPM	bit patterned media
BPO	benzoyl peroxide
D	plate spacing
DMF	N,N-dimethylformamide
DMSO	dimethyl sulfoxide
E_H	energy contribution from enthalpy
E_S	energy contribution from entropy
EBL	electron beam lithography
EUV	extreme ultraviolet
F	group contribution method component
F_h	free energy of the block copolymer horizontally aligned
F_o	free energy of the block copolymer in the bulk
F_v	free energy of the block copolymer vertically aligned
f	volume fraction
G	Gibbs free energy
GPC	gel permeation chromatography

H	enthalpy
ICP	inductively coupled plasma
IPA	isopropyl alcohol
k	thermal conductivity; index of the substance adjacent to B block
k_d	initiator dissociation constant
k_p	polymer propagation constant
k_t	polymer termination constant
k_1	Rayleigh's equation constant
L	period of a block copolymer
L_o	equilibrium period of a block copolymer
LFL	lower flammability limit
MEK	methyl ethyl ketone (2-butanone)
MSDS	material safety data sheet
MW	molecular weight
N	degree of polymerization
n	number of molecules; integer number of domain spacings
NA	numerical aperture
NIL	nanoimprint lithography
NMR	nuclear magnetic resonance
P	pressure
$P^{vap}(T)$	vapor pressure of a gas at temperature T
PDMS	polydimethylsiloxane
PEO	poly(ethylene oxide)
PFS	polyferrocenylsilane
PI	polyisoprene

PMMA	poly(methyl methacrylate)
PMR	perpendicular recording media
PMTMSMA	poly(methyltrimethylsilyl methacrylate)
PS	polystyrene
PVBzAz	poly(vinylbenzyl azide)
PVBzCl	poly(vinylbenzyl chloride)
$\dot{Q}$	heat flow rate
q	heat flux
R	ideal gas constant
r	the distance between two endpoints
RAFT	reversible-addition fragmentation chain transfer
RF	radio frequency
RIE	reactive ion etch
ROMP	ring-opening metathesis polymerization
rpm	revolutions per minute
S	entropy
SEM	scanning electron microscope
T	absolute temperature
T_g	glass transition temperature
t	film thickness
THF	tetrahydrofuran
TMS	trimethylsilyl
UFL	upper flammability limit
UV	ultraviolet
$\hat{V}$	molar volume

XST	cross-linkable surface treatment
x	direction of heat flow
z	volume fraction of gas in mixture
Γ	$\gamma_{AS} / \gamma_{AB}$
Δ	difference
ΔH_v	latent heat of vaporization
γ_{ij}	interfacial tension between objects i and j
δ	solubility parameter; $(\gamma_{BS}-\gamma_{AS}) / \gamma_{AB}$
ζ	number of molecules
η	reaction efficiency
θ	angle of incidence
λ	wavelength; ratio of the BC period to the equilibrium period
ρ	density
σ	interfacial energy per area of interface
υ	kinetic chain length
χ	polymer-polymer interaction parameter
$\chi_{P\text{-}S}$	polymer-solvent interaction parameter
ω	spin speed
$[M]$	total monomer concentration
$[I]$	initiator concentration
∇	gradient operator
$\sum$	summation operator

Bibliography

1. Bates, F. S.; Fredrickson, G. H., *Physics Today* **1999,** *52* (2), 32-38.
2. Ross, C. A., et al., *J. Vac. Sci. Technol., B: Microelectron. Nanometer Struct.--Process., Meas., Phenom.* **2008,** *26* (6), 2489-2494.
3. Colburn, M., et al., *J. Vac. Sci. Technol., B* **2001,** *19* (6), 2162-2172.
4. Schwartz, E. L., et al., *Proc. SPIE* **2010,** *7639* (Pt. 1, Advances in Resist Materials and Processing Technology XXVII), 76390G/1-76390G/11.
5. Ross, C. A., et al., *Proc. SPIE* **2010,** *7637* (Alternative Lithographic Technologies II), 76370H/1-76370H/7.
6. Cushen, J. D., et al. In *Analysis of the Flory-Huggins interaction parameter of silicon-containing block copolymers*, Abstracts of Papers, 241st ACS National Meeting & Exposition, Anaheim, CA, United States, March 27-31, 2011, 2011; pp PMSE-405.
7. Bates, F. S.; Fredrickson, G. H., *Annu. Rev. Phys. Chem.* **1990,** *41*, 525-57.
8. Jung, Y. S.; Ross, C. A., *Nano Lett.* **2007,** *7* (7), 2046-2050.
9. Albert, J. N. L.; Epps, T. H., III, *Mater. Today (Oxford, U. K.)* **2010,** *13* (6), 24-33.
10. Paik, M. Y., et al., *Macromolecules (Washington, DC, U. S.)* **2009,** *43* (9), 4253-4260.
11. Bosworth, J. K., et al., *PMSE Prepr.* **2007,** *96*, 659-660.
12. Li, Y., et al., *Appl. Surf. Sci.* **2011,** *257* (18), 8093-8101.
13. Jeong, J.-W., et al., *Nano Lett.* **2011,** *11* (10), 4095-4101.
14. Huang, E., et al., *Macromolecules* **1998,** *31* (22), 7641-7650.
15. Peng, J., et al., *J. Chem. Phys.* **2004,** *120* (23), 11163-11170.

16. Bosworth, J. K., et al., *ACS Nano* **2008,** *2* (7), 1396-1402.
17. Mokarian-Tabari, P., et al., *ACS Nano* **2011**, ACS ASAP.
18. Tung, S.-H.; Xu, T., *Macromolecules (Washington, DC, U. S.)* **2009,** *42* (15), 5761-5765.
19. Vayer, M., et al., *Thin Solid Films* **2010,** *518* (14), 3710-3715.
20. http://www.deepspar.com/wp-data-loss.html. **2007**.
21. http://www.intel.com/content/www/us/en/silicon-innovations/moores-law-technology.html. **2011**.
22. http://www.cmg.org/measureit/issues/mit41/m_41_2.html. **2007**.
23. http://www.osa-opn.org/archives/0507/features/feature5.aspx. **2012**.
24. https://www1.hitachigst.com/hdd/research/storage/pm/index.html. **2010**.
25. http://www.dataclinic.co.uk/hard-disk-superparamagnetic-effect.htm. **2011**.
26. http://www.tomshardware.com/reviews/hitachi-7k1000-terabyte-hard-drive,1584-3.html. **2007**.
27. http://willson.cm.utexas.edu/Research/Sub_Files/Immersion/index.php. **2006**.
28. http://semimd.com/blog/2011/11/25/asml%E2%80%99s-euv-roadmap-points-to-new-wavelength/. **2011**.
29. Yang, X., et al., *ACS Nano* **2009,** *3* (7), 1844-1858.
30. Ruiz, R., et al., *Science (Washington, DC, U. S.)* **2008,** *321* (5891), 936-939.
31. Rodwogin, M. D., et al., *ACS Nano* **2010,** *4* (2), 725-732.
32. Stoykovich, M. P.; Nealey, P. F., *Mater. Today (Oxford, U. K.)* **2006,** *9* (9), 20-29.
33. Park, S., et al., *ACS Nano* **2008,** *2* (4), 766-772.
34. Phillip, W. A., et al., *ACS Appl. Mater. Interfaces* **2010,** *2* (3), 847-853.
35. Kim, H.-C., et al., *Chem. Rev. (Washington, DC, U. S.)* **2010,** *110* (1), 146-177.

36. Bang, J., et al., *Adv. Mater. (Weinheim, Ger.)* **2009,** *21* (47), 4769-4792.

37. Hellwig, O., et al., *Appl. Phys. Lett.* **2010,** *96* (5), 052511/1-052511/3.

38. In, I., et al., *Langmuir* **2006,** *22* (18), 7855-7860.

39. Ryu, D. Y., et al., *Macromolecules (Washington, DC, U. S.)* **2007,** *40* (12), 4296-4300.

40. Ham, S., et al., *Macromolecules (Washington, DC, U. S.)* **2008,** *41* (17), 6431-6437.

41. Han, E., et al., *Macromolecules (Washington, DC, U. S.)* **2008,** *41* (23), 9090-9097.

42. Matsen, M. W.; Bates, F. S., *Macromolecules* **1996,** *29* (4), 1091-8.

43. Odian, G., *Principles of Polymerization*. 4th ed.; Wiley, New York, 2004.

44. Bates, C. M., et al., *Langmuir* **2010**, ACS ASAP.

45. http://www.cpmt.org/mm/pkglab/theory/spin_theory.html. **2006**.

46. Bita, I., et al., *Science (Washington, DC, U. S.)* **2008,** *321* (5891), 939-943.

47. Son, J. G., et al., *Advanced Materials* **2010**, n/a-n/a.

48. Takenaka, M., et al., *J. Polym. Sci., Part B: Polym. Phys.* **2010,** *48* (22), 2297-2301.

49. Kim, S., et al., *Macromolecules (Washington, DC, U. S.)* **2007,** *40* (12), 4102-4105.

50. Kim, S., et al., *Mater. Res. Soc. Symp. Proc.* **2007,** *961E* (Nanostructured and Patterned Materials for Information Storage), No pp given, Paper #: 0961-O17-03.

51. Chuang, V. P., et al., *Adv. Mater. (Weinheim, Ger.)* **2009,** *21* (37), 3789-3793.

52. Thurn-Albrecht, T., et al., *Science (Washington, D. C.)* **2000,** *290* (5499), 2126-2129.

53. Yufa, N. A., et al., *Macromolecules (Washington, DC, U. S.)* **2009,** *42* (7), 2667-2671.

54. Peng, J., et al., *J. Chem. Phys.* **2006,** *125* (6), 064702/1-064702/8.

55. Brandrup, J., et al., *Polymer Handbook*. 4 ed.; Wiley, New York, 1999.

56. Han, E., et al., *Macromolecules (Washington, DC, U. S.)* **2009,** *42* (13), 4896-4901.

57. Kellogg, G. J., et al., *Phys. Rev. Lett.* **1996,** *76* (14), 2503-6.

58. http://www.chemicalland21.com/specialtychem/finechem/BENZOYL%20PEROXIDE.htm. **2012**.

59. Colburn, M. E. Step and flash imprint lithography: A low-pressure, room-temperature nanoimprint lithography. Dissertation, The University of Texas at Austin, United States -- Texas, 2001.

60. Fetters, L. J., et al., *Connection between Polymer Molecular Weight, Density, Chain Dimensions, and Melt Viscoelastic Properties*. 1994; Vol. 27, p 4639-47.

61. Small, P. A., *Journal of Applied Chemistry* **1953,** *3*, 71-80.

62. Jung, Y. S., et al., *Nano Lett.* **2010,** *10* (3), 1000-1005.

63. Cheng, J. Y., et al., *Adv. Mater. (Weinheim, Ger.)* **2006,** *18* (19), 2505-2521.

64. Green, P. F., *Journal of Polymer Science, Part B: Polymer Physics* **2003,** *41* (19), 2219-2235.

65. Cavicchi, K. A.; Russell, T. P., *Macromolecules* **2007,** *40* (4), 1181-1186.

66. Helfand, E.; Wasserman, Z. R., *Macromolecules* **1976,** *9* (6), 879-88.

67. Ohta, T.; Kawasaki, K., *Macromolecules* **1986,** *19* (10), 2621-32.

68. Walton, D. G., et al., *Macromolecules* **1994,** *27* (21), 6225-8.

69. Turner, M. S., *Phys. Rev. Lett.* **1992,** *69* (12), 1788-91.